ETH Library

Polarization and manipulation of a mesoscopic nuclear spin ensemble using a single confined electron spin

Doctoral Thesis

Author(s):
Maletinsky, Patrick

Publication date:
2008

Permanent link:
https://doi.org/https://doi.org/10.3929/ethz-a-005676739

Rights / license:
In Copyright - Non-Commercial Use Permitted

This page was generated automatically upon download from the ETH Zurich Research Collection.
For more information, please consult the Terms of use.

Polarization and Manipulation of a Mesoscopic Nuclear Spin Ensemble Using a Single Confined Electron Spin

Patrick Maletinsky
2008

DISS. ETH NO. 17815

Polarization and Manipulation of a Mesoscopic Nuclear Spin Ensemble Using a Single Confined Electron Spin

A dissertation submitted to the

SWISS FEDERAL INSTITUTE OF TECHNOLOGY ZURICH

for the degree of

Doctor of Natural Sciences

presented by

PATRICK MALETINSKY

Dipl. Phys.
ETH Zürich

born 3rd of June 1979

citizen of Obersiggenthal, AG

Accepted on the recommendation of:

Prof. Atac Imamoglu, examiner
Prof. Thierry Amand, co-examiner

Cover illustration:
Measurement of nuclear spin polarization (encoded in gray-scale) as a function of quantum dot gate voltage and time (horizontal and vertical axis, respectively). For details, see Chap. 7.

Summary

The present thesis is devoted an all-optical study of the physical properties of the mesoscopic ensemble of nuclear spins contained in an individual, self-assembled quantum dot (QD). QDs are artificial entities that allow for the trapping of individual charge carriers in all three spatial dimensions. The trapping length scales are thereby small enough to require a quantum mechanical treatment of the QD charge carrier confinement. The QDs studied here are self-assembled InAs nano-crystals which contain roughly 10^5 nuclei, all of nonzero nuclear spin. The nuclear spins can be manipulated and measured by using the spin of a trapped QD electron as an agent which couples to the nuclei via the hyperfine interaction. Electron spins can be optically oriented due to selection rules of optical interband transitions in the QD semiconductor material. This electron spin orientation is then transferred to the nuclear spins via the hyperfine interaction, leading to a dynamical nuclear spin polarization (DNSP). At the same time, the hyperfine interaction causes a shift of the energy of the electron in contact with spin polarized nuclei. This fact is exploited here to measure the degree of DNSP through the corresponding spectral features in the light which is emitted upon recombination of the optically generated QD electrons.

This thesis starts with a description of the steady state behavior of optically generated DNSP. It is shown that the transfer of spin information between the electron and the nuclei depends strongly on the degree of the nuclear spin polarization itself. The corresponding feedback of DNSP on the electrons takes the form of an effective magnetic field which can be on the order of a few Tesla and renders the coupled electron-nuclear spin system highly nonlinear. In particular, experimental evidence for a hysteretic behavior of the coupled electron-nuclear spin system in an external magnetic field is presented and explained with a classical rate equation model.

The focus of the second part of the thesis lies on the dynamics of DNSP which is studied using a time-resolved photoluminescence technique. In addition to measuring the timescales for buildup and decay, this experiment revealed an unexpected aspect of the dynamics of DNSP: while an optically pumped electron spin can be used to polarize the nuclear spins, the electron can also be very efficient in destroying an established DNSP in the absence of optical excitation. In this case, the electron spin is randomly fluctuating, thereby causing relaxation of the nuclear spins. This electron mediated decay of DNSP is discussed in detail as a function of the electron spin correlation time and of external magnetic fields. If the electron spin fluctuations become too fast, the lifetime of DNSP can increase again due to an effect called motional narrowing which is observed experimentally. Furthermore, the nonlinear behavior of DNSP in the presence of external magnetic fields leads to the observation of DNSP decay curves which are highly non-exponential.

The presented results give new insights into the dynamics of nuclear spins in semiconductor QDs and show possibilities of manipulating the QD nuclear spin ensemble. The results of this thesis could enable a tailoring of the properties of the nuclear spin system with the aim to prolong the coherence time of the QD electron spin. In self-assembled QDs, this time is limited by the slow fluctuations of the nuclear magnetic field which happen on the same timescale as the decay of DNSP which was determined in this work.

Zusammenfassung

Diese Arbeit behandelt eine rein optische Studie der physikalischen Eigenschaften des mesoskopischen Kernspinsystems in einem einzelnen Quantenpunkt (QP). QPe sind künstliche Objekte, welche es erlauben, Ladungsträger in drei Raumdimensionen zu lokalisieren. Die entsprecheneden Längenskalen sind dabei so klein, dass eine quantenmechanische Behandlung des resultierenden Fallenpotentials notwendig wird. Die hier untersuchten QPe sind selbstorganisierte InAs Nanokristalle, welche ca. 10^5 Kerne mit nichtverschwindendem Spin enthalten. Aufgrund der Hyperfeinwechselwirkung, welche Elektron- und Kernspins koppelt, können Kernspins mit Hilfe des lokalisierten QP-Elektrons manipuliert und gemessen werden. Die optischen Auswahlregeln im Halbleitermaterial des QPes erlauben es, den Spin des Elektrons mit optischen Mitteln zu orientieren. Diese Spinorientierung wird anschliessend mittels der Hyperfeinwechselwirkung auf die Kernspins übertragen, was zu einer dynamischen Kernspinpolarisation (DKSP) führt. Gleichzeitig beinhaltet die Hyperfeinwechselwirkung Terme, welche zu einer Verschiebung der Energie des Elektrons führen, wenn es im Kontakt mit spinpolarisierten Kernen steht. Diese Tatsache wird ausgenützt um den Grad der DKSP mittels entsprechender optischer Signaturen im vom QP ausgesandten Licht zu ermitteln.

Im ersten Teil dieser Dissertation wird eine Beschreibung des Gleichgewichtszustands der optisch generierten DKSP gegeben. Es wird gezeigt, dass der Übertrag von Spininformation vom Elektron auf die Kerne stark vom Grad der DKSP abhängt. Die entsprechende Rückkopplung der Kernspins auf das Elektron nimmt die Form eines effektiven Magnetfeldes von der Grössenordnung einiger Tesla an und führt zu starken Nichtlinearitäten im gekoppelten Spinsystem des Elektrons und der Kerne. Insbesondere wird der experimentelle Beweis erbracht, dass DKSP in einem externen Magnetfeld ein hysteretisches Verhalten zeigen kann, welches mittels einer klassischen Ratengleichung beschrieben werden kann.

Der Schwerpunkt des zweiten Teils dieser Arbeit liegt in der Dynamik der DKSP, welche mit Hilfe einer zeitaufgeösten Photolumineszenztechnik studiert wird. Nebst der Messung der relevanten Zeitskalen für den Aufbau und den Zerfall der DKSP wird ein überraschender Aspekt der Kernspindynamik aufgedeckt: während ein optisch gepumptes Elektron genutzt werden kann um eine DKSP zu erzeugen, führt dasselbe Elektron zu einer sehr effizienten Depolarisation der Kerne, wenn die optische Anregung fehlt. In diesem Fall dominieren zufällige Fluktuationen des Elektronspins seine Evolution und führen zu einer Relaxation der Kernspins. Dieser Elektron-mediierte Zerfall der DKSP und die Rolle der Elektron-Spinkorrelationszeit sowie externer Magnetfelder werden im Detail diskutiert. Wenn die Flukturationen des Elektronspins zu schnell werden, kann sich der Kernspinzerfall wieder verlangsamen, was experimentell nachgewiesen wird. Ausserdem wird gezeigt, dass die oben

genannnten Nichtlinearitäten in starken externen Magnetfeldern zu einem nichtexponentiellen Zerfall der DKSP führen.

Die hier präsentierten Resultate werfen ein neues Licht auf die physikalischen Eigenschaften des mesoskopischen Kernspinsystems eines einzelnen QPes und eröffnen neue Möglichkeiten zur Manipulation dieses Systems. Diese Resultate dieser Doktorarbeit könnten eine gezielte Manipulation des Kernspinsystems zur Verlängerung der Kohřenzzeit des QP Elektrons erlauben. Diese Kohřenzzeit ist durch die langsamen Fluktuationen des Kernspinmagnetfeldes limitiert, welche dieselben typischen Zeitskalen wie der hier gemessene Kernspinzerfall aufweist.

Contents

Titel a

Summary c

Zusammenfassung e

Contents g

List of symbols and abbreviations i

1 Introduction 1

2 Self-Assembled Quantum dots 5
- 2.1 Basic electronic properties of bulk III-V semiconductors 5
- 2.2 Growth of self-assembled quantum dots 7
- 2.3 Charge carrier confinement in quantum dots 8
- 2.4 Experimental methods 10

3 Electron and Nuclear Spin Systems in a Single Quantum Dot and Implications for Electron Spin Coherence 13
- 3.1 Electron spin system 14
- 3.2 Nuclear spin system 14
  - 3.2.1 The concept of a nuclear spin temperature 16
- 3.3 Hyperfine interaction 17
- 3.4 Hyperfine-induced electron spin decoherence 19

4 Optical Pumping of Nuclear Spins in Low Fields 23
- 4.1 Nuclear spin cooling in the Knight field of the QD electron 23
- 4.2 Direct measurement of the Knight field of the QD Electron 25

5 Bistability of the Electron Nuclear Spin System 29
- 5.1 Modelling of the data 31
- 5.2 Hysteresis in the magnetic field sweeps 34
- 5.3 Discussion 37

6 Nuclear Spin Polarization in Transverse Magnetic Fields 39
- 6.1 Theory of the Hanle effect 40
  - 6.1.1 Modifications due to the nuclear field 40
  - 6.1.2 The influence of nuclear quadrupolar interactions 41

6.2 Experimental signatures of the nuclear field in Hanle effect measurements . . . 43
6.2.1 Negatively charged exciton . . . 43
6.2.2 Positively charged exciton . . . 45
6.2.3 Conclusion . . . 47

7 Time-resolved Measurement of Nuclear Spin Polarization 49
7.1 Dynamics of nuclear spin polarization in low magnetic fields . . . 49
7.1.1 Technique for time-resolved measurement of nuclear spin polarization . . . 49
7.1.2 Buildup and decay of nuclear spin polarization . . . 50
7.1.3 Electron mediated nuclear spin decay . . . 50
7.1.4 Control experiments . . . 51
7.1.5 Mechanisms for the electron-mediated nuclear spin decay . . . 53
7.1.6 Low field nuclear spin dynamics . . . 54
7.1.7 Spin temperature considerations for the pump-probe measurements . . . 56
7.2 Nonlinear nuclear spin dynamics in high magnetic fields . . . 57
7.2.1 Buildup and decay of nuclear spin polarization . . . 58
7.2.2 Motional narrowing of nuclear spins . . . 59
7.2.3 Nonlinear decay of nuclear spin polarization . . . 61
7.2.4 Open questions and conclusions . . . 62

8 Conclusion & Outlook 63

A Appendix A
A.1 Experimental setup . . . A
A.2 Measurement of the gate voltage switching time and sample RC time constant . . . E

B Bibliography I

List of publications VII

Acknowledgement IX

Curriculum Vitae XI

List of Figures XIII

List of symbols and abbreviations

f_{el}	Fraction of time that a QD is occupied by a single electron
$g_{\mathrm{el,h,ex}}$	g-factor (for electron, hole and exciton, respectively)
j	Total angular momentum (spin and orbital)
$\mathbf{k}$	Wave vector (of excitation light)
l	Orbital angular momentum
$m^*_{\mathrm{el,h}}$	Effective (for electron and hole, respectively)
A_i	Hyperfine constant of nucleus i
B_{el}	Knight field
B_{ext}	External magnetic field
B_{loc}	Local dipolar nuclear field
B_{nuc}	Overhauser field
D	Diffusion constant
E_{em}	Emission energy
$\hat{\mathbf{I}}^i, I^i$	Nuclear spin operator and quantum number
N	Number of quantum dot nuclei
$\hat{\mathbf{S}}, S$	Electron spin operator and projection om $z-$axis
T_1	Spin relaxation time
T_2,(T_2^*)	Spin dephasing time (ensemble averaged)
T_{d}	Nuclear spin diffusion time
$T_{1\mathrm{e}}$	Nuclear spin relaxation time due to electrons
V_{g}	Gate voltage
Q	Nuclear quadrupolar moment
γ_i	Gyromagnetic ratio of nucleus i
ν_0	Unit cell volume
$\rho_c^+(\rho_c^-)$	Circular polarization of PL light (under σ^+- (σ^--) polarized excitation
$\sigma^+(\sigma^-)$	Circular light polarization of positive (negative) helicity
σ^x	Linear light polarization along x
τ_{el}	Electron spin correlation time
Ψ	Electron wave function
Ω_{el}	Electron Larmor frequency
ΔE_{OS}	Overhauser shift
$\Delta E^{\mathrm{Z}}_{\mathrm{el,e,ex}}$	Zeeman splitting (for electron, hole and exciton, respectively)

$1\text{eV} = 1.6 \cdot 10^{-19}$ J	1 electronvolt
$e = 1.6 \cdot 10^{-19}$ A·s	Electron charge
$g_0 = 2$	Free electron g-factor
$\hbar = 6.582 \cdot 10^{-10}$ μeVs	Reduced PLANCK's constant
$\mu_\mathrm{B} = 58$ μeV/T	BOHR magneton
$k = 86$ μeV/K	BOLTZMANN constant
$\mu_0 = 4\pi \cdot 10^{-7}\text{N/A}^2$	Permeability of free space

As	Arsenic
AEI	Anisotropic exchange interaction
CB	Conduction band
CCD	Charge coupled device (camera)
DNSP	Dynamical nuclear spin polarization
EIT	Electromagnetically induced transparency
e^-	Electron
Ga	Gallium
HH	Heavy hole
In	Indium
LH	Light hole
LO	Longitudinal optical (phonon)
ML	Monolayer
NMR	Nuclear magnetic resonance
OS	Overhauser shift
PL	Photoluminescence
QD	Quantum dot
QI	Quadrupolar interaction
SIL	Solid immersion lens
SNR	Signal to noise ratio
SO	Split off band
Ti	Titanium
VB	Valence band
WL	Wetting layer
X^n	Exciton of charge n

1 Introduction

This thesis treats an optical investigation of nuclear spin effects in individual, self-assembled semiconductor quantum dots (QDs). We study the behavior of the coupled electron-nuclear spin system with experiments which consist of two basic steps. First, optical excitation of a QD with circularly polarized light is used to dynamically polarize the nuclear spins in the QD. Second, the nuclear spin polarization is detected by measuring the energy-shift of a QD emission line due to the effective magnetic field of the spin polarized nuclei.

When an electron spin system is driven out of thermal equilibrium through an external agent, electron spin relaxation drives the electrons back to a thermal state. Since this relaxation is partly happening via the nuclear spin reservoir, angular momentum is transferred to the nuclei and a net nuclear polarization can be established [1]. An efficient way of achieving this situation is optical excitation of spin polarized electrons in bulk semiconductors. Optically induced dynamical nuclear spin polarization (DNSP) was first demonstrated in silicon [2] and was later on studied extensively for nuclei close to paramagnetic impurities in GaAs [3].

Individual, optically active, self-assembled QDs present an excellent system for studying optically induced DNSP in more depth, thereby revealing subtleties of the electron-nuclear spin system that were experimentally not accessible before. Several aspects distinguish the QD system from its bulk counterpart mentioned above: The narrow QD emission lines enable a direct measurement of electron nuclear interaction energy. This is not possible in bulk systems where typical widths of emission lines are an order of magnitude larger than the electronic energy shifts induced by polarized nuclei. In addition, the possibility of addressing a single QD has the advantage of removing effects of sample inhomogeneities and crosstalk between individual islands of spin polarized nuclei. Due to the different atomic composition and strain distribution of the QD as compared to its surrounding host material, the ensemble of $\sim 10^4 - 10^5$ QD nuclear spins can be considered as truly isolated from the environment. Therefore, the coupled electron-nuclear spin system of a QD is an implementation of a well isolated system of a single electron spin, coupled to a slowly varying, small nuclear spin reservoir, i.e., the central spin problem [4].

More recent interest in the dynamics of QD nuclear spins has arisen from the experimental and theoretical findings that the slow fluctuations of the nuclear spins constitute the dominant source of decoherence of QD electron spins. Since these fluctuations have long coherence times, the resulting electron-spin decoherence is non-Markovian and hence the evolution of the electron spin is highly complex [5, 6, 7]. It has been argued that by controlling the nuclear spin fluctuations, for instance by producing a substantial nuclear spin polarization or by performing a series of projective measurements on the nuclear spins [8], one could potentially suppress this decoherence mechanism [9].

Optical orientation of QD nuclear spins has been demonstrated experimentally by a few groups [10, 11, 12, 13, 14, 15, 16, 17]. However, the degree of DNSP achieved in these experiments has been limited to $\sim 10 - 20\%$ in low external magnetic fields and did not exceed 60% in high fields. In order to reach even higher degrees of DNSP, a detailed analysis of both the formation dynamics and the limiting factors of DNSP is required. Since DNSP is a balance between nuclear spin polarization by the QD electron and nuclear spin depolarization by the "lattice", a measurement of the corresponding timescales as well as an identification of the factors that influence the nuclear spin dynamics is of great interest and relevance. Inherent properties of the QD nuclear spin system, like the respective role of nuclear spin diffusion, quadrupolar interactions and trapped excess QD charges on the degree of DNSP can be investigated using time-resolved measurements of the nuclear spins. Furthermore, experimental determination of the nuclear spin decay time directly yields the correlation time of the fluctuations of the Overhauser field along the axis in which the nuclei are polarized - a crucial quantity for understanding the limits of electron spin coherence in QDs [18].

Scope of this thesis

In this work, we give an overview of our experimental assessment of the above mentioned points. In Chap. 2 we start by giving an introduction to the physics of self-assembled QDs in general with a particular focus on the methods used to deterministically define the exact charging state of a single QD. Furthermore, we introduce the basic technique of photoluminescence, our method of choice for the investigation of individual QDs. For the study of QD nuclear spins, the knowledge of the relevant interactions for both the nuclear spin system and the electron spin system is essential. We will discuss the Hamiltonians describing these two spin system as well as the coupling between the electron and the nuclear spins in Chap. 3. In the same chapter, we discuss the influence of the electron-nuclear spin coupling on the coherence property of the electron spin.

We then turn to our experimental results and present our experimental findings on the physics of the QD nuclear spin system. We start by presenting the experimental signatures of nuclear spin polarization at zero magnetic field in Chap. 4 and explain the existence of this polarization with the stabilizing effect that the electron exerts on the nuclear spins via an effective magnetic field - the Knight field. By applying an external magnetic field which compensates the Knight field, we were able to perform the first measurement of the Knight field of a single electron confined to a QD. We proceed by discussing the behavior of nuclear spin polarization in external magnetic fields, applied both parallel (Chap. 5) and perpendicular (Chap. 6) to the axis of optical orientation. In the first case, the nonlinear nature of the coupled electron-nuclear spin system becomes apparent as soon as the external magnetic field is on the order of the nuclear magnetic field. There, DNSP may have a hysteretic response to the applied field. The second case, the second situation reveals information about the atomic structure of the QDs by enabling an indirect observation of nuclear quadrupolar interactions.

The static measurements of nuclear spin polarization are completed by measuring the relevant timescales of buildup and decay of a nuclear spin polarization. This is done by implementing a pump-probe experiment for the nuclear spins, which we discuss in Chap. 7. These measurements allowed us to identify the dominant nuclear spin relaxation mechanisms in self-assembled QDs. We find that the nuclear spin lifetime depends drastically on the number of electrons that occupy the QD. If this number is even, the nuclear spin lifetime is on the order of minutes, if its odd, the nuclear spins decay within a few milliseconds. We discuss the reason for this electron-mediated nuclear spin decay as well as a study of the nuclear spin lifetime in various magnetic fields in the end of this thesis.

Appendix A.1 gives some details of our experimental setup and a list of the most important optical elements used there. In Appendix A.2, a detailed description of the fast switching of the QD gate is given. This switching was needed to perform the time dependent measurements of DNSP presented in Sect. 7.1.3 and allows for a convenient determination of the RC time constant in a gated QD structure based on a simple, single QD photoluminescence experiment.

Part of the results presented in Chap. 4,Chap. 5 and Chap. 7 have been published in References [15], [19] and [20], respectively. These references have separately been listed at the end of this thesis.

2 Self-Assembled Quantum dots

The present chapter discusses the basic physics of self-assembled quantum dots and the experimental methods used to investigate them. Starting from the band structure of bulk III-V semiconductors, the theory of charge carrier confinement in quantum dots is developed. Furthermore, the gated structures used for controlling the exact number of excess quantum dot charges are described.

The QDs studied in this work are self-assembled islands of a semiconductor material embedded in the solid state matrix of another semiconductor of higher bandgap. This chapter gives a basic overview of the physics of these optically active systems and the experimental methods used to fabricate and investigate them. The band structure of direct bandgap semiconductors describes the behavior of charge carriers in these solid state environments. Electrons and holes can essentially be described as free particles having a reduced effective mass which accounts for the periodicity of the crystalline potential. Small semiconductor crystals with dimensions on the order of 10 nm can be grown by taking advantage of the natural “clustering” or “self-assembly” of materials grown under the right conditions. These nanocrystals can be used to trap electrons and holes which can then be investigated by optical means. By incorporating the QDs in a field effect structure, their charging state can be set deterministically and monitored using a photoluminescence technique.

2.1 Basic electronic properties of bulk III-V semiconductors

In order to understand the electronic and optical properties of the QDs studied in this work, the knowledge of the basic properties of the band-structure of the involved materials in the center of the Brillouin zone (i.e. at the Γ-point) is essential. We therefore give a short introduction to the band diagram of these materials, which has a similar structure in nearly all III-V semiconductor compounds.

The electronic band structure of crystals arises from hybridization of the valence electrons of the constituent atoms. Since for all group III and V elements, these electrons come from s or p like orbitals, the resulting electron bands will obey the same symmetries, which determine the total angular momentum j of the charge carriers occupying the specific bands. For the semiconductor materials relevant in this work, the valence band (VB) arises from hybridization of p-shell electrons, while the conduction band (CB) originates from electronic states having s-type symmetry. The resulting structure of VB and CB, valid for nearly all III-V semiconductors is sketched in Fig. 2.1 [21].

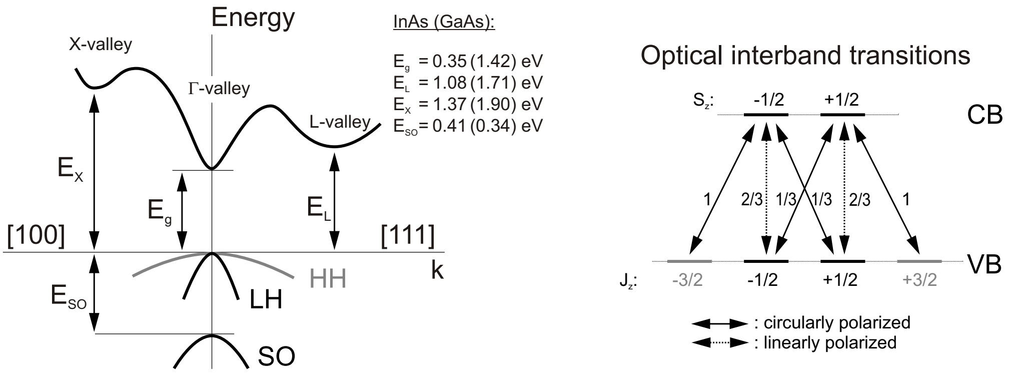

Figure 2.1: Schematic illustration of the band structure of most III-V semiconductors (left panel). Around the Γ-point ($\mathbf{k} = 0$), conduction band (CB) and valence band (VB) are well approximated by a free particle dispersion with effective masses m^*_e and m^*_h, respectively. The VB is divided into heavy hole (HH), light hole (LH) and a split-off (SO) bands. Right panel: Dipole-allowed interband transitions at photon energies close to E_g. Light fields of linear and circular polarization couple HHs (gray) and LHs (black) to VB electrons. The numbers near the arrows which represent the respective transitions indicate their relative oscillator strengths. Driving the interband transition with circularly polarized light, a maximum of 50 % spin polarization of CB electrons can be achieved

Having zero orbital angular momentum, the CB has a two-fold spin degeneracy and a parabolic dispersion, corresponding to the dispersion of a free particle with an effective mass m^*_e. Using basic $\mathbf{k} \cdot \mathbf{p}$ perturbation theory, the effective mass can be found to be roughly inversely proportional to the bandgap E_g [22]. Typical numbers for the effective CB electron mass are $m^*_\mathrm{e,GaAs} \approx 0.06 m_\mathrm{e}$ and $m^*_\mathrm{e,InAs} \approx 0.023 m_\mathrm{e}$ for GaAs and InAs, respectively, where m_e is the free electron mass [21].

The situation is slightly more complex for the VB, which carries an orbital momentum of $l = 1$ that couples to the electron spin though spin orbit interaction. As a result, the sub-band having total angular momentum $j = \frac{1}{2}$ is split off by several hundred meV and can be neglected for most practical purposes in this work. The remaining $j = \frac{3}{2}$ states are degenerate at the Γ-point but show a dispersion which depends on $|j_z|$, the absolute value of the z-component of the total electron angular momentum along the k-vector. The mobile charge carriers in the two resulting subbands are referred to as heavy and light holes (HH and LH, with $|j_z| = \frac{3}{2}$ and $|j_z| = \frac{1}{2}$, respectively) with effective masses $m^*_\mathrm{HH,InAs} \approx 0.41 m_e$ and $m^*_\mathrm{LH,InAs} \approx 0.026 m_e$ in InAs [21].

The fact that the spin-orbit interaction splits off the $j = \frac{1}{2}$ band in bulk III-V semiconductors is at the heart of optical spin orientation in these materials [23]. Fig. 2.1(right panel) shows the dipolar-allowed optical transitions between valence and conduction band at the Γ-point together with the relative weights of the corresponding Clebsch-Gordan coefficients. Driving these transitions with resonant, circularly polarized light, a net spin polarization of 50 % arises in the CB. If the $j = \frac{1}{2}$ band were not split-off, the same photons would also excite electrons from this band and the photogenerated CB electrons would have no net spin polarization.

The degeneracy of the $j = \frac{3}{2}$ valence band at the Γ-point can be further lifted by

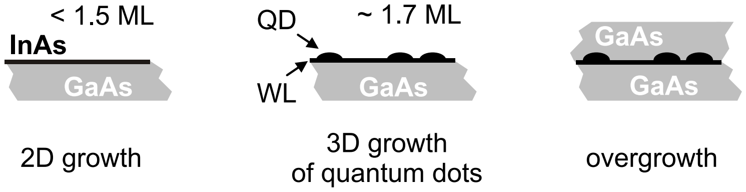

Figure 2.2: Schematic illustration of the QD growth process: InAs is deposited on an atomically flat (100) semi-insulating GaAs substrate. At a critical InAs thickness of ∼ 1.7 ML, instabilities due to the lattice mismatch of InAs and GaAs lead to the spontaneous formation of InAs droplets above the wetting layer. Capping of the QDs with GaAs completes the growth procedure

confining the VB electrons in space as we will show in the following paragraph. As a result, spin polarizations close to 100% can be achieved through optical pumping in these structures.

2.2 Growth of self-assembled quantum dots

The InAs QDs investigated in this work were grown using molecular beam epitaxy. The self-assembled growth is based on strain driven formation of low-bandgap InAs droplets on top of a mono-crystalline GaAs substrate with a high bandgap [24]. When depositing InAs on a GaAs substrate, the growth characteristics of InAs changes abruptly at a certain critical InAs layer thickness. The growth changes from a two-dimensional, planar ML deposition to the formation of three-dimensional islands in the Stranski-Krastanow growth mode, as illustrated by Fig. 2.2 [25]. The reason for this transition from two- to three-dimensional growth is the ∼ 7% lattice mismatch between InAs and GaAs. This mismatch causes mechanical strain when depositing InAs on top of GaAs. At a critical thickness of ∼ 1.7 ML, the gain in minimizing strain energy is bigger than the cost of an increased surface energy, resulting in the spontaneous formation of InAs QDs with a typical thickness of $3-5$ nm and a diameter of ∼ 20 nm. After the QD formation, a thin layer of InAs underlying the QDs still covers the GaAs substrate, this layer is referred to as the wetting layer (WL).

The formation of QDs on top of the wetting layer is followed by an overgrowth with GaAs which results in regions of low bandgap InAs, surrounded by a high-bandgap GaAs matrix. This difference in bandgap leads to the confinement of CB electrons and VB holes in the InAs-rich regions. The emission energy of recombining excitons in as-grown QDs lies at approximately 1.1 eV - a wavelength rather inconvenient for conventional, Si-based photodetectors used in most optical spectrometers. The QDs are therefore treated with an additional annealing step during the overgrowth procedure: when the QDs are partially covered by the GaAs overgrowth layer, the sample temperature is temporarily increased to allow for material exchange between the QD and its surrounding. This annealing process increases the intermixing of Ga to the InAs QDs and reduces the height of the QDs. As a result, the QD emission energy is shifted to ∼ 1.3 eV. QDs treated in this way are referred to as “partially covered islands” due to their particular shape.

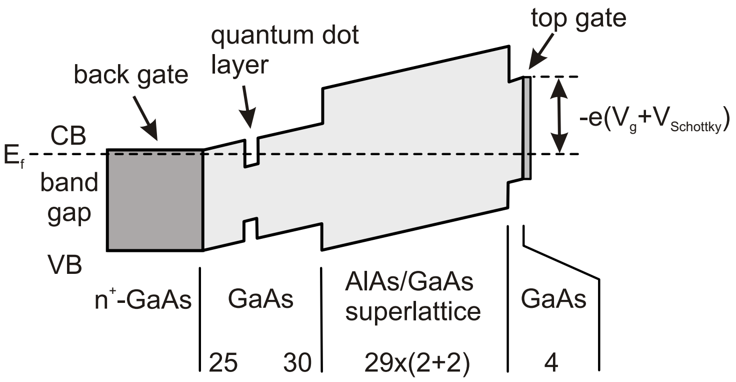

Figure 2.3: Energies of the edges of conduction and valence band (CB and VB, respectively) in the field effect structure used in this work; dimensions are given in nm. The electric field at the QD position determines the QD charging state and is controlled by a gate voltage V_g which is applied across the structure. The Schottky voltage V_{Schottky} is a constant which depends on the details of the top-gate contact an which is on the order of 1 V

The GaAs overgrowth layer has a total thickness of 30 nm. It is followed by 29 periods of a AlAs/GaAs (2/2 nm) superlattice barrier layer, acting as a blocking barrier for conduction band electrons, and capped by 4-nm GaAs. A semitransparent Ti film forms a Schottky-contact on top of the sample which is used to adjust the energy of the QD ground state with respect to the Fermi-energy. 25 nm below the QD layer, a highly doped n^{++}-GaAs layer forms the back (Ohmic) contact of the sample, pinning the Fermi-energy in the device. Fig. 2.3 shows a sketch of the energies of CB and VB in the field effect structure containing QDs. It is seen that by applying a bias voltage between top and back contact, the QD ground state energy can be shifted below the Fermi-energy of the electron reservoir, leading to charging of the QD. Coulomb-blockade thereby ensures that only individual charges are injected into the QD, which allows for a deterministic preparation of the QD charge state [26].

2.3 Charge carrier confinement in quantum dots

The low bandgap of InAs compared to the surrounding GaAs leads to a confinement of electrons and holes to the two-dimensional system consisting of the WL and the QDs. This confinement along the sample growth direction z leads to a shift of the CB and VB states, which can be estimated by the particle spectrum in a one dimensional, infinitely deep trapping potential of width L_z: $E_n = \frac{\hbar^2}{2m^*}(\frac{\pi n}{L_z})^2$. The corresponding level spacing is on the order of 20 meV for $L_z = 5$ nm, so that typically only the ground state $n = 0$ of the confining potential in the growth direction is populated.

Since the extent of the WL in the z-direction is considerably smaller than the QD thickness, the confinement energy along the z-direction is increased in the WL compared to the QDs. This leads to an additional lateral trapping of charge carriers to the QDs, and to charge carrier confinement in all three dimensions. The resulting QD confinement potential in the plane of the WL is sketched in Fig. 2.4. The

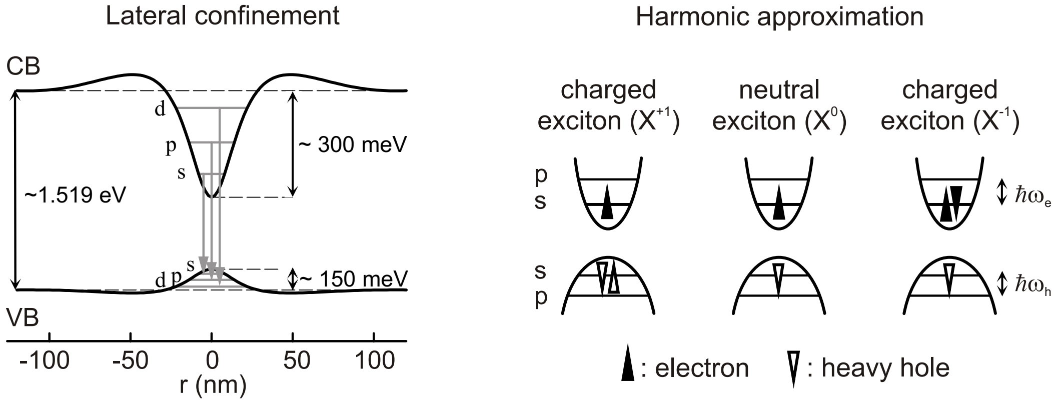

Figure 2.4: Sketch of the QD confinement potential and of its harmonic approximation (left panel). The QD is surrounded by bulk GaAs, having a bandgap of ~ 1.519 eV. The approximate depths of the electron and hole confining potentials are given in the figure. The discrete quantum confined levels are labelled in analogy with atomic orbitals. The level spacings for electrons and holes are on the order of $\hbar\omega_e = 50$ meV and $\hbar\omega_h = 10$ meV, respectively. The carrier confinement in the lowest QD shells is well approximated by a 2D harmonic potential (right panel). Three examples for QD excitons (neutral and singly, negatively and positively charged) are given in the figure

confinement potential is deeper for electrons than for holes due to the details of the band-alignment between InAs and GaAs. Furthermore, the quantum mechanical level spacing $\hbar\omega_{e,h}$ arising from carrier confinement is considerably smaller for holes than for electrons due to the larger effective mass of VB holes compared to CB electrons. For the lowest lying electron and hole states (denotes as s,p,... in analogy to atomic orbitals) localized in the QD, a parabolic confinement potential is a good approximation.

Due to the different masses of heavy and light holes, a confinement of these charge carriers results in a splitting of the HH and the LH states. This splitting is on the order of 20 meV in QDs of height $L_z = 5$ nm and one order of magnitude larger in the thin WL. Heavy-light hole splitting therefore eliminates the restrictions of optical spin orientation present in bulk semiconductors mentioned in Sect. 2.1 and in principle allows for the creation of photogenerated VB electrons with 100 % spin polarization. We note however, that quantum confinement leads to population of states with $\mathbf{k} \neq 0$, which induces an admixture of heavy and light hole states. This mixing makes nominally forbidden optical transitions partially allowed, reducing the spin polarization of optically generated electrons again.

Optical excitation leads to the formation of localized excitons in a QD which can be detected through the light emitted upon recombination of the excitons. Since the QD ground state in the VB has HH character, the trapped QD holes have angular momentum projections on the k-vector of $j_z = \pm\frac{3}{2}$, while for QD electrons $S_z = \pm\frac{1}{2}$. The circular polarization of the emitted recombination light thus carries direct information about the spin of the recombining charges. Furthermore, the incorporation of the QDs into the field effect structure described in Sect. 2.2 allows for deterministic charging of the QDs and therefore to the formation of charged excitons. Fig. 2.4 (right panel) shows two examples of the most relevant QD charge complexes in this work: The neutral exciton (X^0) and the singly negatively charged exciton (X^{-1}). The harmonic approximation of the QD trapping potential allows for a convenient calculation of the Coulomb interactions between the different confined QD charges [27]. In this way, the many-body spectrum of the QD can be obtained, which allows for the identification of the different QD emission lines in a PL experiment with respect to their excitonic origin.

2.4 Experimental methods

The QD sample described in Sect. 2.2 was chosen to show a low QD density of less than 0.1 μm^{-2}, that allowed for the addressing of a single QD using a micro-photoluminescence (micro-PL) setup. Our standard micro-PL setup is described in detail in Appendix A.1. The setup was based on the combination of a ZrO_2 solid immersion lens (SIL) in Weierstrass configuration, directly fixed onto the sample, and PL collection optics of numerical aperture 0.25. Depending on the discussed experiment, the sample was placed either in a helium-bath cryostat equipped with a superconducting magnet, reaching a maximum magnetic field strength of 10 T, or in a helium flow cryostat. There, variable low magnetic fields of $B_{\text{ext}} < 20$ mT or, alternatively, fixed magnetic fields of $B_{\text{ext}} \approx 200$ mT were applied using external Helmholtz coils or a permanent magnet, respectively. In the case of the flow cryostat, PL was collected using a microscope objective mounted outside of the cryostat, while for the bath cryostat, we used a lens directly fixed onto the sample mount inside the helium-bath.

The spectroscopy system consisted of a spectrometer of 0.75 m focal length and a liquid-nitrogen cooled charge coupled device (CCD) camera. The spectral resolution of this system was limited to ~ 30 μeV by the finite CCD pixel separation. However, the precision to which the emission energy of a given spectral line can be determined, could be increased to ~ 2 μeV by calculating a weighted average of the emission line over the relevant CCD pixels [19]. Alternatively, by using a scanning Fabry-Perot interferometer of 62 μeV free spectral range and a finesse $\gtrsim$70 as a narrow-band frequency filter in front of the spectrometer, a spectral resolution on the order of 1 μeV was achieved [15].

The PL polarization and spin splitting were studied by resonantly exciting a single QD in one of its excited (p-shell) states at $T \approx 5$ K ($T = 1.7$ K in case of the bath cryostat). The PL spectral lines associated with different charging states of a single QD can be identified from the PL intensity contour plot as a function of the bias voltage and emission energy (Fig. 2.5(a)) [26, 28]. The emission line coming from neutral exciton (X^0) recombination exhibits a fine-structure splitting of ~ 20 μeV due to the anisotropic electron-hole exchange interaction (AEI) [29]. The emission from the negatively (positively) charged trion X^{-1} (X^{+1}) arises from optical excitation of QD charged with a single electron (hole). The photons emitted upon X^{-1} (X^{+1}) recombination are red (blue) shifted by ~ 4.6 meV (~ 1.9 meV) with respect to the X^0 line.

Unless stated otherwise, the discussed experiments were performed on the negatively charged exciton X^{-1} at the center of its PL stability region with respect to

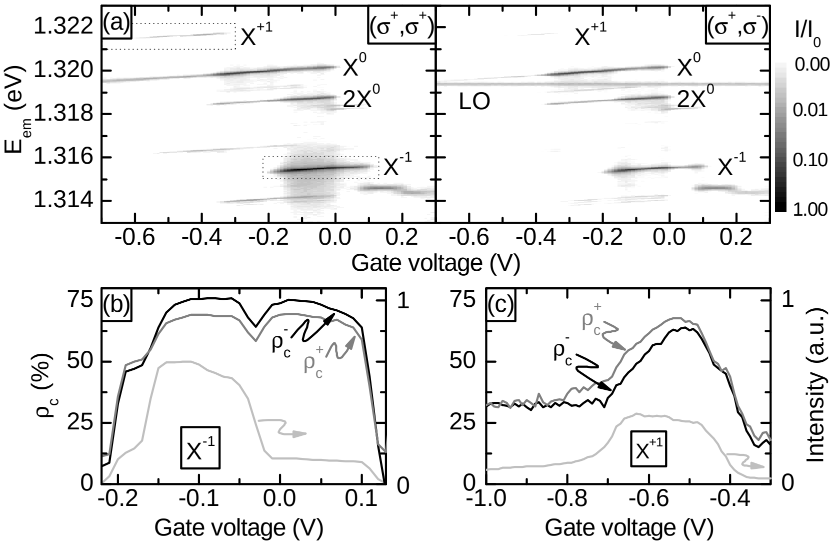

Figure 2.5: Photoluminescence from a single charge-tunable QD. (a) Contour plot of the PL intensity as a function of applied bias voltage under σ^+-polarized excitation and co- (cross-) circularly polarized detection ((σ^+,$\sigma^{+(-)}$), respectively). The intensity is normalized with respect to the X^{-1} peak-intensity of $I_0 = 3 \cdot 10^4$ counts/sec. The excitation laser energy is tuned to a p-shell resonance of the singly charged QD at 1.356 eV, ~36.6 meV above the bulk GaAs LO phonon line indicated in (a). Panels (b) and (c) show the integrated intensities of X^{-1} and X^{+1} emission in the (σ^+,σ^+) configuration (light gray), as well as the degree of circular PL polarization $\rho_c^{\pm}$ under $\sigma^{\pm}$-excitation. For (c), the laser is tuned into a p-shell resonance for X^{+1}

gate voltage. In this regime, electron co-tunnelling to the nearby reservoir is minimized [30] and the QD is occupied by a single electron in its ground state. Optical excitation is performed in a resonant way into the p-shell, which lies approximately one LO phonon energy above the emission energy of X^{-1} ($E_0 = 1.3155$ eV)[1]. The carriers created in the p-shell then relax to the QD ground state on a timescale of ~ 30 ps due to a combination of phonon-mediated relaxation and co-tunnelling through the electron reservoir. For all our experiments, the excitation power is set close to saturation of the observed emission line. We found that these excitation conditions lead to a maximal preservation of PL light polarization ($|\rho_c^{\pm}| \approx 75\%$ at $B = 0$ T) after excitation with circularly polarized light.

The polarization of the excitation laser and of the PL are denoted as $(\sigma^\alpha, \sigma^\beta)$, where σ^α and σ^β are the excitation and detection polarization, respectively. The index α or β takes one of four values: linear polarization along the crystal axes $(x : [1\bar{1}0], y : [110])$ or circular polarization (±: light helicity of ±1). The degree of circular polarization is defined as $\rho_c^{\pm} \equiv (I^{\pm} - I^{\mp})/(I^{+} + I^{-})$, where I^{β} denote the intensity of PL in the $(\sigma^{\pm}, \sigma^{\beta})$ configuration. The polarization characteristics of the system is calibrated using the strongly polarized emission of the LO phonon of the GaAs substrate (Fig. 2.5(a)) [22]. The combined fidelity of polarization preparation and detection was thereby found to be better than 98%.

---

[1] Another possible scenario for QD excitation would be the creation of a ground state (s-shell) exciton with simultaneous emission of an LO phonon. We exclude this mechanism by various experimental observations: we observe several distinct QD excitation resonances at different energies. The GaAs LO phonon line for these resonances can thereby lie above or below the corresponding excitonic emission energy. The observed resonances have widths on the order of 100 μeV, in accordance with recent experimental observations of p-shell excitation resonances [31]. Only a few of these resonances lead to the high degree of PL circular polarization and to the nuclear spin polarization effects that will be discussed later. These facts corroborate or model of resonant excitation into the p-shell.

Circularly polarized, resonant p-shell pumping of a single electron (hole) charged QD generates optically oriented trions with hole (electron) spin $j_z = +3/2$ ($S_z = -1/2$) or $j_z = -3/2$ ($S_z = +1/2$), under σ^{+}- and σ^{-}-pumping, respectively (See Chap. 2.1 and [13, 31]). The intra-dot excitation ensures maximal carrier spin preservation during relaxation, which is confirmed by the high degree of circular polarization of the PL emission lines (Fig. 2.5(b) and (c)). The initial state of X^{+1} is composed of two holes in a singlet-state and one electron. Therefore, σ^{+}- (σ^{-}-) polarized PL from X^{+1} indicates that the optically created electron was in the $S_z = -1/2$ ($S_z = 1/2$) state. Analogously, for X^{-1}, circular polarization of the emitted light reflects both the spin of the hole in the QD before photon emission and the initial spin of the residual QD electron after photon emission. A high degree of circular polarization of X^{-1}-emission thus indicates a highly spin polarized residual electron in the QD.

3 Electron and Nuclear Spin Systems in a Single Quantum Dot and Implications for Electron Spin Coherence

The theory of the spin systems of quantum dot electrons and nuclei is described in this chapter. While electron spins are well described by the Zeeman interaction and their coupling to an electron reservoir, nuclear spin-spin interactions need to be taken into account to understand the properties of the nuclear spin system. The electronic and the nuclear spins are coupled through the hyperfine interaction whose properties will be discussed together with its implications for the coherence properties of the electron spin.

Circularly polarized excitation and the analysis of the polarization of PL light are powerful experimental tools for manipulating and measuring the polarization of the electron spin in a single QD. The high degree of QD PL polarization described in Sect. 2.4 indicates that electron spin relaxation mechanisms in the investigated QDs are relatively weak. Since the electron spin system is in thermal contact with the nuclear spin system through the hyperfine interaction, spin polarization is transferred from one to the other, thereby cooling the nuclear spin system. At the same time, the coupling of the nuclear spins to their environment will heat up the nuclear spins, leading to a finite nuclear spin temperature in a dynamical equilibrium. In this section, we give an overview of the basic spin interactions and relaxation mechanisms of the QD electron and nuclear spins and discuss the coupling mechanism between the two spin systems. Finally, we discuss how this coupling affects the coherence properties of the electron spin.

The total Hamiltonian $\hat{H}$ for a single electron in contact with an ensemble of nuclear spins can be written as

$$\hat{H} = \hat{H}_{\mathrm{Z}}^{\mathrm{el}} + \hat{H}_{\mathrm{Z}}^{\mathrm{nuc}} + \hat{H}_{\mathrm{dip}} + \hat{H}_{\mathrm{HF}}. \tag{3.1}$$

$\hat{H}_{\mathrm{Z}}^{\mathrm{el}}$ and $\hat{H}_{\mathrm{Z}}^{\mathrm{nuc}}$ denote the electron and nuclear Zeeman Hamiltonian, respectively, while $\hat{H}_{\mathrm{dip}}$ describes the nuclear dipole-dipole interactions and $\hat{H}_{\mathrm{HF}}$ the hyperfine interaction, which couples the electron and nuclear spins. We will discuss the individual terms of this Hamiltonian in more detail in the following paragraphs.

3.1 Electron spin system

The electron spin system considered in this work consists of a residual QD electron in the case of X^{-1} and of the (metastable) photo-generated QD electron in the case of X^{+1}. Information about the electron spin is obtained by measuring the circular polarization of PL light.

When placed in a magnetic field, the spin of a QD electron experiences the Zeeman interaction, described by the Hamiltonian

$$\hat{H}_{\mathrm{Z}}^{\mathrm{el}} = g_{\mathrm{el}}^{*}\mu_{B}\hat{\mathbf{S}}_{\mathrm{el}} \cdot \mathbf{B}, \tag{3.2}$$

where μ_{B} is the Bohr magneton, g_{el}^{*} the effective electron g-factor and $\hat{\mathbf{S}}_{\mathrm{el}}$ the electron spin operator ($\hat{\mathbf{S}}_{\mathrm{el}} \equiv \frac{1}{2}\hat{\boldsymbol{\sigma}}$, with the Pauli-matrices $\hat{\boldsymbol{\sigma}}$).

For a consistent notation with respect to the sign of the g-factors, we also note the Zeeman Hamiltonian for holes, which we write as $\hat{H}_{\mathrm{Z}}^{\mathrm{h}} = -g_{\mathrm{h}}^{*}\mu_{B}\hat{\mathbf{S}}_{\mathrm{h}} \cdot \mathbf{B}$[32], with the effective hole g-factor g_{h}^{*} and the hole spin operator $\hat{\mathbf{S}}_{\mathrm{h}}$. In this representation, the heavy-hole wave functions with $j_z = \pm\frac{3}{2}$ convert to pseudo-spins with $\widetilde{j}_z = \pm\frac{1}{2}$. The experimentally found g-factors g_{el}^{*} and g_{h}^{*} are both negative in our system. We note that in this work, we only consider singly charged excitons. Exchange interactions therefore play no role for the energies of the recombining excitons [29] and will not be discussed here.

Due to the tight confinement of electrons in self-assembled QDs, the electron spin is well protected from spin-relaxation by electron-phonon coupling via spin-orbit interaction, which is otherwise very effective in a solid state environment. This typically extends electron T_1 times in QD systems up to 1 s in moderate magnetic fields [33]. However, the coupling of the QD electron to the nearby electron reservoir introduces an additional - albeit controllable - decay channel for the electron spin. The QD electron can make a virtual transition to the Fermi sea of the reservoir and be replaced by a spin-flipped electron from the same reservoir. The rate of these co-tunneling events depends critically on the tunnel barrier between the QD and the electron reservoir and therefore on the details of the QD heterostructure. For the structures used in this work, the resulting T_1 time of the electron has an upper bound of $\sim$ 3 ns at gate voltages in the center of the $1e^{-}$ stability region and decreases rapidly towards the edges of this region [30]. This tunability of the electron spin lifetime will be an essential feature in the measurements of the nuclear spin lifetime that will be discussed in Chap. 7.

3.2 Nuclear spin system

The QDs considered in this work consist of InAs with an admixture of Ga due to material diffusion during the growth process. The nuclear spins present in our QDs therefore consist of three nuclear species with their naturally occurring isotopes: ^{115}In (95.3%), ^{113}In (4.7%),^{75}As,^{69}Ga (60.1%), ^{71}Ga (39.9%) - their natural abundances are given in brackets. Indium has a total spin of 9/2 while all other nuclei have spin 3/2. In the following, we will only consider the most abundant nuclear species for simplicity and neglect the at least $\sim$ 10% admixture of Ga in our dots.

Each nucleus i is characterized by its spin I^i and the gyromagnetic ratio γ_i, describing the response to a static external magnetic field $\mathbf{B}$:

$$\hat{H}_{\mathrm{Z}}^{\mathrm{nuc},i} = -\gamma_i \hbar \hat{\mathbf{I}}^i \cdot \mathbf{B}, \tag{3.3}$$

where $\hat{\mathbf{I}}^i$ is the (dimensionless) spin-operator of the ith nucleus. The total nuclear Zeeman Hamiltonian is then a sum over all the nuclear spins: $\hat{H}_{\mathrm{Z}}^{\mathrm{nuc}} = \sum_i \hat{H}_{\mathrm{Z}}^{\mathrm{nuc},i}$. The gyromagnetic ratios for In and As are $\gamma_{^{115}\mathrm{In}} = 9.365$ MHz/T and $\gamma_{^{75}\mathrm{As}} = 7.315$ MHz/T.

Interactions of nuclear spins dominate the energy spectrum of the nuclei at low magnetic fields and lead to spin-transport in high fields. The simplest, and in semiconductors usually dominant nuclear spin-spin interaction is the dipolar coupling between two nuclear spins i and j. It can be written as [34]:

$$\hat{H}_{\mathrm{dip}}^{i,j} = \frac{\mu_0 \hbar^2 \gamma_i \gamma_j}{4\pi r_{ij}^3} \left(\hat{\mathbf{I}}^i \cdot \hat{\mathbf{I}}^j - 3 \frac{\left(\hat{\mathbf{I}}^i \cdot \mathbf{r}_{ij}\right)\left(\hat{\mathbf{I}}^j \cdot \mathbf{r}_{ij}\right)}{r_{ij}^2} \right), \tag{3.4}$$

where $\mathbf{r}_{ij}$ is the vector of length r_{ij} joining the two nuclei, and μ_0 is the permeability of free space. The dipolar Hamiltonian of the total nuclear spin system is then a sum over all nuclear spin pairs: $\hat{H}_{\mathrm{dip}} = \sum_{i<j} \hat{H}_{\mathrm{dip}}^{i,j}$.

A common decomposition of this Hamiltonian divides $\hat{H}_{\mathrm{dip}}$ into "secular" parts which commute with $\hat{H}_{\mathrm{Z}}^{\mathrm{nuc}}$ and "non-secular" parts which don't commute with $\hat{H}_{\mathrm{Z}}^{\mathrm{nuc}}$ [34]. For a given nuclear spin species, the secular part is composed of terms which are proportional to $\hat{I}_z^i \hat{I}_z^j - \frac{1}{4}(\hat{I}_+^i \hat{I}_-^j + \hat{I}_-^i \hat{I}_+^j)$, where $\hat{I}_+^i$ and $\hat{I}_-^i$ are the raising and lowering operators of the ith nuclear spin. The secular part is therefore spin-conserving and responsible for nuclear spin diffusion within the lattice. The non-secular part on the other hand contains terms which don't conserve the total angular momentum of the nuclear spin system and can lead to depolarization of nuclear spins in low magnetic fields. The strength of the interaction $\hat{H}_{\mathrm{dip}}$ is usually characterized by a "local field" B_{loc}, which is the effective magnetic field generated on the site of a nucleus by its neighboring nuclear spins [34]. For bulk GaAs, B_{loc} is on the order of 0.1 mT [3]. It can be shown that the non-secular terms of $\hat{H}_{\mathrm{dip}}$ only contribute to the evolution of the nuclear spin systems for magnetic fields $B_{\mathrm{ext}} \leq B_{\mathrm{loc}}$. Below these fields, the non-secular nuclear dipole-dipole interactions depolarize the nuclear spins very effectively within the decoherence-time $T_2 \approx 10 - 100$ μs. We note that this decoherence time does not refer to a decoherence process in the sense of a loss of information from the nuclear spins to a reservoir, resulting in a decay of the off diagonal elements of the nuclear spin density matrix. Rather it corresponds to an "collapse" of the off-diagonal elements of the nuclear spin density matrix and to the time of the establishment of a nuclear spin temperature, as will be discussed in Sect. 3.2.1.

Nuclear spin relaxation in III-V semiconductors has been experimentally investigated in detail using standard NMR techniques [35]. The resulting T_1 times in InAs and GaAs were on the order of 1000 s for Ga and As and roughly 200 s for In at a temperature of 4 K. These values however were shown to be limited by nuclear spin relaxation by paramagnetic impurities, a mechanism absent in individual QDs.

The remaining relevant nuclear spin relaxation mechanism is quadrupolar relaxation. This process results from nuclear transitions induced by the coupling of the nuclear quadrupole moment to phonon-generated electric field gradients at the nuclear site. The corresponding phonon-induced relaxation rate scales with the square of the temperature T and dominates over the temperature-independent relaxation by paramagnetic impurities for $T > 20$ K. We therefore estimate the nuclear T_1-time in our QDs to be further reduced by 2 orders of magnitude compared to the reported values [35]. Even though the nuclear T_1-time could be reduced again by the strong lattice deformations in self-assembled QDs (cf. Chap. 6), we assume the nuclear spin-lattice relaxation to be completely negligible for our experiments. The only remaining mechanism leading to a decay of nuclear spin polarization in a QD is spin-diffusion out of the QD into the surrounding bulk material. The spin-diffusion constant in GaAs has been measured experimentally to be $D = 10^{-13}$ cm^2 s^{-1} [36]. The typical timescale for diffusion out of a QD with a diameter $d \approx 20$ nm is therefore $d^2/D \approx 1$ min. However, the different nuclear species and local lattice structure within the QD compared to its surrounding bulk material should further reduce the diffusion constant and increase the diffusion time. Experimental work on nuclear spin diffusion between quantum wells has shown that this reduction amounts at least to a factor of 10 [37].

3.2.1 The concept of a nuclear spin temperature

A solid state nuclear spin system, in contrast to its counterparts in liquids or gases, can usually be described by a single constant of motion, its mean energy or, equivalently, its temperature. The validity of this spin temperature approximation is based on two assumptions [38]. First, due to nuclear spin-spin interactions, the off-diagonal elements of the nuclear density matrix all evolve at different frequencies spread over an energy interval $\Delta E \approx \hbar\gamma B_{\mathrm{loc}}$. As far as the expectation values of observables are concerned, these elements can therefore be taken to be equal to zero after a time $T_2 \approx \hbar/\Delta E$, after which the nuclear spin density matrix is effectively diagonal. This is the random phase approximation. By further assuming that all observables of the nuclear spin systems are unique, smooth functions of the energy, one can fully describe the properties of the nuclear spin system by knowing its mean energy. The nuclear spin density matrix is then diagonal and the values of the diagonal elements are given by a Boltzmann distribution with the nuclear spin temperature T.

Describing the nuclear spin system by a spin temperature is therefore valid for times $t > T_2$ after the preparation of a certain nuclear spin state. The relaxation of this nuclear spin temperature to the temperature of its environment (the “lattice”) is denoted as T_1. In the presence of an external magnetic field exceeding B_{loc}, nuclear spin temperature is equivalent to a polarization along the direction of the magnetic field. Bringing the system to zero field, the polarization is destroyed by nuclear spin-spin interactions on a timescale T_2, the nuclear spin temperature (or entropy) however is conserved for a much longer time T_1, even at zero field. This fact can experimentally be tested by re-introducing the nuclear spin system into a magnetic field and by measuring its nuclear spin polarization. In corresponding experiments on bulk Lithium [39], it was indeed found that the nuclear spin temperature is conserved over a long time, even though nuclear spin polarization is destroyed in zero field - a result that can only explained in the context of a nuclear spin temperature [38].

3.3 Hyperfine interaction

The dominant contribution to the coupling between the electron- and the nuclear-spin systems in III-V semiconductors originates from the Fermi contact hyperfine interaction. For an electron in a QD and in first order perturbation theory, this interaction can be written as [3, 5, 40]:

$$\hat{H}_{\mathrm{hf}} = \frac{\nu_0}{8} \sum_i A_i |\psi(\mathbf{R}_i)|^2 \hat{\mathbf{S}}_{\mathrm{el}} \cdot \hat{\mathbf{I}}^i, \tag{3.5}$$

where ν_0 is the volume of the InAs-crystal unit cell containing eight nuclei, $\psi(\mathbf{r})$ is the electron envelope wave function[1], and $\mathbf{R}_i$ is the location of the ith nucleus. $A_i = \frac{2}{3}\mu_0 g_0 \mu_{\mathrm{B}} \hbar \gamma_i |u(\mathbf{R}_i)|^2$ is the hyperfine coupling constant and g_0 the free electron g-factor. A_i depends on the value of the electron Bloch function $u(\mathbf{R}_i)$ at the nuclear site. For all the nuclei in our system it is positive and on the order of 50 μeV (i.e., $A_{\mathrm{In}} = 56$ μeV and $A_{\mathrm{As}} = 46$ μeV [41]). We note that only electrons in the conduction band couple to the nuclear spins through (3.5). For carriers in the valence band of *III-V* semiconductors, this interaction vanishes due to the p-type symmetry of $u(\mathbf{R}_i)$ [42].

With the identity $\hat{\mathbf{S}}_{\mathrm{el}} \cdot \hat{\mathbf{I}}^i = \hat{I}^i_z \hat{S}_z + \frac{1}{2}(\hat{I}^i_+ \hat{S}_- + \hat{I}^i_- \hat{S}_+)$, where $\hat{S}_+$ and $\hat{S}_-$ are the electron spin raising and lowering operators, respectively, (3.5) can be decomposed into two parts [23]: A dynamical part ($\propto I^i_+ S_- + I^i_- S_+$), allowing for the transfer of angular momentum between the two spin systems, and a static part ($\propto I^i_z S_z$), affecting the energies of the electron and the nuclear spins.

The dynamical contribution leads to a thermal equilibration of the electron and the nuclear spin systems. In an external magnetic field exceeding B_{loc} in strength, this leads to a polarization of the nuclear spins. Neglecting other spin relaxation mechanisms and polarization of the electronic or nuclear spins due to thermalization in the external magnetic field, the mean nuclear spin polarization $\langle I^i_z \rangle$ along the quantization axis z is linked to the electron spin polarization S_z through the Curie-law like relation [43]:

$$\langle I^i_z \rangle = I^i B_{I^i}(x), \quad \text{with} \quad x = I^i \ln\left(\frac{1+2S_z}{1-2S_z}\right). \tag{3.6}$$

B_{I^i} is the Brillouin function of order I^i. For small electron spin polarizations $S_z \ll 1/2$, (3.6) can be expanded to $\langle I^i_z \rangle \approx 4/3 I^i (I^i + 1)\langle S_z \rangle$, while for $S_z \approx 1/2$, $\langle I^i_z \rangle \approx I^i$.

The static part of the hyperfine interaction leads to the notion of the "effective magnetic fields", either seen by the electron due to spin polarized nuclei (Overhauser field $\mathbf{B}_{\mathrm{nuc}}$), or by the nuclei due to a spin polarized electron (Knight field $\mathbf{B}_{\mathrm{el}}$). Here, we only consider their projection along the z-axis, which we denote as B_{nuc} and B_{el}, respectively. The corresponding Knight field operator $\hat{B}^i_{\text{el}}$ for the ith nuclear spin is

---

[1] In our convention, $|\psi(\mathbf{r})|^2$ is normalized to $\frac{8}{\nu_0}$. Typical values of $\psi(\mathbf{r})$ are therefore $\sqrt{\frac{8}{\nu_0 N}}$ for $\mathbf{r}$ being within the QD.

$$\hat{B}^i_{\text{el}} = -\frac{1}{\hbar\gamma_i}\frac{\nu_0}{8}A_i|\psi(\mathbf{R}_i)|^2\hat{S}_z. \tag{3.7}$$

Its expectation value $B^i_{\text{el}} = \langle S|\,\hat{B}^i_{\text{el}}\,|S\rangle$ depends on the electron spin state $|S\rangle$ and on the exact location of the nucleus i. For a fully polarized electron bound to a shallow donor[2] in GaAs, the maximal value of B^i_{el} has been estimated to be 13 mT for Ga and 22 mT for As. These values, however, are further reduced to $f_{\text{el}}B^i_{\text{el}}$ if the QD is occupied by a single electron only in a finite fraction f_{el} of the total measurement time [3].

Analogously, the Overhauser field operator can be written as

$$\hat{B}_{\text{nuc}} = \frac{1}{g^*_{\text{el}}\mu_{\text{B}}}\frac{\nu_0}{8}\sum_i A_i\,|\psi(\mathbf{R}_i)|^2\,\hat{I}^i_z, \tag{3.8}$$

with the expectation value $B_{\text{nuc}} = \langle\mu|\,\hat{B}_{\text{nuc}}\,|\mu\rangle$ for a given nuclear spin state $|\mu\rangle$. This effective field leads to a total electron Zeeman splitting in the presence of both nuclear and external magnetic fields:

$$\Delta E^Z_{\text{el}} = g^*_{\text{el}}\mu_{\text{B}}(B_{\text{ext}} + B_{\text{nuc}}). \tag{3.9}$$

The change of the electron Zeeman splitting due to spin polarized nuclei is referred to as the Overhauser shift (OS), ΔE_{OS}. For a fully polarized nuclear spin system in bulk InAs, the total OS amounts to $\Delta E^{\text{max}}_{\text{OS}} = 0.5\,\frac{9}{2}\,56\mu\text{eV}+0.5\,\frac{3}{2}\,46\mu\text{eV} = 161\ \mu\text{eV}$, with the first contribution coming from the In nuclei and the second from the As nuclei. The weighting factors of 0.5 thereby correspond to the stoichiometric ratio of In and As in InAs. For a typical electron g-factor of $g_{\text{el}} = 0.7$, this corresponds to a nuclear magnetic field of $B_{\text{nuc}} = 4$ T

Singly charged excitons are ideal candidates for a spectroscopic study of DNSP in QDs. In these charge complexes, exchange interactions between the carriers play no role [29] and the magnetic field dispersion of the spin splittings of excitonic recombination lines is solely due to Zeeman interaction of the spins with (effective) magnetic fields. For X^{-1}, the total Zeeman splitting $\Delta E^{\text{Z}}_{X^{-1}}$ of the PL recombination line is given by the difference of the Zeeman splittings of the initial and final states of exciton recombination. It thus amounts to

$$\Delta E^{\text{Z}}_{X^{-1}} = -g^*_{\text{h}}\mu_{\text{B}}B_{\text{ext}} - g^*_{\text{el}}\mu_{\text{B}}(B_{\text{ext}} + B_{\text{nuc}}), \tag{3.10}$$

where g^*_{el} and g^*_h are the electron- and hole g-factors, respectively.

Exciting the QD with linearly polarized light creates residual electrons in a superposition of spin up and down, resulting in no nuclear polarization and therefore in $B_{\text{nuc}} = 0$. Thus, comparing the Zeeman splittings of X^{-1} under linearly- and circularly polarized excitation ($\Delta E^{\text{Z,lin.}}_{X^{-1}}$ and $\Delta E^{\text{Z},\sigma^\pm}_{X^{-1}}$, respectively) gives a direct measure of ΔE_{OS} and B_{nuc}:

$$\Delta E_{\text{OS}} = \Delta E^{\text{Z},\sigma^\pm}_{X^{-1}} - \Delta E^{\text{Z,lin.}}_{X^{-1}} = -g^*_{\text{el}}\mu_{\text{B}}B_{\text{nuc}}. \tag{3.11}$$

The analysis of the spin splittings of X^{+1} is analogous and will not be given here.

---

[2] With a Bohr radius of 10 nm - comparable to our QD confinement length.

3.4 Hyperfine-induced electron spin decoherence

As we argued in Sect. 3.1, QD electron spins are well protected from relaxation and their evolution of the spin is governed by the Zeeman interaction of the electron with (effective) magnetic fields. Besides the externally applied magnetic field, the electron experiences the strong nuclear magnetic field B_{nuc}. This field can attain values of several T for fully polarized nuclei and can therefore significantly contribute to the QD electron spin dynamics. If the nuclear spins are not explicitly prepared in a specific spin state, each nuclear spin points in a random direction and the mean nuclear spin polarization of the ensemble of nuclear spins is a random variable with a Gaussian distribution, having a width $\propto \sqrt{N}$. The fluctuating nuclear field can therefore be estimated to be $\Delta B_{\mathrm{nuc}} \simeq A/\sqrt{N} g_{\mathrm{el}}^{*}\mu_{\mathrm{B}}$, which is on the order of 10 mT for typical QD sizes with $N \approx 10^{5}$.

In low external magnetic fields, $B_{\mathrm{ext}} \approx \Delta B_{\mathrm{nuc}}$, the evolution of the direction of the electron spin is therefore mostly determined by its interaction with the nuclear spins. The transverse components of B_{nuc} with respect to the electron spin direction lead to coherent Larmor precession of the electron spin. Equivalently, the flip-flop terms in (3.5) drive transitions between the electron spin up and down states, thereby coupling these two states and defining a new quantization direction for the electron spins.

In a magnetic field $B_{\mathrm{ext}} \gg \Delta B_{\mathrm{nuc}}$, where the electron Zeeman splitting largely exceeds the hyperfine coupling strength of the electron with the random nuclear field, electron-nuclear flip-flop events become energetically forbidden and the components of the nuclear field transverse to B_{ext} can be neglected. However, the longitudinal components of the nuclear field fluctuations lead to a fluctuation of the energies of the electron spin states. This fluctuation in turn leads to a decoherence of the electron spin with a corresponding T_2^{*} time [40]:

$$T_2^{*} = \frac{\hbar}{g_{\mathrm{el}}^{*}\mu_{\mathrm{B}}\sqrt{2\Delta B_{\mathrm{nuc}}^{2}/3}}. \tag{3.12}$$

With $\Delta B_{\mathrm{nuc}} \approx 10$ mT, T_2^{*} is of the order of 3 ns, in accordance with recent transport measurements in a QD system [44]. We note that this apparent decoherence on a timescale T_2^{*} only comes from the fact that real experiments constitute an average over many measurements, each of which is realized under another nuclear spin configuration. In each run, the electron therefore has another Larmor precession frequency, which combined with the experimental averaging leads to an apparent damping of the electron spin precession. For a given nuclear spin state, however, the evolution of the electron-nuclear spin system is perfectly coherent as long as the direction and magnitude of the nuclear field are not altered. The effect of time- (or ensemble-) averaging can be eliminated by using spin-echo techniques [45] which unwind the effect of a static nuclear field on the electron spins. Under such conditions, the electron spin dephasing time in electrostatically defined QDs was found to be $T_2 \approx 1\,\mu$s at $B_{\mathrm{ext}} = 100$ mT - 2 orders of magnitude longer than T_2^{*} [44].

The remaining electron spin decoherence is a consequence of the evolution of the nuclear spin system and in particular of the z-component B_{nuc}^{z} of the nuclear field. This evolution was neglected in deriving (3.12) and the arguments leading to the finite T_2^{*} time were given based on the picture of the “frozen fluctuations” of the nuclear field. In order to understand the dephasing processes for a QD electron (characterized by a time T_2), it is therefore necessary to understand the mechanisms which cause the evolution of ΔB_{nuc} and the timescale at which this evolution happens.

In Sect. 3.2 it was shown that nuclear spin lattice relaxation is negligible in the temperature range relevant to the experiments discussed here. The only interactions relevant for the evolution of the nuclear field are therefore the nuclear dipole-dipole interactions (3.4) and the hyperfine interaction with conduction band electrons (3.5). The main effect of both of these interactions in changing B^z_{nuc} are flip-flop processes between different nuclei (i and j), which change the nuclear field because the two coupled nuclei might have different interaction strengths with the electron spin (i.e., $|\psi(\mathbf{R}_i)|^2 \neq |\psi(\mathbf{R}_j)|^2$).

Nuclear dipolar interaction strengths are characterized by the local dipolar field B_{loc} (cf. Sect. 3.2). The evolution of a nuclear spin due to interactions with its neighbors therefore happens at a rate corresponding to the nuclear Larmor precession frequency of about 10 kHz in the field B_{loc}. For external magnetic fields exceeding B_{loc}, the only relevant contribution for the evolution of B^z_{nuc} are the secular terms of the dipole-dipole interaction which lead to diffusion and re-distribution of the nuclear spins. The corresponding rate of change of B^z_{nuc} due to dipolar interactions is therefore further reduced. The time required to change a given nuclear field by a magnitude ΔB_{nuc} has been estimated to be $\sim 0.01 - 10$ s [46].

The role of the hyperfine interaction for the evolution of the nuclear spin system is twofold. First, the Knight field B_{el} of a QD electron leads to precession of the nuclear spins around the electron spin at a rate given by the nuclear Larmor frequency in a field B_{el}. Being on the order of 1 mT [15], the Knight field leads to nuclear spin evolution on timescales comparable to the corresponding estimates for the dipolar interactions. This evolution, however gets suppressed in external magnetic fields exceeding B_{el}, where electron-nuclear flip-flop processes vanish to first order. The second effect of the hyperfine interaction on the nuclear spins are electron-mediated, long ranged nuclear spin-spin interaction. This second order process termed "indirect interaction" consists of a virtual electron-nuclear spin-flip followed by a spin-"flop" of the electron with another nuclear spin. The resulting decorrelation time of the nuclear magnetic field has been shown to scale as $N^{3/2}\Delta E^{\text{Z}}_{\text{el}}/A^2$ for $A/\Delta E^{\text{Z}}_{\text{el}} \ll 1$[47], with a rough estimate of 1 ms for $N = 10^5$, $A = 50$ μeV and $\Delta E^{\text{Z}}_{\text{el}} = 200$ μeV. This estimate, however, is an upper bound for the rate of change of the nuclear field that neglects, for instance, effects of the Knight field gradient which will further slow down this rate. For cases where the approximation $A/\Delta E^{\text{Z}}_{\text{el}} \ll 1$ is not valid, no theoretical predictions for the evolution of the nuclear spin system due to indirect interactions exist.

Calculating the electron spin dephasing rate caused by the slow but random nuclear field fluctuations occurring on a timescale of $\sim 100\mu$s turns out to be a difficult task [48]. This rate not only depends on the timescale of nuclear field fluctuations, but also on the correlations of these fluctuations as well as on the width of the initial nuclear field distribution. Still, attempts have been made to calculate this quantity including the interaction mechanisms discussed above [5, 49]. The results of these calculations lead to an electron T_2-time of $1 - 100$ μs, in rough agreement with experimental results [44].

Since most solid state systems contain nuclei with non-zero spin, the only way to further increase the electron spin coherence time is to manipulate the nuclear spins. The goal of such a manipulation is then to suppress fluctuations of the mean nuclear spin, thereby leaving the electron to interact coherently with a static nuclear field. Two methods for suppressing nuclear spin fluctuations have been proposed up to now. They involve creating a very high degree of nuclear spin polarization [5] or, alternatively, repeated projective measurements of the nuclear field [8], causing a "quantum Zeno effect" on the nuclear spins.

4 Optical Pumping of Nuclear Spins in Low Fields

Experimental evidence for dynamical nuclear spin polarization induced by a single, optically oriented electron in zero external magnetic field is presented. Nuclear dipole-dipole interactions are suppressed by the relatively strong effective magnetic field that the quantum dot electron exerts on the nuclear spins. By applying external magnetic fields, this Knight field can be compensated, allowing for a direct measurement of its magnitude, which turns out to be on the order of one mT.

In low external magnetic fields, the evolution of the nuclear spin system is governed by the nuclear dipole-dipole interactions, characterized in strength by a local magnetic field B_{loc} (cf. Sect. 3.2). If the total magnetic field seen by the nuclei is smaller than B_{loc} , nuclear angular momentum is not a conserved quantity. Instead, the nuclear spins evolve into a highly entangled many body state due to their dipolar coupling. In order to observe any nuclear spin polarization, it is therefore necessary to apply a magnetic field exceeding B_{loc}. This fact has been observed experimentally in different QD systems [14, 50] as well as in various bulk NMR experiments [38]. Remarkably, in a situation of tight electron confinement, the Knight field B_{el} can attain values exceeding the local field B_{loc}, thereby "stabilizing" the nuclear spin polarization and allowing for the observation of dynamical nuclear spin polarization (DNSP) even in the absence of an externally applied magnetic field.

4.1 Nuclear spin cooling in the Knight field of the QD electron

Creating a Knight field strong enough to suppress the non-secular terms of the dipole-dipole interaction requires a sizable QD electron spin polarization. We realize this situation by exciting our QDs resonantly in one of their excited ("p-shell") states as described in Sect.2.4.

Figure 4.1(a) shows the emission spectrum of X^{-1} at zero external magnetic field obtained by using a scanning Fabry-Perot interferometer (cf. Appendix A.1) under linearly and circularly polarized excitation. Under σ^x-polarized laser excitation, no fine structure splitting is observed, confirming the absence of nuclear spin polarization. Exciting the QD with $\sigma^{\pm}$-polarized light, spin doublets with a splitting appear of $\sim 13\ \mu$eV. For X^{-1}, PL peaks that are co-circular with the excitation laser have lowest energy for both σ^+- and σ^--excitation (Fig. 4.1(a)), indicating that the direction of the effective magnetic field causing the observed splitting is determined by

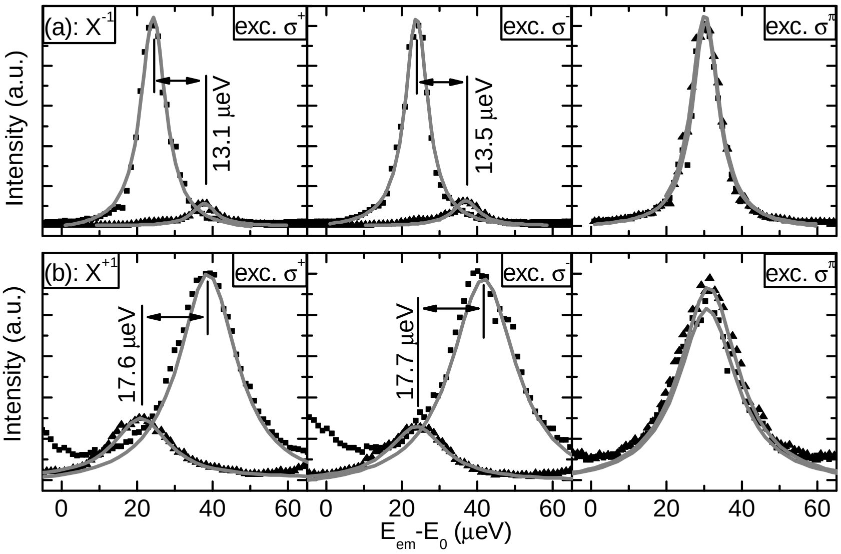

Figure 4.1: Exciton spin splitting induced by the Overhauser field. High-resolution PL spectra measured with a Fabry-Perot scanning interferometer (spectral resolution $\sim 1\,\mu$eV) under $B_{\text{ext}} = 0$. The polarizations of the excitation laser are denoted in the figure. PL is detected co- and cross- polarized with respect to the excitation polarization (squares and triangles, respectively). Under circularly polarized excitation of X^- (a) as well as of X^{+1} (b), a significant nuclear spin polarization with the corresponding OS denoted in the figure develops. In contrast, linearly polarized excitation does not lead to nuclear spin polarization. An energy offset of $E_0 = 1.3155$eV (1.3215eV) is subtracted from the X^- (X^+) data

the direction of the QD electron spin. We therefore attribute the observed splitting to DNSP and further test this hypothesis by performing an analogous measurement using X^{+1} trion excitation (Fig. 4.1(b)). For X^{+1} , the observed energy sequence in PL emission is reversed, indicating that for a given excitation polarization the electron spin is polarized in opposite directions in the case of trions [14]. This is consistent with the respective electron spin systems for X^{-1} and X^{+1} that were identified in Sect. 3.1.

Generally, the expectation value of the Overhauser field in an external magnetic field $\mathbf{B}_{\text{ext}}$ and in the presence of nuclear dipolar interactions can be expressed as [3, 23, 43, 51]:

$$\mathbf{B}_{\text{nuc}} = b_n^* \frac{\langle \mathbf{S} \rangle \cdot \mathbf{B}_{\text{tot}}}{B_{\text{tot}}^2 + \xi B_{\text{loc}}^2} \mathbf{B}_{\text{tot}}, \tag{4.1}$$

where $\mathbf{B}_{\text{tot}} = \mathbf{B}_{\text{ext}} + \mathbf{B}_{\text{el}}$ is the total effective magnetic field seen by the nuclei and $B_{\text{tot}} = |\mathbf{B}_{\text{tot}}|$. $\langle \mathbf{S} \rangle$ is the average QD electron spin, ξ is a numerical factor of order unity and b_n^* is a proportionality constant determined by (3.6) and (3.8) and by the rates of nuclear spin relaxation[1]. The fact that we observe DNSP even if $B_{\text{ext}} = 0$[2]

---

[1] As we will show in Chap. 5, the rate of nuclear spin relaxation due to electrons depends on the magnetic field as well. This dependence explains the behavior of DNSP in magnetic fields $B_{\text{ext}} \gg B_{\text{loc}}$.

[2] We measured the stray field in our set-up to be 0.05 ± 0.01 mT at an angle of $\sim 25°$ to the optical axis.

suggests that the Knight field of a single spin-polarized electron is strong enough to ensure $B_{\mathrm{el}} > B_{\mathrm{loc}}$.

4.2 Direct measurement of the Knight field of the QD Electron

Based on (4.1), it could be concluded that the application of an external field that cancels the Knight field should result in the complete disappearance of DNSP. Figure 4.2(a) shows the dependence of the observed Overhauser shift ΔE_{OS} of X^{-1} on B_{ext}. A dip in the OS at $B_{\mathrm{ext}} = -B_{\mathrm{el}} \approx \pm 0.6$ mT is observed under excitation with $\sigma^{\pm}$-polarized light, which gives a direct measurement of the average Knight field B_{el} experienced by the QD electrons. As indicated by (3.7), the direction of B_{el} is solely determined by the direction of the spin of the QD electron[3] and is always antiparallel to the direction of the electron spin. Excitation of the QD with σ^{+}-polarized light leaves a residual electron with spin up in the QD; this implies that the Knight field indeed has to point in the negative direction, while the nuclear spins are polarized in the positive direction. From this, one can conclude that the sign of the nuclear spin temperature under optical spin cooling in the Knight field is opposite to the sign of the nuclear gyromagnetic ratio γ_i. For all the nuclei in our system, $\gamma_i > 0$, which leads to a negative nuclear spin temperature at $B_{\mathrm{ext}} = 0$.

The Knight fields we measured with this method range from ± 0.6 mT to $\sim \pm 3$ mT, depending on the degree of PL polarization, the excitation light intensity and the QD that was studied. The measured values indicate a time-averaged electron spin polarization between 3% and 30%. A fully polarized electron spin would have given rise to a Knight field on the order of $10 - 20$ mT (cf. Sect.3.3). Predicting an exact number for this maximal value of B_{el} in a self-assembled QD however is difficult due to large uncertainties in the exact confinement length-scale and in the composition of the QD.

Even when $B_{\mathrm{ext}} = -B_{\mathrm{el}}$ in Fig. 4.2(a), ΔE_{OS} is only reduced from ~ 16 μeV to ~ 12 μeV, indicating that the cancellation of the Knight field B_{el} by the external field is not complete. One reason for the incomplete reduction in DNSP at $B_{\mathrm{ext}} = -B_{\mathrm{el}}$ is the inhomogeneity of the Knight field. Since B_{ext} is homogeneous, the condition $B_{\mathrm{tot}} = 0$ is satisfied only for a small class of nuclei at any given B_{ext}. The rest of the nuclei still experience a sizable total magnetic field and as a result, the Overhauser field is only slightly modified when $B_{\mathrm{ext}} = -B_{\mathrm{el}}$. To demonstrate the role of the inhomogeneous nature of the Knight field, we extended (4.1) to account for the inhomogeneity: We assume an in-plane Gaussian electron wave-function $|\psi(\mathbf{R}_i)|^2 \propto exp[-(x_i^2 + y_i^2)/l^2]$ which we convolve with (4.1) to estimate the total contribution of the different classes of QD nuclei. The choice of a maximum Knight field of 1.5 mT in the center of the dot, $B_{\mathrm{loc}} = 0.11$ mT and a confinement length scale $l = 20$ nm gives a reasonable description of the experimental data (solid curves in Fig. 4.2(a)), even though we only assumed a single nuclear species.

An additional reason for the finite value of ΔE_{OS} even at $B_{\mathrm{ext}} = -B_{\mathrm{el}}$ is the fact that a significant fraction of the QD nuclei experience a large quadrupolar splitting

---

[3] We note that the nuclear gyromagnetic ratio γ_i drops out of the expression (3.7) for B_{el}, since $A \propto \gamma_i$; the sign of γ_i therefore plays no role for the sign of B_{el}.

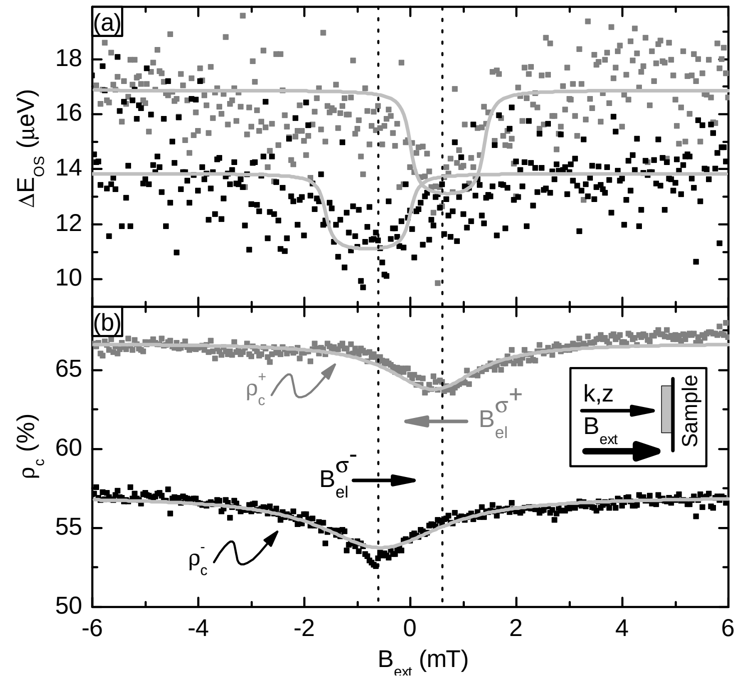

Figure 4.2: Overhauser shift ΔE_{OS} (a) and PL polarization (b) as a function of applied external magnetic field B_{ext}. Here, the measured spin splitting is determined by a weighted average of the X^{-1} spectral lines measured by the spectrometer. The light gray curves in (a) and (b) are fits according to the model described in the text. Observation of correlated dips in the spin splitting and in ρ_c as a function of B_{ext} suggests an average Knight field $B_{\mathrm{el}} \approx 0.6$ mT seen by the nuclei. Under σ^+- (σ^--) excitation, the corresponding Knight field $B_{\mathrm{el}}^{\sigma^+}$ ($B_{\mathrm{el}}^{\sigma^-}$) is parallel (anti-parallel) to the wave-vector $\mathbf{k}$ of laser excitation. The schematic in the inset of (b) sketches the orientations of the laser wave-vector and a positive external magnetic field

due the strain in the QD. The quadrupolar interaction can dominate the spectrum of the QD nuclei and render them insensitive to the effect of dipole-dipole interactions. However, we neglect this effect in the present chapter and postpone its detailed discussion to Chap. 6.

Remarkably, a minimum in the degree of PL polarization is also observed for the same B_{ext} where ΔE_{OS} has a minimum (Fig. 4.2(b)): this is at first surprising since polarization of the X^{-1} trion line is solely determined by the hole-spin which has a negligible coupling to the nuclear spins. A possible explanation is based on AEI: after the resonant excitation of the QD, the electron excited into a *p*-shell state is expected to tunnel out into the n-doped GaAs layer in $\lesssim 10$ ps [30]. After tunneling, the QD is neutral and the remaining electron-hole pair is subject to AEI which rotates the spins of the electron and the hole [52]. This coherent rotation is interrupted by the formation of an electron spin singlet after re-injection of an additional electron from the n-doped GaAs layer into the QD *s*-shell in $\tau_{\mathrm{el}} \approx 20$ ps, as required by the charging condition. Because tunneling is a random process, the time the QD spends in the neutral state is random and the post-tunneling hole-spin state is partially randomized, which leads to a finite ρ_c.

As the application of a magnetic field reduces the effect of AEI, the Overhauser-field competes with the exchange-mediated reduction of electron and hole spin polarization and a reduction in DNSP will lead to a reduction in ρ_c, consistent with our observation in Fig. 4.2(b). The PL polarization in the presence of an Overhauser shift $\Delta E_{\rm OS}$ and an exchange-splitting $\Delta E_{\rm ex}$ due to AEI can be described by the formula [53]:

$$\rho_c = \frac{1 + \Delta E_{\rm OS}^2 \tau_{\rm el}^2/\hbar^2}{1 + (\Delta E_{\rm OS}^2 + \Delta E_{\rm ex}^2)\tau_{\rm el}^2/\hbar^2}, \tag{4.2}$$

provided other spin relaxation processes are neglected. Fitting the polarization $\rho_c(X^{-1})$ with the measured spin splitting in Fig. 4.2(a), $\tau_{\rm el} = 30$ ps is obtained[4]. By reducing the QD excitation power below saturation of the X^{-1} PL line, a decrease in both OS and ρ_c arises. This observation further confirms our model of exciton spin preservation during relaxation from the *p*- to the *s*-shell due to the nuclear magnetic field (4.2).

The electron (spin) exchange with the n-doped GaAs layer also explains how spin pumping of the QD electron is achieved in a negatively charged QD: irrespective of the electron spin state before light excitation, the sequential tunneling ensures that the QD ends up in a trion state where the electrons form an *s*-shell singlet. Preservation of hole-spin during relaxation in these QDs then implies that the post-recombination electron is always projected into the same spin-state.

---

[4] As shown in Fig. 2.5(b), the PL from this QD exhibits a different degree of PL polarization under σ^+- and σ^--polarized excitation: the origin of this asymmetry is not clear and was not observed on all QDs studied.

5 Bistability of the Electron Nuclear Spin System

The dependence of optically induced dynamical nuclear spin polarization on longitudinal external magnetic fields is studied. The experiment shows that the coupled electron-nuclear spin system behaves in a highly nonlinear way, which is modelled in a classical rate equation picture. A striking manifestation of the nonlinearity of this system is the experimental observation of bistability of the electron-nuclear spin system.

The behavior of dynamical nuclear spin polarization (DNSP) is qualitatively different in low and high external magnetic fields. While the low field case was studied in the previous section, we now investigate a situation where the coupled electron-nuclear spin system is exposed to a magnetic field which is on the order of the Overhauser field B_{nuc}. There, the external magnetic field can fully compensate the nuclear field B_{nuc}, thereby greatly enhancing the transfer of angular momentum between the electron and the nuclear spins which depends on the effective Zeeman splitting of the electron spin.

In external magnetic fields, nuclear spin polarization manifests itself in a difference in emission energies between excitation with circularly and linearly polarized light as was discussed in Sect. 3.3. Fig. 5.1(c) shows the X^{-1} emission energies of a single QD under excitation with circularly polarized light as a function of external magnetic fields. Gray (black) denotes excitation with σ^+- (σ^--) polarized light, while squares (triangles) stand for detection of co- (cross-) circularly polarized light with respect to the excitation polarization. The polarizations for excitation and detection are denoted as $(\sigma^\alpha, \sigma^\beta)$ where σ^α and σ^β correspond to excitation and detection, respectively. The data shown in Fig. 5.1(c) was obtained in a single sweep from $B_{\mathrm{ext}} = -2$ T to $B_{\mathrm{ext}} = +2$ T, varying excitation and detection polarization for each value of the magnetic field in the order $(\sigma^+, \sigma^-) \Rightarrow (\sigma^+, \sigma^+) \Rightarrow (\sigma^-, \sigma^+) \Rightarrow (\sigma^-, \sigma^-)$ such that any memory of the nuclear spin system was erased during the sweep. The data for $|B_{\mathrm{ext}}| < 500$ mT was taken with smaller magnetic field steps in order to highlight the detailed behavior of DNSP at low fields. Every data point represents the center of mass of the emission peak of X^{-1} taken from a single spectrum with 1 s integration time and a signal to noise ratio of $\sim 100 : 1$ for co-circular detection (Fig. 5.1(b)). The effects of nuclear polarization can be seen in the range of $|B_{\mathrm{ext}}| \lesssim 1.2$ T where emission energies for a given detection polarization depend strongly on the helicity of the excitation light. Excitation with σ^+-light creates a residual electron with its spin pointing in the positive z-direction (see Fig. 5.1(a)). According to (3.5) and (3.8), this creates a nuclear spin polarization in the same direction and, due to the negative sign of the g^*_{el}, a nuclear field pointing in the

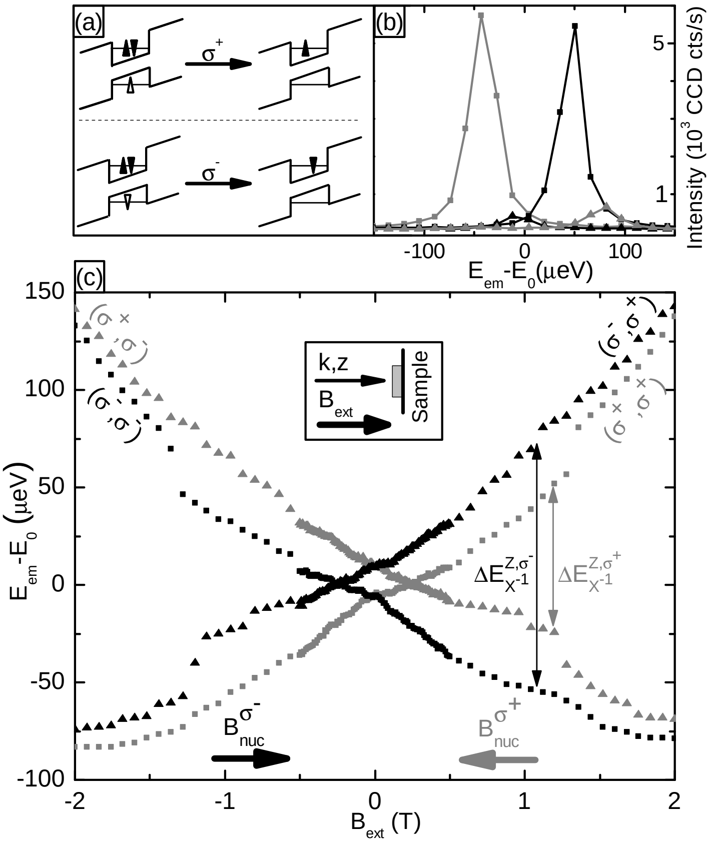

Figure 5.1: (a) Configurations of X^{-1} before and after the emission of a $\sigma^{\pm}$-polarized photon. Open (filled) triangles denote the spin of the hole (electron). (b) Raw spectra at $B_{\text{ext}} = -0.96$ T for the four excitation/detection configurations in the circular basis: gray (black) denotes excitation with σ^{+}- (σ^{-}-) polarized light. Detection is co- or cross-circular (squares and triangles, respectively). (c) Energy dispersion of X^{-1} under circularly polarized excitation: The emission energies (E_{em}) are different for σ^{+}- and σ^{-}-polarized excitation due to DNSP and the resulting effective nuclear magnetic field $B_{\text{nuc}}^{\sigma^{+}}$ ($B_{\text{nuc}}^{\sigma^{-}}$) under σ^{+}- (σ^{-}-) excitation (orientation indicated by the arrows in the figure). An energy $E_0 = 1.3155$ eV was subtracted from E_{em}. The inset shows the relative orientation of k-vector, quantization axis z and positive magnetic field

negative z-direction. This scenario is consistent with the polarization sequences and lineshifts observed in Fig. 5.1(c). Above 1.2 T, the emission energies of the QD are almost independent of excitation light polarization, indicating that nuclear effects become very small. Another striking feature in this data is the symmetry under simultaneous reversal of the excitation light helicity and the sign of the magnetic field. However, the data is not symmetric under the reversal of only one of these parameters. This asymmetry indicates that the system distinguishes between nuclear fields pointing along or against the external magnetic field - we will see in the following that it is more efficient for the electron-nuclear spin system to create a nuclear field pointing against B_{ext} than one that points along this field.

In order to obtain a more quantitative picture of the magnetic field dependent DNSP, we performed the following analysis steps on the data (see Fig. 5.2): We first extract the Zeeman splittings for excitation with σ^+- and σ^--polarized light from the raw data shown in Fig. 5.1(c). To this data, we fit a linear Zeeman splitting such that the fit coincides with the data at magnetic fields $B_{\text{ext}} > 1.8$ T, where nuclear polarization is very small (Fig. 5.2(a)). The excitonic g-factor, $g^*_{\text{ex}} \equiv g^*_{\text{el}} + g^*_{\text{h}} = -1.87$ that we find with this fitting procedure matches within a few percent to an independent measurement of g^*_{ex} that we performed with linearly polarized excitation (not shown here). The Overhauser shift can now be extracted from this fit with the help of (3.11); the result is plotted in Fig. 5.2(b). There is a striking difference when polarizing the nuclei along or against the external field. Nuclear polarization with B_{nuc} pointing along the applied field is rather inefficient and shows a slight decrease with increasing magnitude of the applied field. Polarization with B_{nuc} pointing against the external magnetic field on the other hand shows a much richer behavior: The nuclear polarization first increases almost linearly as the magnitude of the external field increases and then shows a sudden drop when $|B_{\text{ext}}| \approx 1.2$ T. At $B_{\text{ext}} = 0$, DNSP abruptly changes its dependence on magnetic field and $\mathrm{d}B_{\text{nuc}}/\mathrm{d}B_{\text{ext}}$ shows a quick change, resulting in a "kink" of $B_{\text{nuc}}(B_{\text{ext}})$.

From the spectral data we can also extract information about the hole spin polarization before- and the residual electron spin polarization after recombination of X^{-1}. For this, we define a degree of QD spin polarization as $\rho_c^\pm \equiv (I_{(\sigma^\pm,\sigma^\pm)} - I_{(\sigma^\pm,\sigma^\mp)})/(I_{(\sigma^\pm,\sigma^+)} + I_{(\sigma^\pm,\sigma^-)})$ under $\sigma^\pm$-excitation. $I_{(\sigma^\alpha,\sigma^\beta)}$ are the intensities of the dominant X^{-1} PL-peaks in the corresponding analyzer/polarizer configurations. At $B_{\text{ext}} = 0$, $\rho_c^\pm$ is equivalent to the PL circular polarization defined in Sect. 2.4. At finite B_{ext}, however, $\rho_c^\pm$ measures the relative weight of the two Zeeman split emission lines[1] and is therefore a measure of hole spin preservation during relaxation from the p- to the s-shell. The measured quantity $\rho_c^\pm$ is plotted in Fig. 5.2(c) as a function of external magnetic field. It is roughly constant and on the order of 85% over a wide range of magnetic fields. Only for the fields where the exciton Zeeman splitting vanishes due to its cancellation with the OS, $\rho_c^\pm$ dips to roughly 65%. This behavior is consistent with the rotation of the exciton spin during relaxation of the optically created electron from the excited p-shell state to the s-shell via the electron reservoir which was already observed in Sect. 4.2.

As in the data presented in Chap. 4, there is a certain asymmetry in the data shown in Fig. 5.2(c) that remains unexplained: ρ_c^- is larger than ρ_c^+ at high magnetic fields and the dip in ρ_c^+ at lower fields is less pronounced than for ρ_c^-. A possible reason for this asymmetry could be the different excitation efficiencies in the QD for σ^+- and σ^--excitation.

5.1 Modelling of the data

Most of the above-mentioned effects of optically induced DNSP in the presence of an external magnetic field can be described by a simple rate equation model proposed earlier [14, 40, 50] and originally based on publications by D'yakonov [54] and Abragam [34]. The rate equation is based on the condition for dynamical equilibrium (3.6) between the electron and the nuclear spin system in the absence of any coupling to the environment. This equilibrium is reached on a typical timescale

---

[1] These lines are perfectly circularly polarized as evidenced by the raw spectra shown in Fig. 5.1(b).

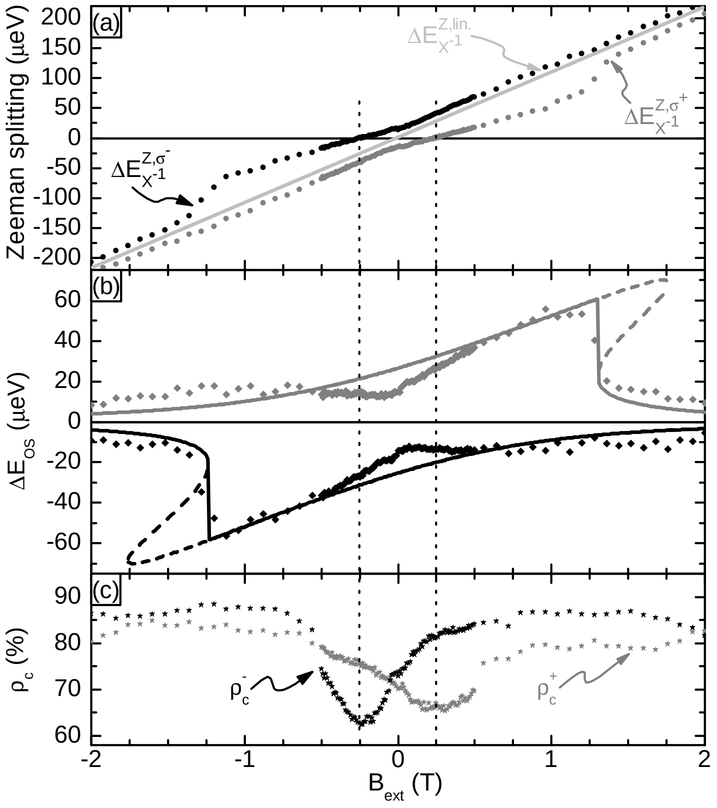

Figure 5.2: Nuclear Polarization in external magnetic fields: (a) Spin splitting of X^{-1} under circularly polarized excitation. Gray and black symbols correspond to excitation with σ^+- and σ^--polarized light, respectively. The solid line is a linear fit to the data as described in the text. (b) Deviation of the spin splitting between circular and linear excitation: Overhauser shift for σ^+- and σ^--excitation (gray and black diamonds, respectively). The solid and dashed lines are the results of the fits according to the model discussed in the text. (c) QD spin polarization $\rho_c^\pm$ under $\sigma^\pm$-excitation extracted from PL intensities as described in the text. The polarization shows a minimum at the magnetic field where the exciton Zeeman splitting is zero, consistent with our model of carrier relaxation (Chap. 4)

given by the nuclear spin relaxation time $T_{1\mathrm{e}}$, which can be estimated to be [23]

$$\frac{1}{T_{1\mathrm{e}}} = \frac{1}{T_{1\mathrm{e}}^0} \frac{1}{1+\Omega_{\mathrm{el}}^2 \tau_{\mathrm{el}}^2}. \tag{5.1}$$

Here, τ_{el} is the electron spin correlation time which broadens the electronic spin states. $\Omega_{\mathrm{el}} = \Delta E_{\mathrm{el}}^Z/\hbar$ is the electron Larmor frequency which depends on the degree of nuclear polarization through (3.8) and (3.9). For a given nuclear species, the nuclear spin relaxation time for a negligible electron Zeeman splitting is given by $1/T_{1\mathrm{e}}^0 = f_{\mathrm{el}}\tau_{\mathrm{el}}(A_i/N\hbar)^2$, with N the number of QD nuclei and f_{el} the fraction of time the QD is occupied with a single electron. This expression for $1/T_{1\mathrm{e}}^0$ is valid in the regime of "motional narrowing", where $A_i/N\hbar \ll \tau_{\mathrm{el}}^{-1}$. The quantity $A_i/N\hbar$ corresponds to the precession frequency ω_{L} of a nuclear spin in the Knight field B_{el} of the QD electron. The nuclear Larmor precession in the field B_{el} is interrupted by a re-initialization of the electron spin after a time interval of length τ_{el} during which the nuclear spins have rotated by an angle $|\delta\Phi| = \omega_\mathrm{L}\tau_\mathrm{el}$. This leads to a random walk of the nuclear spin on the Bloch-sphere with $\sqrt{\langle\Phi^2\rangle} = \delta\Phi\sqrt{n}$ after n steps. With $n = t/\tau$ and by defining T_1 as the time after which the angle $\sqrt{\langle\Phi^2\rangle}$ has evolved to 1 and by adding the factor of finite electron occupancy f_el, the before mentioned expression for $1/T_{1\mathrm{e}}^0$ results. In this derivation, we assumed a homogenous electron wave function $\psi(\mathbf{r}) \propto \sqrt{8/\nu_0 N}$ which is constant within the QD volume and zero outside.

By adding a nuclear spin decay channel which is dominated by nuclear spin diffusion out of the QD on a timescale T_d, we end up with a rate equation of the form

$$\frac{d\langle I_z^i\rangle}{dt} = -\frac{1}{T_{1\mathrm{e}}}(\langle I_z^i\rangle - I^i B_{I^i}(x)) - \frac{1}{T_\mathrm{d}}\langle I_z^i\rangle \qquad (5.2)$$

$$\simeq -\frac{1}{T_{1\mathrm{e}}}(\langle I_z^i\rangle - I^i) - \frac{1}{T_\mathrm{d}}\langle I_z^i\rangle. \qquad (5.3)$$

Due to the high degree of electron spin polarization deduced from the measured large value of $\rho_c^\pm$, we take the limit of (3.6) for $S_z = 1/2$, where $B_{I^i}(x) = 1$ to arrive at (5.3).

This equation was obtained for the coupling of a single electron to a single nuclear spin species. It can be approximately generalized to the case of an ensemble of different nuclei in the QD by considering the mean nuclear spin polarization $\langle I_z\rangle = \frac{1}{N}\sum_i\langle I_z^i\rangle$. For this, we replace the hyperfine constant A_i in (5.1) and the nuclear spin I^i in (5.3) each by its average value $\overline{A}$ and $\overline{I^i}$ over the two dominant nuclear spin species. With the values for A_i and I^i noted in Sect. 3.3, this results in $\overline{A} = 0.5A_\mathrm{In} + 0.5A_\mathrm{As} = 51\ \mu\mathrm{eV}$ and $\overline{I^i} = \frac{6}{2}$. We take these numbers to be fixed in the following, even though the In content varies drastically within a QD and accurate estimates of $\overline{A}$ and $\overline{I^i}$ are difficult to obtain.

We note that this model was previously applied to situations where DNSP was induced by neutral excitons [40, 50]. There, anisotropic exchange interaction plays a crucial role and has to be included in the detuning factor in (5.1). In this work however, DNSP is induced by a single, spin-polarized electron for which exchange interaction plays no role[2].

Since the electron-mediated nuclear spin relaxation time $T_{1\mathrm{e}}$ itself depends on nuclear spin polarization, (5.3) leads to the following self-consistent nonlinear steady state solution $\langle I_z^\mathrm{ss}\rangle$ for the mean nuclear spin polarization:

$$\langle I_z^\mathrm{ss}\rangle = \frac{\overline{I^i}}{1 + \frac{T_{1\mathrm{e}}^0}{T_\mathrm{d}}(1 + (\frac{\tau_\mathrm{el}}{\hbar})^2(g_\mathrm{el}^*\mu_\mathrm{B}B_\mathrm{ext} + A\langle I_z^\mathrm{ss}\rangle)^2)}. \qquad (5.4)$$

We note that averaging (5.3) over the different nuclear species, our choice of a homogenous electron wavefunction and the fact that we neglected the magnetic field dependence of T_d can all limit the validity of this model.

In order to fit our experimental data, we numerically solved the implicit equation (5.4). The result of such a fit is shown in Fig. 5.2(b). The model qualitatively reproduces the data. Still, some features, like the before-mentioned "kink" of DNSP around $B_{\mathrm{ext}} = 0$ as well as the high residual nuclear spin polarization at high external magnetic fields, could not be explained within the model or any reasonable extension [50] to the rate equation picture employed here. In the region 1.2 T$< B_{\mathrm{ext}} <$ 1.8 T the model predicts three solutions: two stable states, one with a low and one with a high degree of DNSP and an unstable solution of intermediate nuclear spin polarization (the last two solutions correspond to the dashed lines in Fig. 5.2). Since in this experiment we changed the excitation polarization from σ^+ to σ^- for each magnetic field value, the system always followed the solution with minimal nuclear spin polarization. The fact that the drop in DNSP in this measurement was rather smooth compared to the model prediction was probably due to the long timescale of the buildup of DNSP right before its disappearance: since in the experiment every point was taken with an integration time of 1 s, the nuclear system did not have time to reach its steady state polarization before the excitation light polarization was switched. This explanation will be further confirmed by the time-dependant measurements of DNSP presented in Sect. 7.2. The parameters used for the fitting curve in Fig. 5.2(b) were $T^0_{1\mathrm{e}}/T_{\mathrm{d}} = 1.2$,$\tau_{\mathrm{el}} = 42$ ps, $g^*_{\mathrm{el}} = -0.69$, which are all realistic values for our QD.

---

[2] We can rule out the possibility that DNSP is induced by the intermediate state where the QD is neutral during electron relaxation through the reservoir. In this case the direction of the nuclear field would be opposite to the one observed in the experiment.

The surprisingly short electron spin correlation time found in the fit can be explained with the resonant excitation scheme that we used in our experiments. The QD is excited from its ground state into the *p*-shell and after relaxation through an intermediate neutral excitonic state, PL emission is observed from carriers recombining from the *s*-shell. Since this system is pumped close to saturation, the lifetime and thus the correlation time of the residual electron is limited by the relaxation time from the *p*-shell to the n^{++}-GaAs layer by tunnelling. This timescale is expected to be on the order of 10 ps and the value of 42 ps we find here is in good agreement with the value found independently in Sec. 4.

The parameters obtained in this fit also allow us to estimate the nuclear spin relaxation time $T^0_{1\mathrm{e}}$. Using the value $\tau_{\mathrm{el}} = 42$ ps, the corresponding value for $f_{\mathrm{el}} = 0.035$ (assuming an X^{-1}-lifetime of 1 ns) and N$= 10^4 - 10^5$, we obtain $T^0_{1\mathrm{e}} = 1 - 100$ ms, which is in reasonable agreement with the corresponding direct measurement of $T_{1\mathrm{e}}$ that will be discussed in Chap. 7.

5.2 Hysteresis in the magnetic field sweeps

In this section, we focus on the bistable behavior of the coupled electron-nuclear spin system in the magnetic field range close to the “breakdown” of DNSP. Fig. 5.3(a) shows a graphical representation of the solutions of the nonlinear equation (5.4). The result suggests that the maximal achievable degree of DNSP in our system leads to a maximal OS given by $\Delta E^{\max}_{\mathrm{OS}} = A\overline{I^i}(1 + T^0_{1\mathrm{e}}/T_{\mathrm{d}})^{-1}$. This value is reached when nuclear spin relaxation is maximized, i.e., when the total electron Zeeman splitting is zero (cf. (5.1)). It can also be seen from the figure that there is a regime of external magnetic fields where two stable solutions for DNSP coexist. One solution leads to a high degree of nuclear polarization, reaching $\mathrm{OS}_{\max}$ at its maximum, while the other one shows a low degree of nuclear polarization. The graphical solution also shows that bistability is an inherent property of the solutions of (5.3) for systems where $\mathrm{OS}_{\max}$ is at least on the order of the width of the density of states of the

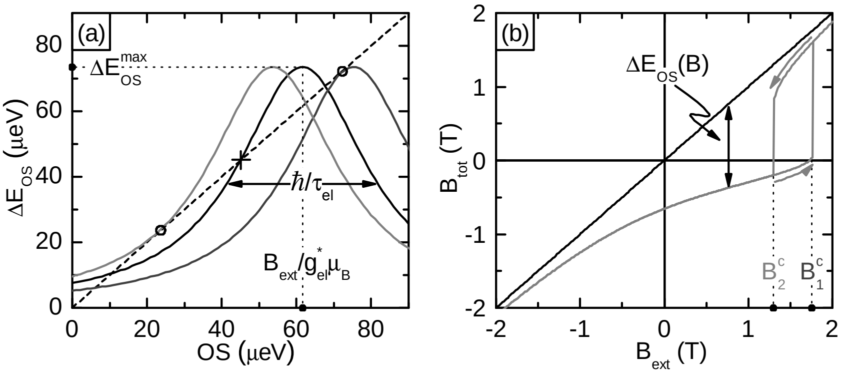

Figure 5.3: (a) Graphical solution of (5.4): The right (left) hand side is represented by the solid curves (dashed line). These terms correspond to gain and loss of DNSP, respectively. Circles (cross) indicate the stable (unstable) solutions for nuclear spin polarization. The center of the Lorentzian shifts proportionally to the external magnetic field, explaining the magnetic field dependence of DNSP. The dark (light) gray curve show the situation at the critical field B_1^c (B_2^c). The figure illustrates that: 1.) Bistability can only be observed if the maximal slope of the Lorentzian is bigger than 1 and 2.) the difference between B_1^c and B_2^c is on the order of the width of the electron spin states in units of magnetic fields $\hbar/\tau_{\mathrm{el}} g_{\mathrm{el}}^* \mu_{\mathrm{B}}$. (b) Total magnetic field B_{tot} seen by the QD electron under optical orientation of nuclear spins with σ^+-polarized light (gray curve). The curve is calculated from (5.3) with the parameters found from the fit presented in Fig. 5.2. The model shows that when the nuclear magnetic field B_{nuc} opposes the external field (i.e., for $0 < B_{\mathrm{ext}} < 1.74$ T), the nuclei overcompensate B_{ext} and the electron sees a total magnetic field $B_{\mathrm{tot}} < 0$. When the nuclear field saturates to its highest value, B_{tot} is very close to zero and the nuclear spin polarization becomes unstable

electronic spins ($\hbar/\tau_{\mathrm{el}}$), which is typically the case for localized carriers such as in QDs, but not for bulk systems. The two stable solutions can be understood as follows: When increasing an external field while creating a nuclear field in the opposite direction, the electron Zeeman splitting is reduced compared to the case where nuclear spin polarization is absent. Therefore, the nuclear spin relaxation rate $T_{1\mathrm{e}}^{-1}$ remains at a high value such that DNSP can be maintained. As soon as $\mathrm{OS}_{\mathrm{max}}$ is reached, however, the system can no further compensate for an increasing external magnetic field. DNSP will start to drop, which leads to a negative feedback on $T_{1\mathrm{e}}^{-1}$ and eventually causes an abrupt jump of DNSP to a low value at an external field B_1^c. When ramping the external field down again, now in the absence of nuclear polarization, the system will initially remain in a state of low DNSP since $T_{1\mathrm{e}}^{-1}$ is still low. At the same time, DNSP will slightly increase and compensate B_{ext}, due to the increasing rate $T_{1\mathrm{e}}^{-1}$ of nuclear polarization with decreasing magnetic field strength. At a field B_2^c, the positive feedback of the reduced electron Zeeman splitting on $T_{1\mathrm{e}}^{-1}$ will take over and an abrupt jump to a state of high nuclear polarization will occur. As illustrated by Fig. 5.3(a), the difference between the fields B_1^c and B_2^c is on the order of the width of the electronic spin states in units of magnetic fields.

In order to observe the hysteretic behavior of DNSP we performed a magnetic field dependent PL experiment as described above, now by exciting the QD with

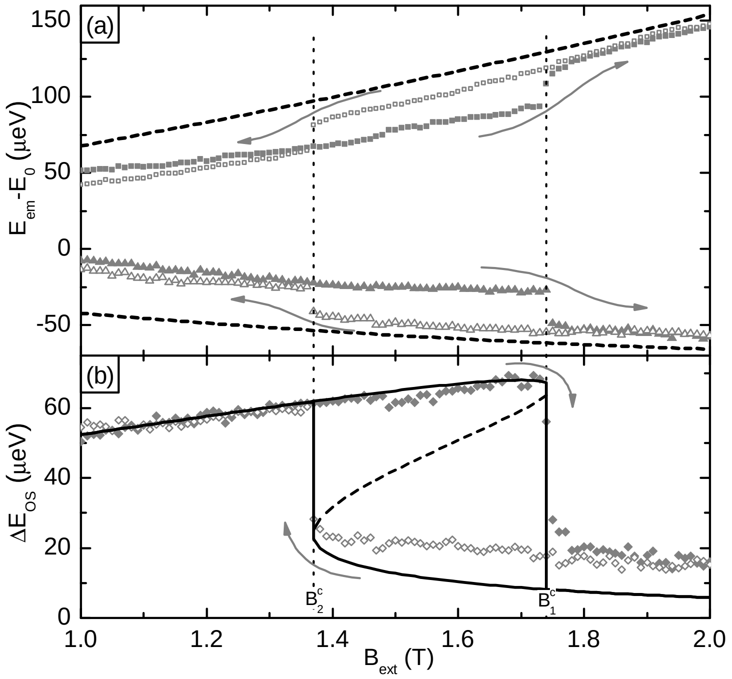

Figure 5.4: Hysteresis behavior of the coupled electron-nuclear spin-system: Magnetic field sweeps under excitation with constant light polarization (σ^+). (a) Energy dispersion of X^{-1}, sweeping magnetic field up or down (as indicated by arrows). Squares (triangles) denote co- (cross-) circular detection with respect to excitation polarization. The dashed line is a fit to the case of linearly polarized excitation. (b) Overhauser shifts extracted from the data shown in (a) for the magnetic field sweeping up and down (solid and open diamonds, respectively). The black line shows the simulations described in the text

light of constant helicity and by ramping the magnetic field from low to high values and back again. Hysteretic behavior can be expected if the nuclear field created in that way is pointing against the external magnetic field. In our system such a situation is realized when exciting the QD with σ^+-polarized light while applying an external field in the positive z-direction.

Figure 5.4 shows data obtained in this regime: Going from low to high field amplitude, DNSP is significant up to a magnetic field of $B_1^c = 1.74$ T, where it suddenly drops. Sweeping the magnetic field back to low field amplitudes, DNSP reappears at a field $B_2^c = 1.36$ T, a value different from B_1^c. The difference of 380 mT between these two field is on the order of $\hbar/(\tau_{\mathrm{el}} g^*_{\mathrm{el}} \mu_{\mathrm{B}})$ as predicted by the model.

A fit of (5.4) to the data is also shown in Fig. 5.4. The parameters used for this fit were $T^0_{1\mathrm{e}}/T_{\mathrm{d}} = 1.25$, $\tau_{\mathrm{el}} = 39$ ps, $g^*_{\mathrm{el}} = -0.69$, consistent with the parameters used in the fit shown in Fig. 5.2. As in the previous fit, the residual nuclear polarization at high fields observed in this experiment is slightly higher than what is predicted by the model.

5.3 Discussion

We note that at the point of maximal Overhauser shift ($B_{\text{ext}} = B_1^{\text{c}} = 1.74$ T), our model predicts that B_{nuc} is almost completely cancelled by B_{ext} (see Fig. 5.3(b)). This point is therefore of particular interest because it enables a direct measurement of the maximal nuclear field $B_{\text{nuc}}^{\text{max}} = \Delta E_{\text{OS}}^{\text{max}}/g\mu_B = B_1 = 1.74$ T. Remarkably, the remaining exciton Zeeman splitting at this point is solely due to the Zeeman interaction of the hole with B_{ext}. We can therefore directly obtain the hole g-factor for an individual QD and find $g_h^* = -1.2$. This observation has found applications in the precise and systematic study of electron and hole g-factors in semiconductor QDs [55].

Our experiment along with the model also shows that the maximal nuclear polarization of $\sim 43\%$[3] achieved in our system is limited by the fraction $T_{\text{d}}/T_{1\text{e}}^0$, i.e., the ratio between nuclear spin decay time and electron mediated nuclear spin relaxation time. While T_{d} is a parameter given by the nature of the QD, $T_{1\text{e}}^0$ could potentially be modified by varying the pump power or the details of the excitation process [41]. In particular, due to the energetically narrow p-shell excitation resonances in our system, it is likely that the QD excitation process becomes less efficient as we increase the magnetic field. Indeed, by adjusting the energy of the excitation laser to a p-shell resonance at $B_{\text{ext}} = 5$ T, we were able to observe DNSP along with the previously discussed, bistable behavior, on the same dot at $B_{\text{ext}} \approx 4$ T. Fig. 5.5 shows the corresponding data for a magnetic field sweep with constant excitation light polarization. The resulting value of $\Delta E_{\text{OS}}^{\text{max}}$ in this experiment was 130 μeV, corresponding to a nuclear spin polarization of 80% - to the best of our knowledge, the highest degree of DNSP achieved by optical orientation of nuclear spins in an individual, self-assembled QD.

We extended the rate equation (5.2) and included the dynamics of the mean electron spin $\langle S_z \rangle$ by expanding (3.6) to first order in $\langle S_z \rangle$. The evolution of $\langle S_z \rangle$ is described by a rate equation similar to (5.3). The main differences between the electron and the nuclear spin dynamics are that the electron spin system, in the absence of other relaxation mechanisms, reaches the thermal equilibrium state (3.6) at a rate $N/T_{1\text{e}}$. Compared to the nuclear spin relaxation rate, the electron spin relaxation is faster by the number of nuclei N in the system. In addition, the electron spin is repumped into its initial state $S_z^0 = \rho_c^{\pm}/2$ at a rate corresponding to the X^{-1} recombination rate on the order of 1 ns^{-1}. This extension, however, did not lead to any new insights on the behavior of the nuclear spin system. A numerical study of this extended model suggested though that the mean value of the electron spin decreases linearly with increasing nuclear spin polarization. The electron spin thus seems to follow the intricate dynamics of the nuclear spin system. This observation motivates further studies on the positively charged exciton where PL light polarization gives a direct measure of the mean electron spin [56].

The qualitative disagreement of the model with our data in the low field regime where the measured DNSP shows a clear “kink” as a function of magnetic field indicates that our simple approach does not give a full description of the nonlinear processes that lead to an equilibrium value of DNSP in a QD. A further extension

---

[3] We estimate the degree of nuclear spin polarization by comparing $\Delta E_{\text{OS}}^{\text{max}} = 70$ μeV to the OS for a fully polarized nuclear spin system, which was given in Sect. 3.3.

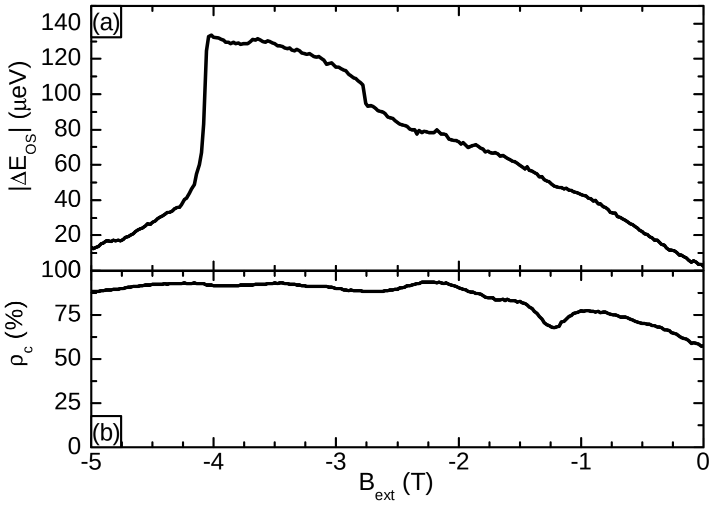

Figure 5.5: Nuclear Polarization in high external magnetic fields. The energy of the excitation light is tuned to a p-shell resonance at $B_{\mathrm{ext}} = 5$ T, shifting the critical field $|B_1^{\mathrm{c}}|$ to higher values compared to Fig 5.2, where the excitation laser was tuned to a resonance at $B_{\mathrm{ext}} = 0$. The presented data was extracted from the raw spectra according to the procedure described for Fig. 5.2. (a) Overhauser shift for continuous excitation with σ^--polarized light. The maximal OS, $\Delta E_{\mathrm{OS}}^{\mathrm{max}} \approx 130$ μeV corresponds to a nuclear spin polarization of $\sim 80\%$. (b) PL light polarization ρ_c^- under σ^--excitation. Since the excitation energy was optimized for $B_{\mathrm{ext}} = 5$ T, DNSP is negligible at zero field and the minimum in ρ_c^- occurs at $B_{\mathrm{ext}} = 0$. A further local minimum of ρ_c^- is observed at $B_{\mathrm{ext}} \approx -1.2$ T and is probably a result of the specific nature of the p-shell excitation resonance.

of the model could include light-induced nuclear spin relaxation due to the nuclear quadrupolar interaction [57] which could induce an additional loss of nuclear spin polarization at low external magnetic fields. Another possible nuclear depolarization mechanism relevant at low fields is the coupling of the nuclear Zeeman spin temperature to the nuclear dipolar spin temperature [38]. Since the heat conductivity for dipolar spin temperature is at least on the same order than the one for the Zeeman spin temperature [58], the rate of nuclear spin depolarization in the QD will increase as soon as the two temperature reservoirs couple. This coupling of nuclear Zeeman and dipolar reservoirs might therefore also explain the observed “kink” of DNSP at low fields. While our rate equation approach was purely classical, it could also be conceived that the quantum mechanical nature of the electron spin system would alter the behavior of DNSP at low fields and explain the unpredicted features in our measurement. In order to confirm this hypothesis, further theoretical and experimental studies are required.

6 Nuclear Spin Polarization in Transverse Magnetic Fields

In the framework of the nuclear spin temperature, the polarization of a cooled nuclear spin system has to be aligned with an external magnetic field. Here it is shown that this statement can be partly relaxed if the external magnetic field is on the order of the Knight field or if the nuclear spins experience strong quadrupolar interactions. For this purpose, the behavior of nuclear spin polarization in transverse magnetic fields is studied through the Hanle effect - the depolarization of electron spins in transverse magnetic fields.

In the preceding chapters, we studied nuclear spin polarization as a function of external magnetic fields applied in the direction of light excitation and electron spin orientation. This study is complemented by examining nuclear effects in a situation where the external magnetic field is applied transverse to the electron spin polarization. As we argued in Sect. 3.2.1, in cases where the nuclear spin system can be described by a nuclear spin temperature, a finite nuclear spin polarization necessarily has to be aligned along the total magnetic field the nuclei are exposed to. One would therefore not expect the nuclear spin system to acquire a polarization due to optically oriented electrons if an external magnetic field is applied transverse to the direction z in which the electrons were oriented. Taking into account a more detailed description of the nuclear spin system, however, this statement is only partly true. In a situation of Knight field enabled nuclear spin cooling, described in Chap. 4, the nuclei feel a total magnetic field which is tilted away from the optical axis if the transverse magnetic field is on the order of B_{el}. As the projection of the electron spin on this oblique axis is nonzero, the nuclear spins can be polarized, although the applied magnetic field is purely transverse. Furthermore, the QD nuclei are subject to a substantial quadrupolar splitting induced by the large strain in self-assembled QDs. As a result of this splitting, the nuclear gyromagnetic ratio γ becomes strongly anisotropic and can almost vanish in the direction transverse to the QD growth direction. In this case, nuclear spins are insensitive to transverse magnetic fields $B_{\text{ext},\perp}$ and DNSP can be observed even if $B_{\text{ext},\perp}$ largely exceeds B_{el}. In this chapter we will discuss the theory of DNSP in transverse magnetic fields and the resulting evolution of the electron spin system. The precession and relaxation of charge carriers can be studied by measuring the Hanle effect - the depolarization of PL light in magnetic fields applied transverse to the axis of optical spin orientation. We will present measurements of the Hanle effect for X^{-1} and X^{+1} PL and discuss how nuclear spins affect the observed Hanle curves.

6.1 Theory of the Hanle effect

The evolution of an electron spin in a magnetic field is a combination of Larmor precession in the total magnetic field seen by the electron and electron spin relaxation, which is described by the Bloch equation

$$\frac{d\langle \mathbf{S}\rangle}{dt} = \frac{g^*_{\mathrm{el}}\mu_B}{\hbar}\mathbf{B}\times\langle \mathbf{S}\rangle - \frac{\langle \mathbf{S}\rangle - \mathbf{S}_0}{\tau}. \tag{6.1}$$

Here, $\mathbf{S}_0 = (0,0,S_0)$ is the average, optically generated electron spin polarization in the absence of a magnetic field and $\tau^{-1} = \tau_{\mathrm{el}}^{-1} + \tau_{\mathrm{S}}^{-1}$ is the total rate of loss of electron spin orientation, which is a combination of the finite electron lifetime τ_{el} and the electron spin relaxation rate τ_{S}^{-1}. In steady state and in the presence of a magnetic field lying in the x-z plane, the resulting steady state electron spin polarization along the z-axis amounts to

$$\langle S_z\rangle = S_0\frac{B_{1/2}^2 + B_z^2}{B_{1/2}^2 + B_z^2 + B_x^2}. \tag{6.2}$$

For $B_z = 0$, this corresponds to a Lorentzian dependence of the mean electron spin polarization on the transverse magnetic field B_x, with a half-with $B_{1/2} = \frac{\hbar}{g^*_{\mathrm{el},\perp}\mu_B\tau}$, and $g^*_{\mathrm{el},\perp}$ being the transverse electron g-factor. Measuring the Hanle effect is therefore a useful tool to directly determine the reduced lifetime $g^*_{\mathrm{el},\perp}\tau$ of the recombining exciton.

6.1.1 Modifications due to the nuclear field

Equation 6.2 describes the Hanle effect of optically oriented electrons, which can be observed by monitoring the polarization of PL light. This, in turn, depends on the mean electron spin polarization along the direction of light collection. The situation becomes more complicated when taking into account the nuclear spin system and the resulting nuclear magnetic field B_{nuc} that acts on the electron spins. In this case, the magnetic field appearing in (6.1) and (6.2) has to be replaced by $\mathbf{B} = \mathbf{B}_{\mathrm{ext}} + \mathbf{B}_{\mathrm{nuc}}$. By using the low-field dependence of DNSP described by (4.1), the component of $\mathbf{B}_{\mathrm{nuc}}$ relevant in (6.1) can be expressed as $\mathbf{B}_{\mathrm{nuc}} = K\mathbf{B}_{\mathrm{ext}}$, with $K = b_n^* S_0 \frac{B_z + B_{\mathrm{el,z}}}{B^2 + \xi B_{\mathrm{loc}}^2}$ [3]. Since in this expression $B_{\mathrm{el,z}} \propto \langle S_z\rangle$, the resulting equation of motion for the electron spin is nonlinear. Due to the presence of $\mathbf{B}_{\mathrm{nuc}}$, the external magnetic field is "amplified" by a factor $(1+K)$, where the "amplification factor" K can be on the order of 10^6 for transverse magnetic fields $B_{\mathrm{ext},\perp}$ with $B_{\mathrm{ext},\perp} \lesssim B_{\mathrm{el}}$ [3]. As a result, the PL polarization drops upon application of a small transverse magnetic field on the order of the Knight field. For transverse magnetic fields $B_{\mathrm{ext},\perp} \gg B_{\mathrm{el}}$, nuclear spins cannot be polarized anymore because the total magnetic field seen by the nuclei is orthogonal to the direction of electron spin polarization. The Hanle curve therefore falls back to its original Lorentzian lineshape in this magnetic field region. The total resulting depolarization of PL as a function of transverse magnetic field takes the form of a Lorentzian with a "W-shaped" dip of width B_{el} in the center, as illustrated by the numerical simulation shown in Fig. 6.1(a). The "amplification factor" K can in principle take both signs, positive or negative. While in the former case the

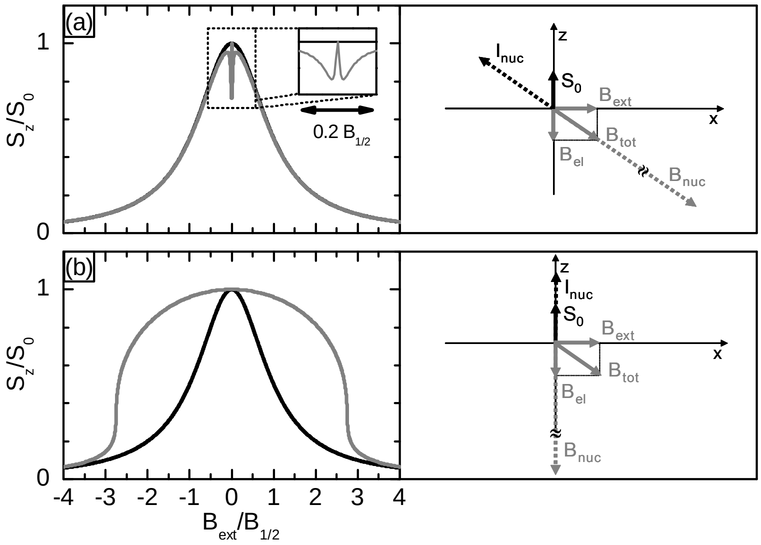

Figure 6.1: (a) Anomalous Hanle effect due to the nuclear field (gray) compared to the normal Hanle effect (black). When B_{ext} is on the order of the Knight field B_{el}, the nuclei see a total magnetic field which is oblique resulting in a tilt of the nuclear spin polarization away from the optical axis z. Since $B_{\text{nuc}} \gg B_{\text{el}}$, B_{ext} is significantly enhanced due to the transverse component of B_{nuc}, resulting in a fast depolarization of the electron spin even in low fields. The corresponding relative orientation of $B_{\text{ext}}, B_{\text{el}}$ and B_{nuc} is shown in the right panel. The orientation of B_{nuc} is drawn for the case $g^*_{\text{el}}\gamma_i < 0$. The parameters used in (a) are $b^*_n = 10\ B_{1/2}$,$B_{\text{loc}} = B_{\text{el}} = 5{\cdot}10^{-3}\ B_{1/2}$ and $S_0 = 0.5$. (b) Anomalous Hanle effect due to the nuclear field, under the influence of quadrupolar interactions (gray). These interactions stabilize the nuclear field along the z-axis, which in turn protects the electron spin from depolarization in a transverse magnetic field. The right panel shows the relative directions of $B_{\text{ext}}, B_{\text{nuc}}$ and B_{el}. The parameters used for simulating the curve in (b) according to the extension of (6.1) discussed in the text are $b^*_n = 10\ B_{1/2}$ and $S_0 = 0.5$

nuclear field aligns with B_{ext} leading to the described narrowing of the Hanle curve, B_{nuc} can compensate B_{ext} and substantially broaden the Hanle curve in the latter case. The sign of $K/\langle S_z\rangle$ (at $B_z = 0$), which distinguishes these two cases, is given by the sign of b^*_n which in turn is given by $-\text{sign}(g_{\text{el}}\gamma_i)$. Since this quantity is positive in our case, we would at first expect a narrowing of the Hanle curve due to nuclear effects in our InAs QDs.

6.1.2 The influence of nuclear quadrupolar interactions

The properties of the nuclear spin system are further modified by taking into account the nuclear quadrupolar interactions (QI). The resulting modifications of the Hanle curve was recently discussed both theoretically and experimentally in [59]. The QI describes the coupling of a nucleus of spin I to electric field gradients. This coupling arises because the charge distribution within a nucleus shows deviations from spherical symmetry, which to first order can be described by a quadrupolar moment Q [60]. For a uniaxial, symmetric electric field gradient $V_{z'z'}$, with its principal axis

z', the resulting Hamiltonian of the nuclear QI is [61]

$$\begin{aligned} H_{\mathrm{Q}} &= \frac{h\nu_Q}{2}\left(\hat{I}_{z'}^2 - \hat{I}^2/3\right), \\ \text{with } \nu_Q &= \frac{3eV_{z'z'}Q}{2I(2I-1)h}, \end{aligned} \tag{6.3}$$

In bulk Zincblende crystalline structures, the electric field gradients at the nuclear sites are zero. However, by applying strain to the structure, the crystal lattice gets distorted and electric field gradients can arise. Due to the strain-driven formation of self-assembled QDs discussed in Sect. 2.2 the electric field gradients can be expected to be particularly strong in the case of the QDs studied here. The symmetry of the QD thereby requires that the mean QD strain axis coincides with the QD growth direction, so that $z' = z$. The electric field gradient can be expressed through the corresponding component of the deformation tensor e_{zz} through the linear relation $V_{zz} = S_{11}e_{zz}$. The constant S_{11} has been measured experimentally for a variety of III-V semiconductors [62] and was found to be $S_{11} = 5.4 \cdot 10^{22}$ V/m^2 for In nuclei in InAs. The exact degree of deformation along the z-axis is difficult to obtain experimentally; atomistic calculations of the structural properties of QDs predict e_{zz} to be in the range $4\% - 8\%$ with the maximum strain in the periphery, and the minimal value in the center of the QD [63]. With the quadrupolar moment for In, $Q_{\mathrm{In}} = 0.76 \cdot 10^{-28}$ m^2, this results in a maximal quadrupolar splitting of $\nu_q \approx 3.3$ MHz corresponding to the Larmor frequency of an In nucleus in an external magnetic field of 3.5 T.

Since the Hamiltonian 6.3 commutes with the operators $\hat{I}$ and $\hat{I}_z$, I and m_z are still good quantum numbers for the nuclear spins. Contrary to a pure Zeeman interaction, the energies corresponding to the states $|I, m_z\rangle$, however, are now proportional to m_z^2, with a constant energy offset. If an external magnetic field B_{ext} is applied to these nuclei, the states $|I, m_z\rangle$ with different $|m_z|$ are not coupled to first order in B_{ext}. Nuclear spin states in an $|m_z|$ manifold can then be treated as effective spin-1/2 particles with a highly anisotropic nuclear gyromagnetic ratio γ [23]. In particular, if a magnetic field $B_{\mathrm{ext},\perp}$ is applied perpendicular to the quantization axis z, γ is zero and the nuclear spins do not feel the presence of $B_{\mathrm{ext},\perp}$ to first order.

In the present QD system, the quantization axis for the quadrupolar Hamiltonian lies along the axis of the growth direction which is perpendicular to the external magnetic field in the Voigt geometry. The nuclear spins are therefore not affected by an applied transverse magnetic field $B_{\mathrm{ext},\perp}$ and B_{nuc} is always oriented along the QD growth direction. The modification of the Bloch equation 6.2 therefore consists in replacing $\mathbf{B}$ by $\mathbf{B}_{\mathrm{ext}} + \mathbf{B}_{\mathrm{nuc}}$, where $\mathbf{B}_{\mathrm{nuc}} = b_n\left(\mathbf{S} \cdot \mathbf{e}_z\right)\mathbf{e}_z$ [59]. Here, $\mathbf{e}_z$ is a unit vector along the QD growth direction and b_n is a fitting parameter denoting the strength of the nuclear field.

With the influence of QI the qualitative picture of the role of the nuclear spins in the Hanle effect changes again. Instead of amplifying small external magnetic fields and thus leading to an enhanced depolarization of the electron spin in $B_{\mathrm{ext},\perp}$, the nuclear spins subject to a strong quadrupolar splitting act as a strong, static magnetic field along the growth direction. This field stabilizes the electron spin and leads to a broadening of the Hanle curve. This is exemplified in Fig. 6.1(b) which shows a numerical solution of (6.1) including the effect of a nuclear field stabilized by the QI.

6.2 Experimental signatures of the nuclear field in Hanle effect measurements

In order to experimentally investigate the two discussed effects of nuclear spins on the Hanle curve of QD excitons, we measured the degree of circular PL polarization ρ_c as a function of transverse magnetic field both on the positively and on the negatively charged excitons in an individual QD. In addition to the PL polarization we monitor the total Zeeman splitting ΔE_Z between the co- and cross-polarized PL peaks with respect to the excitation light polarization. While for small transverse magnetic fields, ΔE_Z is a direct measure of nuclear spin polarization, ΔE_Z arises from the Zeeman interaction of the QD electron with both the transverse external magnetic field $B_{\mathrm{ext},\perp}$ and the longitudinal nuclear magnetic field B_{nuc}.

6.2.1 Negatively charged exciton

We first measure the Hanle effect on the recombination line of X^{-1}. This charge complex consists of two electrons in a singlet state and a single QD hole (cf. Fig. 2.4). After radiative recombination of one of the electrons with the hole, a single electron is left in the QD. The polarization of the emitted photon is thereby determined by the spin polarization of the QD hole right before radiative recombination. The evolution of the hole spin is described by a Bloch equation analogous to (6.1). Since holes do not couple to the nuclear spins in III-V semiconductors (cf. Sect. 3.3) one would expect the corresponding Hanle curve to show no anomalies due to nuclear spins, which would allow for a direct measure of $\tau_{\mathrm{h}} g^*_{\mathrm{h},\perp}$. Fig. 6.2 shows a measurement of the Hanle curve of X^{-1} for σ^+- and σ^--polarized excitation along with the corresponding measurement of ΔE_Z as a function of $B_{\mathrm{ext},\perp}$. For $|B_{\mathrm{ext},\perp}| > 3$ mT, the Hanle curve is well fitted by a Lorentzian of half-width $B_{1/2} = 420$ mT. Assuming that the hole lifetime in the excitonic state is limited by the radiative lifetime of X^{-1}, $\tau_{X^{-1}} \approx 1$ ns [64] the resulting transverse hole g-factor is $g^*_{\mathrm{h},\perp} \approx 0.03$. This value agrees reasonably well with the reported values of $g^*_{\mathrm{h},\perp}$, which are greatly reduced compared to the longitudinal g-factor $g^*_{\mathrm{h},\parallel}$ due to the heavy-light hole splitting in structures of reduced dimensionality [65]. Apart from the expected Lorentzian dependence on $B_{\mathrm{ext},\perp}$, ρ_c shows an anomalous feature at $|B_{\mathrm{ext},\perp}| < 3$ mT (cf. Fig. 6.1(a)). We attribute this "spike" at $B_{\mathrm{ext}} = 0$ to the tilting of B_{nuc} upon application of transverse external magnetic fields on the order of B_{el}, as discussed above. It is at first surprising that the PL polarization of X^{-1} depends on nuclear spin polarization. However, while the spin of the QD hole is not expected to couple to nuclear spins directly, the nuclear field can stabilize the hole spin during relaxation from the p-shell in which it was created to the s-shell in which it recombines. Such an effect was already discussed both in Chap. 4 and Chap. 5, where the observed correlation between nuclear spin polarization and PL polarization (Fig. 4.2 and Fig. 5.2, respectively) was assigned to a competition between hyperfine interaction and exchange coupling in the intermediate neutral exciton state, which occurs during carrier spin relaxation through

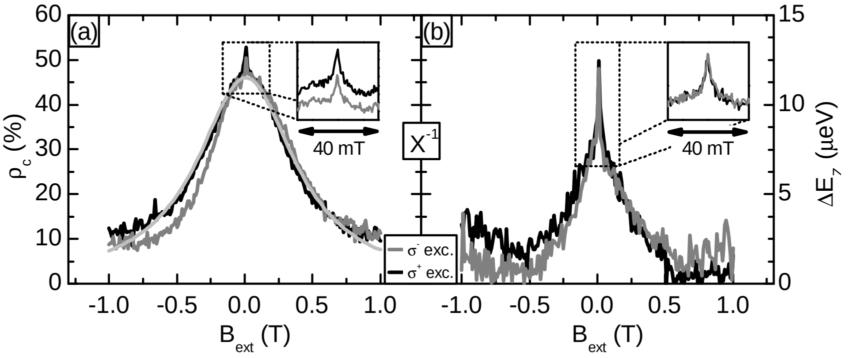

Figure 6.2: Measurement of PL polarization (Hanle curve, (a)) and exciton Zeeman splitting (b) of X^{-1} as a function of transverse magnetic field strength. The insets show a close-up of the corresponding curves over a width of 40 mT around $B_{\text{ext}} = 0$. For larger fields, the Hanle curve fits well to a Lorentzian of half-width $B_{1/2} = 420$ mT, corresponding to $\tau_{\text{h}} g^{*}_{\text{h},\perp} = 20$ ps. The central feature of half width ~ 2 mT is a signature of the strong longitudinal nuclear field, which preserves the hole spin during relaxation from the p- to the s-shell. The exciton Zeeman splitting ΔE_{Z} shows the same feature which arises from a tilting of the nuclear polarization upon application of a weak external magnetic field on the order of B_{el}. Due to the stabilizing effect of quadrupolar interactions, signatures of nuclear spin polarization can be seen in ΔE_{Z} for transverse magnetic fields of up to 500 mT

the electron reservoir. The data presented in Fig. 6.2(a) therefore has a qualitative difference to the Hanle curve described in Fig. 6.1(a): In the present case, the form of the Hanle curve is a consequence of the stabilizing effect of the longitudinal component of B_{nuc} on the hole spin during relaxation, while in the previously discussed case it is a consequence of the depolarizing effect of the transverse component of B_{nuc} on the electron spin before recombination. This qualitative difference explains, why we do not observe the recovery of the PL polarization as soon as $B_{\text{ext},\perp} > B_{\text{nuc}}$ that is apparent in Fig. 6.1(a). The anomalous behavior of ρ_c around $B_{\text{ext}} = 0$ is accompanied by a corresponding decrease of DNSP upon application of $B_{\text{ext},\perp}$ on the order of 3 mT. This further confirms the correlation between nuclear spin polarization and the degree of polarization of X^{-1} PL light.

The measurement of ΔE_Z is performed by calculating a weighted average over the exciton emission peaks in co- and cross circular polarization detection with respect to the excitation light polarization[1], a technique discussed in more detail in Sec. 2.4. While this is a direct measurement of the nuclear magnetic field, as long as $B_{\text{ext},\perp}$ is small (cf. Sect. 3.3), the situation gets more complicated, when the transverse field is on the order of the nuclear field (i.e. $|B_{\text{ext},\perp}| \gtrsim 500$ mT). In this case, $B_{\text{ext},\perp}$ leads to a mixing of the electron spin states in the final state of exciton recombination, and discriminating the emission peaks of the two exciton spin states by the polarization of the emitted light is no longer possible. Using larger external magnetic fields on the order of $3-6$ T (not shown here), we were able to resolve the splitting of the PL emission line without relying on polarization discrimination. We can thereby determine the transverse excitonic g-factor which we find to be $g^*_{\mathrm{ex},\perp} = 0.46$. The corresponding Zeeman splitting of $\sim 10\ \mu\mathrm{eV}$ that we expect for $|B_{\mathrm{ext}}| = 500$ mT can not be resolved by our spectrometer. We therefore believe that the features of the exciton Zeeman splitting ΔE_Z that we observe for $|B_{\mathrm{ext}}| \lesssim 500$ mT are due to DNSP. The fact that we observe effects of nuclear spin polarization in transverse magnetic fields of up to 500 mT is a clear indication that the stabilizing effect of nuclear QI is significant in our QD structures. We will further study these effects by investigating the Hanle effect on the positively charged exciton.

---

[1] In order to establish the necessary symmetry upon reversal of the sign of B_{ext}, we subtracted a linear offset of -3.25 μeV/T from the data presented in Fig. 6.2(b). This offset might be due to a slight misalignment between B_{ext} and k.

6.2.2 Positively charged exciton

Studying the Hanle effect on X^{+1} allows for a direct measurement of the spin of the QD electron before exciton recombination (cf. Fig. 2.4). X^{+1} consists of two holes in a singlet state and a single electron. It decays radiatively to a state with a single hole in the QD. The polarization of the emitted photon is therefore determined by the spin polarization of the QD electron before radiative recombination. As we showed in Chap. 4, excitation of X^{+1} can lead to a substantial degree of nuclear spin polarization and we therefore expect the Hanle curve to show deviations from a Lorentzian due to the nuclear magnetic field. Fig. 6.3(a) shows measurements of the Hanle effect on X^{+1} with light of constant circular polarization as well as under a 2 kHz square-wave polarization modulation from σ^+ to σ^-. If the helicity of the excitation light is constant, the Hanle curve is broadened and highly distorted from a Lorentzian. This is a consequence of DNSP of nuclear spins experiencing a strong QI. Furthermore, the nonlinearity induced by the nuclear field scales with both the degree of PL polarization and the degree of nuclear spin polarization as one can see by comparing the data obtained under σ^+- and σ^--polarization. At $|B_{\mathrm{ext},\perp}| = 570$ mT, the stabilizing effect of the nuclear field on electron spin polarization breaks down and the curves for constant excitation light polarization coincide with the one where the excitation polarization was modulated[2]. Even though the cross-over between these two regimes is rather abrupt, we did not observe any effect of hysteresis as a function of $B_{\mathrm{ext},\perp}$ in this measurement, although this might be expected due to the nonlinearity that arises from including a nuclear field $\mathbf{B}_{\mathrm{nuc}} \propto \mathbf{B}_z$ to (6.1). Furthermore, taking into

---

[2] We note that the symmetry with respect to the sign of B_{ext} of the data shown in Fig. 6.3(a) strongly depends on the exact angle θ between the magnetic field and the sample growth direction. In order to observe the symmetric curves presented here, the magnetic field had to be tilted away from the sample normal by $\theta \approx 1.5° \pm 0.1°$ for one QD and by $\theta \approx 0.5° \pm 0.1°$ for another dot. This observation could be explained by the direction z' of the principal axis of strain, which might deviate slightly from the sample growth direction z and which will vary from dot to dot. If θ deviated by more than $\sim 0.1°$ form the indicated values, the Hanle curves became asymmetric upon reversal of sign(B_{ext}) but remained symmetric under the simultaneous reversal of sign(B_{ext}) and the helicity of the excitation light.

Furthermore, we could drastically modify the exact shape of the Hanle curves by changing the energy of the excitation laser to another p-shell resonance. Most of these resonances showed qualitatively the same behavior as the presented data. In some cases, however, the Hanle curves obtained under polarization modulated excitation were identical to the ones obtained without the modulation and both showed strong deviations from a Lorentzian. In these cases the shape of the Hanle curve was not due to nuclear effects but rather a consequence of the Larmor precession of carriers during p- to s-shell relaxation which can also strongly influence the shape of the Hanle curve [23].

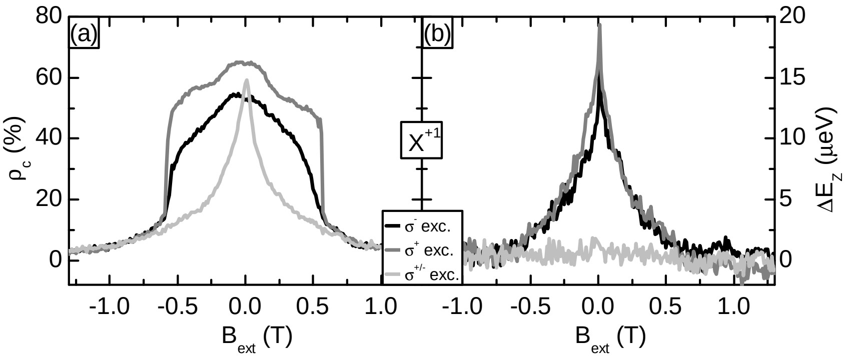

Figure 6.3: Hanle curve (a) and exciton Zeeman splitting (b) of X^{+1} as a function of transverse external magnetic field under excitation with light of constant helicity and modulation of the excitation light helicity at 2 kHz. Under excitation with constant light polarization, strong distortions of the Hanle curve occur due to the effect of nuclear spin polarization, stabilized by quadrupolar interactions, which is qualitatively described by (6.1) and its modification due to the nuclear spins discussed in the text. The exciton Zeeman splitting shows a very similar behavior as in the case of X^{-1} excitation, indicating that the Knight field B_{el} is on the same order for X^{-1} and X^{+1} excitation

account the Bloch equation 6.1 and its modification due to B_{nuc} only, we were not able to obtain a quantitative fit to the experimental data presented in Fig. 6.3. The exciton Zeeman splitting ΔE_Z measured on X^{+1} (Fig. 6.3(b)) shows a very similar behavior to the one measured on X^{-1} (Fig. 6.2(b))[3]. This makes sense, since DNSP is comparable for the two cases at $B_{\mathrm{ext}} = 0$ and the response of the nuclear spin system in transverse magnetic fields should be identical between X^{+1} and X^{-1}. The narrow, central feature of ΔE_Z around $B_{\mathrm{ext}} = 0$ which shows the reduction DNSP in transverse magnetic fields on the order of B_{el} indicates that B_{el} is on the same order in X^{+1} and X^{-1}. Surprisingly, this feature in ΔE_Z is not accompanied by a corresponding change of ρ_c of X^{+1} PL light around $B_{\mathrm{ext}} = 0$.

The Hanle curve obtained under modulated excitation polarization has Lorentzian wings but shows an unexpected behavior at $B_{\mathrm{ext}} = 0$, where it has a pronounced “cusp”. This behavior is independent of the frequency of helicity modulation within the experimentally accessible range of modulation frequencies of up to 100 kHz. For modulation frequencies slow enough to allow for the buildup of a nuclear spin polarization (i.e. $\lesssim 100$ Hz), the Hanle curve gradually changes its shape towards the one observed under constant excitation polarization. Hanle curves with a “cusp” at $B_{\mathrm{ext}} = 0$ have been observed earlier [23] and have been attributed to a combination of diffusion of electrons to local traps and simultaneous Larmor precession of the spin of these electrons in B_{ext}. This explanation, however, seems unlikely for our system, where exciton creation happens directly in the QD and carrier diffusion should play no role. Another explanation of the “cusp” at $B_{\mathrm{ext}} = 0$ could be the existence of a small degree of DNSP which is able to follow the modulated light helicity. This fast component of nuclear spin polarization would then lead to an additional stabilization of the electron spin at zero magnetic field.

---

[3] We again subtracted a linear offset of 3 μeV/T from the data presented in Fig. 6.3(b).

6.2.3 Conclusion

The presented Hanle curves of singly charged excitons show signatures of both the tilting of B_{nuc} upon application of a small external magnetic field on the order of B_{el} and the stabilizing effect of QI which fix the axis of nuclear spin polarization in space. At first, these two observations seem to contradict each other. However, the strain in self-assembled QDs is highly non-uniform, inhomogeneous and can even change sign from negative (compressive) to positive (expansive) [63]. It is therefore reasonable to assume that for a certain class of QD nuclei the strain is sufficiently small or suitably oriented [23] to be neglected for the discussed experiments. This class of nuclei would then cause the low field effects observed in Fig. 6.3 and Fig. 6.2(b). In this scenario, the degree of DNSP of nuclei being stabilized by QI would be coupled to the orientation of the remaining nuclei via the QD electron: Tilting B_{nuc} by a small external magnetic field leads to depolarization of the electron spin, which in turn reduces the degree of DNSP of the nuclei which were stabilized by QI. Therefore, even if the total number of nuclei which do not experience any strain is small, the resulting effect on DNSP in $B_{\text{ext},\perp}$ on the order of B_{el} could be large and explain the corresponding, large signatures in Fig. 6.3(b) and Fig. 6.2(b).

Our discussion of the experimental Hanle curves shows that by using (6.1) and its discussed extensions arising from DNSP, we can only qualitatively reproduce the experimental data. Therefore, our model is probably too simplistic to fully describe the influence that QI have on the optical orientation of QD nuclei. In this model, we assumed the main strain axis in the QD to be aligned with the growth direction. While this is a reasonable approximation after averaging over all nuclei, this assumption is violated for most nuclei in the QD. As a result, the transverse, nuclear g-factor will not be zero for most QD nuclei and will alter the description of the nuclear spin system in transverse magnetic field. Also, since the maximal transverse magnetic field applied in our experiment comparable to the quantity $h\nu_q/\gamma$, characterizing the QI, it might be necessary to consider the full quadrupolar and Zeeman Hamiltonian to accurately describe the nuclear spin system. Furthermore, not only the direction, but also the magnitude of strain that the different nuclei experience varies over the dot [63]. This is already apparent from the fact that at least a certain subset of nuclei react to external magnetic fields on the order of the Knight field, leading to the corresponding experimental signatures around $B_{\text{ext}} = 0$ (as shown in the insets in Fig. 6.2). A full description of the QD nuclear spin system should take these inhomogeneities and the effect of the large transverse magnetic field into account and could potentially give a more quantitative description of our experimental findings. An interesting experimental complement would be the observation of nuclear magnetic resonance from a single QD. Judging from the data presented in Fig. 6.2 and 6.3 the quadrupolar shifts and broadenings of the resonance lines should be substantial and would allow for a further investigation of the influence of QI on QD nuclear spins. We note however, that if the resulting broadening of the NMR line is too strong, observation of optically detected NMR from a single dot might be practically impossible.

7 Time-resolved Measurement of Nuclear Spin Polarization

This chapter describes time-resolved measurements of the nuclear spin polarization in an individual quantum dot. It is found that the number of excess quantum dot charges has a big influence on the lifetime of nuclear spin polarization. Furthermore, the dependence of nuclear spin lifetime on external magnetic fields is studied in two distinct regimes. In magnetic fields below one mT, nuclear dipole-dipole interactions greatly reduce the nuclear spin lifetime. Conversely, in fields on the order of one T, the decay of nuclear spin polarization is very slow and non-exponential due to the nonlinear character of the electron-nuclear spin system.

A key ingredient for the understanding of the coupled electron-nuclear spin system is the knowledge of the relevant timescales of the dynamics of nuclear spin polarization. This has already become apparent in Chap. 5, where (5.4) shows that the maximal nuclear spin polarization in a QD is limited by the ratio of buildup and decay times of the nuclear spins. Many other aspects like the respective roles of nuclear spin diffusion, quadrupolar relaxation and trapped excess QD charges influence the dynamics of DNSP and remain essentially unexplored up to now. While the buildup time of DNSP (τ_{buildup}) is likely to depend on the way the nuclear spin system is addressed, the DNSP decay time (τ_{decay}) is an inherent property of the isolated nuclear spin system of a QD. Furthermore, experimental determination of τ_{decay}, which directly yields the correlation time of the fluctuations of the Overhauser field along the axis in which the nuclei are polarized, can be crucial for understanding the limits of electron spin coherence in QDs [18].

7.1 Dynamics of nuclear spin polarization in low magnetic fields

7.1.1 Technique for time-resolved measurement of nuclear spin polarization

In order to study the buildup and decay of DNSP, we extended our standard PL setup (Sect. 2.4) by the ability to perform “pump-probe” measurements [20]. An acousto-optical modulator (AOM) served as a fast switch of excitation light intensity, producing light pulses of variable lengths, with rise- and fall-times $\ll 1\ \mu$s (details about the AOM setup are given in Appendix A.1). We differentiate between “pump” pulses of duration τ_{pump}, used to polarize the nuclear spins, followed by "probe" pulses of length τ_{probe}, used to measure the resulting degree of DNSP. The intensity of each pulse corresponds to the saturation intensity of the observed emission line, maximizing both the resulting OS and the signal to noise ratio (SNR) of the measurement. A mechanical shutter placed in the PL collection path is used to block the pump pulses while allowing the probe pulses to reach the spectrometer. Pump and probe pulses are separated by a waiting time τ_{wait} with a minimal length of 0.5 ms, limited by the jitter of the shutter opening time. In order to measure the buildup (decay) time of DNSP, τ_{pump} (τ_{wait}) are varied, respectively, while keeping all other parameters fixed. The timing and synchronization of the pulses is computer controlled via a digital acquisition card operating at a clock period of 2 μs, which sets the time resolution of the pulse sequences. Individual pump-probe sequences are repeated while the signal is accumulated on the spectrometer CCD in order to obtain a reasonable SNR. We verify a posteriori that individual pump-probe pairs are separated by much more than the measured DNSP decay time.

7.1.2 Buildup and decay of nuclear spin polarization

Figure 7.1(b) and (c) show the results for buildup and decay curves of DNSP obtained with this technique. The resulting curves fit surprisingly well to a simple exponential, yielding $\tau_{\text{buildup}} = 9.4$ ms and $\tau_{\text{decay}} = 1.9$ ms[1]. The small residual OS observed for $\tau_{\text{pump}} = 0$ ($\tau_{\text{wait}} \gg \tau_{\text{decay}}$) in the buildup (decay) time measurement is due to the nuclear polarization created by the probe pulse. Comparing our experimental findings to previous experiments is not straightforward, since, to the best of our knowledge, the dynamics of DNSP at zero external magnetic field has not been studied up to now. However, in experiments performed at external magnetic fields of ~ 1 T, the buildup time of DNSP in QDs was estimated to be on the order of a few seconds [19, 50]. A further shortening of τ_{buildup} arises from the strong localization of carriers in our QDs, which has been shown to be an important ingredient for efficient nuclear spin polarization [37]. Localization of electrons increases the mean value of the Knight field (3.7) and therefore increases the rate of electron-mediated nuclear spin relaxation given by (5.1). Most strikingly, previous experimental results in similar systems revealed DNSP decay times on the order of minutes [36]. It is thus at first sight surprising that we find a DNSP decay time as short as a few milliseconds.

7.1.3 Electron mediated nuclear spin decay

A possible cause for the fast decay of DNSP is the presence of the residual QD electron even in the absence of optical pumping. We study its influence on τ_{decay} with the following experiment: While the nuclear spin polarization is left to decay, we apply a voltage pulse to the QD gate electrodes, ejecting the residual electron from the QD into the nearby electron reservoir. This is achieved by switching the QD gate voltage to a value where the dominant spectral feature observed in PL stems from

---

[1] The rate equation model presented in Chap. 5 predicts deviations from an exponential dependence due to the feedback of DNSP on the nuclear spin cooling rate. However, the limited SNR of our experiment and the finite length of the probe pulses do not allow us to observe these deviations at zero magnetic field.

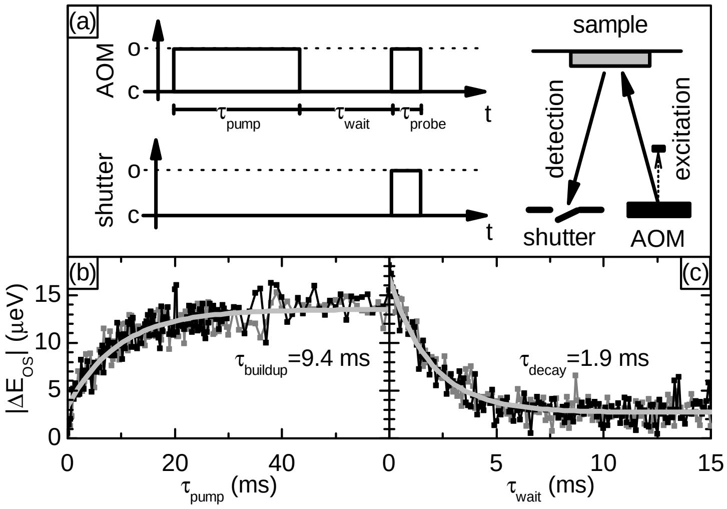

Figure 7.1: (a) Schematic of the pulse sequences used in the buildup and decay time measurements of DNSP. An acousto optical modulator (AOM) deflects the excitation beam on and off the sample, serving as a fast switch (o (c) denote the open (closed) state, respectively). The AOM creates pump (probe) pulses of respective lengths τ_{pump} (τ_{probe}), separated by a waiting time τ_{wait}. A mechanical shutter blocks the pump pulses from reaching the spectrometer, while letting the probe pulses pass. (b) DNSP buildup curves obtained by varying τ_{pump} at fixed τ_{wait} (0.5 ms) and τ_{probe} (0.2 ms). The gray (black) data points correspond to QD excitation with light of positive (negative) helicity. The light gray line is an exponential fit, yielding a buildup time of $\tau_{\mathrm{buildup}} = 9.4$ ms. (c) DNSP decay curves obtained by varying τ_{wait} at fixed τ_{pump} (50 ms) and τ_{probe} (0.5 ms). The color coding is identical to (a). The exponential fit reveals a decay time of $\tau_{\mathrm{decay}} = 1.9$ ms

the recombination of the neutral exciton. Using transient voltage pulses, we are able to perform this "gate voltage switching" on a timescale of 30 μs, which is verified by an experiment which is discussed in detail in Appendix A.2. Before sending the probe pulse onto the QD, the gate voltage is switched back to its initial value in order to collect PL from X^{-1} recombination. The dramatic effect of this gate voltage pulsing on DNSP lifetime is shown in Fig. 7.2(b). On the timescale of the previous measurements, almost no DNSP decay can be observed. By prolonging τ_{wait} up to a few seconds (Fig. 7.2(c)), we estimate the spin decay time of the unperturbed nuclear system to be $\tau_{\mathrm{decay}} \approx 2.3$ s. We note that the increase of τ_{wait} necessary for this experiment results in a reduced SNR, which makes an exact determination of τ_{decay} difficult.

7.1.4 Control experiments

The role of the residual electron in depolarizing the nuclear spins was further confirmed in two independent control experiments. First, we performed a modified version of the gate voltage switching experiment. We polarize the nuclear spins at a gate voltage V_1 (corresponding to the center of the 1-e^- occupation window in gate voltage) with a pump pulse of length $\tau_{\mathrm{pump}} = 50$ ms. After this, we immediately switch the gate voltage to a value V_2, where we let the nuclei evolve for a

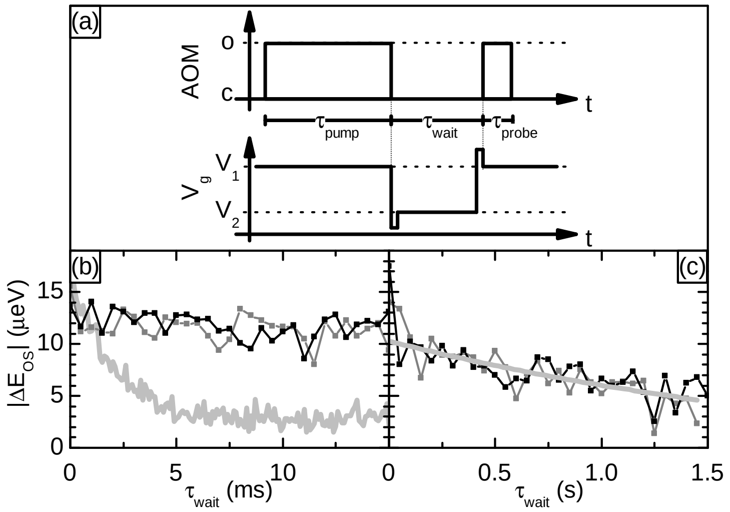

Figure 7.2: (a) Timing diagram for the gate voltage switching experiment: DNSP is established at a gate voltage V_1, corresponding to the center of the X^{-1} stability plateau. During the period τ_{wait}, the QD gate voltage is switched to a value V_2 and the nuclei are left to decay. Using transient pulses, the switching time is 30 μs. (b) Measurement of DNSP decay, with V_2 corresponding to the center of the X^0 stability plateau. As a result, the residual QD electron is ejected during DNSP decay, which dramatically increases DNSP lifetime. The gray (black) data points represent DNSP decay under σ^+- (σ^--) excitation. For comparison, the light gray curve shows the mean of the data presented in Fig. 7.1(b). (c) Same measurement as in (b), but over a longer timescale. The exponential fit (light gray) indicates a decay time constant of $\tau_{\text{decay}} \approx 2.3$ s

time $\tau_{\text{wait}} = 20$ ms. We measure the final degree of nuclear spin polarization with a probe pulse of length $\tau_{\text{probe}} = 1$ ms at the initial gate voltage V_1. Fig. 7.3 shows the resulting OS as a function of the gate voltage V_2 at which the nuclei were left to evolve freely. One can clearly distinguish regions of fast and slow DNSP decay, corresponding to QD occupations with an even or odd number of electrons, respectively. We can increase the number of electrons in the QD up to four. After this point, the diode structure used for QD gating (cf. Fig. 2.3) becomes conductive due to the large applied bias voltage and the QD as well as the WL become completely filled with electrons. The stepwise increase of the QD charge as a function of V_g is accompanied by corresponding changes in the PL spectra (Fig. 2.5)[28], which allow us to determine the absolute number of electrons in the QD.

When two electrons occupy the QD ground state (for 0.1 V$\lesssim V_g \lesssim 0.35$ V), the Pauli principle ensures that they form a spin singlet state, which does not couple the QD nuclei, resulting in a prolonged lifetime of DSNP on the order of seconds. The third electron occupies the next QD orbital (the p-shell), where it can again interact with the QD nuclei and lead to a fast depolarization of nuclear spins on a ms timescale. Injecting a fourth electron into the QD at $V_g \approx 0.6$ V increases DNSP lifetime again. This last observation is at first surprising, since Hunds rule states that the first two electrons occupying the p-shell of a QD should form a spin triplet at $B_{\text{ext}} = 0$ [27] and should therefore still couple to the QD nuclei. Assuming a symmetrical, harmonic QD confinement potential, the singlet-triplet splitting in

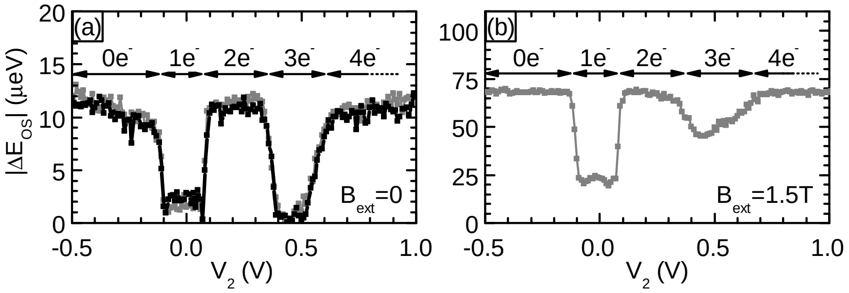

Figure 7.3: (a) Nuclear spin polarization after free evolution of the nuclear spins at a gate voltage V_2. DNSP lifetime has a strong dependence on the charging state of the QD at $V_g = V_2$. If the number of QD electrons is odd, DNSP decays in a ms-timescale, while the decay takes seconds for an even number of electrons. The QD electron occupation number as extracted from a V_g dependent PL measurement is indicated in the figure. Gray (black) data points correspond to QD excitation with σ^+- (σ^--) polarized light; the measurement sequence is the same as for Fig. 7.2, the timing parameters are $\tau_{\text{buildup}} = 50$ ms, $\tau_{\text{wait}} = 20$ ms and $\tau_{\text{probe}} = 1$ ms. (b) Same measurement as in (a) but at $B_{\text{ext}} = 1.5$ T. The behavior of τ_{decay} as a function of V_2 is qualitatively different on the $1e^-$-plateau compared to the $3e^-$-plateau. This is a consequence of motional narrowing, which will be discussed in Chap. 7.2

the p-shell can be extracted from spectral features of PL of X^{-3} [66]. Based on this estimate, this splitting should be on the order of 1 meV in our QDs. However ,the splitting can be reduced for deformed QDs with a broken cylindrical symmetry [67] or even for cylindrically symmetric QDs if the atomistic symmetry of the underlying Zincblende lattice is taken into account [68]. Under these circumstances, Hunds rule is violated and the first two p-shell electrons occupy the same orbital, where they form a spin singlet state. Our data suggests that this scenario is indeed the case for the QD under investigation. It is interesting to note that in this case, the QD nuclear spins act as a probe for the properties of the QD and allow for an efficient test of Hunds rule (in the p-shell) of an individual QD.

The second control experiment we performed, consisted in measuring DNSP dynamics at a constant gate voltage where X^{+1} is the stable QD charge complex (the data is not shown here). As we showed in Chap. 4, optically pumping the X^{+1} exciton can also lead to DNSP. However, in this case, the optically created electron polarizes the nuclear spins and no electron is left in the QD after the pump pulse is turned off. The corresponding DNSP decay channel is therefore not present. As expected, τ_{decay} is also on the order of seconds for this case.

7.1.5 Mechanisms for the electron-mediated nuclear spin decay

We argue that two mechanisms could lead to the efficient decay of DNSP due to the residual QD electron. The first mechanism is caused by the randomization of the electrons spin through co-tunnelling to the close-by electron reservoir. Co-tunnelling happens on a timescale of $\tau_{\text{cot}} \approx 3$ ns for the structure studied in this work [30]. The resulting electron spin depolarization is mapped onto the nuclear spin system via hyperfine flip-flop events. Taking into account the detuning $\Delta E^{\text{Z}}_{\text{el}}$ of the two electron spin levels and using (5.1), the nuclear spin depolarization rate can be estimated to be $T_{1e}^{-1} \approx (A/N\Delta E_{\mathrm{el}}^{\mathrm{Z}})^2/\tau_{\mathrm{cot}}$ [23]. In order to get a rough estimate of the resulting timescale, we take $\Delta E_{\mathrm{el}}^{\mathrm{Z}}$ to be constant and equal to half the maximum measured OS. With these values, we obtain a nuclear spin depolarization time on the order of 10 ms, roughly consistent with our measurement.

A second possible mechanism is the indirect coupling of nuclear spins due the presence of a QD (conduction band) electron [34]. While this process conserves the total angular momentum of the nuclear spin system, it can lead to a decay of the OS by re-distributing the nuclear spin polarization within the QD and by increasing the nuclear spin diffusion rate out of the QD. The resulting decay rate for the nuclear field has been estimated to be on the order of $T_{\mathrm{ind}}^{-1} \simeq A^2/N^{3/2}\Delta E_{\mathrm{el}}^{\mathrm{Z}}$ as discussed in Sect. 3.4. The corresponding estimate for τ_{decay} of approximately 1 ms was obtained for an unpolarized nuclear spin system and in the limit of $\Delta E_{\mathrm{el}}^{\mathrm{Z}} \gg A$. Since this estimate was a "worst case scenario" as discussed in Sect. 3.4 and since the approximation $\Delta E_{\mathrm{el}}^{\mathrm{Z}} \gg A$ is not valid in our case, giving a correct estimate for the corresponding timescale of DNSP decay seems difficult for our situation.

7.1.6 Low field nuclear spin dynamics

Our study of DNSP timescales was complemented by adding a permanent magnet to our sample. The resulting magnetic field is antiparallel to the excitation beam direction and has a magnitude of $B_{\mathrm{ext}} = -220$ mT at the site of the QD. The buildup and decay time measurements in the presence of B_{ext} are shown in Fig. 7.4. In accordance with the discussion of Chap. 5, an asymmetry between the cases of σ^+- and σ^--excitation is observed. The situation where B_{nuc} opposes B_{ext} is more efficient than the one where B_{nuc} aligns with B_{ext}; equilibrium is therefore reached faster and at a higher nuclear spin polarization in the first case, which corresponds to σ^--excitation for the present magnetic field direction. The measurements presented in Fig. 7.4(a) and (b) confirm this picture: we find that τ_{buildup} and τ_{decay} are both increased by a factor of $\sim 2-3$ when the polarization of the excitation light is changed from σ^- to σ^+.

We again performed the "gate voltage switching" experiment in the presence of B_{ext} (Fig. 7.4(c)). Since in this case DNSP decay is not mediated by the residual QD electron, no dependence of τ_{decay} on excitation light helicity was found and only the average between the two data sets (σ^+- and σ^--excitation) is shown. Compared to the case of zero external magnetic field, the decay of nuclear spin polarization is further suppressed. Even though extracting exact numbers is difficult in this case due to the required long waiting times, we estimate τ_{decay} to be on the order of a minute. This further suppression of DNSP decay rate can be induced with a magnetic field as small as ~ 1 mT as shown in the inset of Fig. 7.4(c): Keeping $\tau_{\mathrm{wait}} = 1$ s fixed, we sweep an external magnetic field while measuring the remaining OS. The resulting dip around $B_{\mathrm{ext}} = 0$ has a half-width of ~ 1 mT. This indicates that nuclear spin depolarization at zero magnetic field is governed by the non-secular terms of the nuclear dipole-dipole interactions (3.4) which can be suppressed by applying an external magnetic field that exceeds the local dipolar field $B_{\mathrm{loc}} \approx 0.1$ mT [23]. The exact nature of this zero field decay of DNSP, however, is still unclear since nuclear dipole interactions should depolarize the nuclear spins at zero field in a much shorter time on the order of $T_2 \approx 10-100$ μs. Furthermore, upon application of the probe

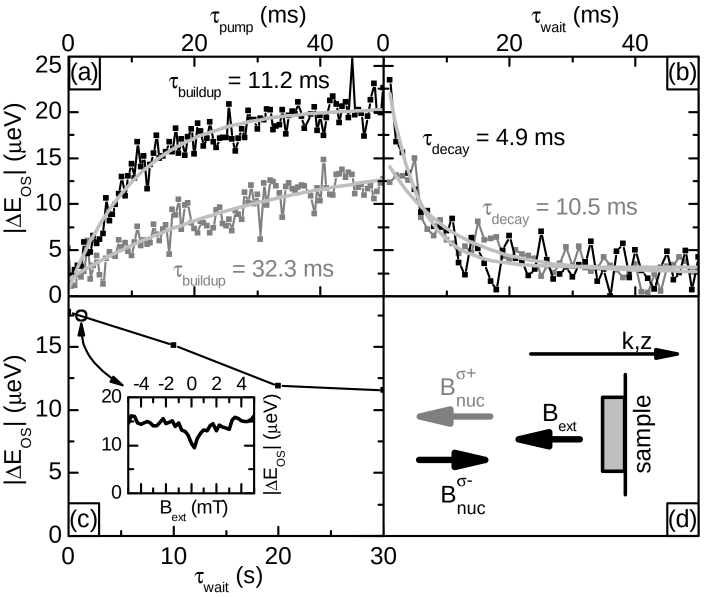

Figure 7.4: Measurements of buildup and decay of DNSP in an external magnetic field $B_{\mathrm{ext}} \approx -220$ mT: (a) Buildup of DNSP. In the presence of B_{ext}, it is more efficient and thus faster to produce a nuclear magnetic field compensating the latter (black, σ^--excitation) than one that enforces it (gray, σ^+-excitation). (b) If DNSP decay is mediated through the residual QD electron, it is again more efficient to depolarize the nuclei if the total effective magnetic field seen by the electron is minimized. The color coding is the same as in (a). Solid curves in (a) and (b) show exponential fits to the data, the resulting buildup- and decay times are given in the figures. (c) Decay of DNSP in the absence of the QD electron. Compared to the zero-field case (Fig. 7.2(c)), DNSP decay time is prolonged to $\tau_{\mathrm{decay}} \approx 60$ s. The inset shows OS after a waiting time of $1s$ as a function of external magnetic field. DNSP decay is suppressed on a magnetic field scale of ~ 1 mT, indicative of DNSP decay mediated by nuclear dipole-dipole interactions. (d) shows the respective directions of the external magnetic field and the nuclear fields $B_{\mathrm{nuc}}^{\sigma^+}$ ($B_{\mathrm{nuc}}^{\sigma^-}$) induced by QD excitation with σ^+- (σ^--) polarized light

pulse which generates a Knight field in the QD, DNSP should reappear due to the long lifetime of nuclear spin temperature (cf. Sect. 7.1.7). We speculate that an interplay of nuclear dipolar interactions and quadrupolar shifts could explain this experimental results at low magnetic fields.

We also investigated the possible role of nuclear spin diffusion and the resulting DNSP of the bulk nuclei surrounding the QD. For this purpose, we studied the dependence of τ_{decay} on the nuclear spin pumping time τ_{pump} for $\tau_{\mathrm{pump}} \gg \tau_{\mathrm{buildup}}$ in the absence of the QD electron. A nuclear spin polarization in the surrounding of the QD would lead to an increase of τ_{decay} with increasing τ_{pump}[36]. However, within the experimental parameters accessible to our experiment, we were unable to see such a prolongation and hence any effect of polarization of the surrounding bulk nuclei. We interpret this fact as a strong indication that we indeed create and observe a very isolated system of spin polarized nuclei. The QD boundaries constitute a barrier for spin diffusion and the small remaining flux of nuclear spin polarization is too low to saturate the bulk material surrounding the dot.

7.1.7 Spin temperature considerations for the pump-probe measurements

To further test the influence of the probe pulse on the measured degree of DNSP, we tested how our experimental results depend on the polarization of the probe pulse. We repeated all experiments presented in this section using probe pulses both with linear polarization or with orthogonal polarization with respect to the pump pulse. This test revealed that our experimental findings are independent of the polarization of the pump pulse. While for experiments performed in the presence of an external magnetic field this shows that our probe pulses indeed does not alter the nuclear spin polarization, this observation is surprising for experiments in zero magnetic field. As we discussed in Sect. 3.2, in the absence of external magnetic fields, nuclear spin polarization is destroyed on a timescale $T_2 \approx 10 - 100$ μs by nuclear dipole-dipole interactions. At the same time, nuclear spin temperature has a lifetime $T_1 \gg T_2$, even at zero magnetic field (see [23], Chap. 5). In Chap. 4, we interpreted our experimental observation of DNSP at zero magnetic field with the presence of a relatively strong Knight field during optical pumping of QD nuclear spins. Since this Knight field is zero in the absence of laser excitation, one would expect DNSP to decay within a time T_2 after switching off the pump pulse. The probe pulse arriving after τ_{wait} (with $T_2 < \tau_{\text{wait}} < T_1$) would then lead to the reappearance of DNSP oriented along the Knight field created by the probe pulse. This is a consequence of the fact that by adiabatically ramping the B_{ext} to zero and back to a finite value in a time smaller than T_1, the nuclear spin temperature, but not necessarily the nuclear angular momentum is conserved. If the helicity of the pump pulse is switched with respect to the probe pulse, the Knight field created by the probe pulse opposes the one created by the pump pulse and we would expect a reversal of the nuclear spin polarization compared to the case of co-circularly polarized pump and probe pulses. The fact that we do not see this reversal of the sign of DNSP suggests that the nuclear T_2 time is on the order of T_1 for the QD nuclear spin system. A possible reason for this could be the strong nuclear quadrupolar interactions in QDs [59] (cf. Chap. 6) which can partly suppress the effect of nuclear dipole-dipole interactions [69].

The switching of the pump and probe pulses in our experiment occurred on timescales of a few 100 ns as mentioned in Sect. 7.1.1. Since this timescale is much shorter than the nuclear T_2^* time, the analysis of the nuclear spin dynamics at low external magnetic fields has to be done carefully. If DNSP at $B_{\text{ext}} = 0$ is indeed enabled by the Knight field of the QD electron, the fast switching of the pump and probe pulses constitutes a non-adiabatic change of the magnetic field the nuclei experience, which might in principle affect the nuclear spin polarization. The behavior of the nuclear spin temperature under a non-adiabatic change of the external magnetic field has been treated in [38]. It was found that if the magnetic field was non-adiabatically switched from an initial value B_i to a final value B_f, the corresponding inverse nuclear spin temperatures $\beta_i (= 1/k_{\text{B}} T_i)$ and $\beta_f (= 1/k_{\text{B}} T_f)$ were related through

$$\beta_f = \beta_i \frac{B_i B_f + B_{\text{loc}}^2}{B_f^2 + B_{\text{loc}}^2}. \tag{7.1}$$

In the case of DNSP at zero magnetic field, the initial magnetic field value is given by the Knight field, $B_i = B_{\mathrm{el}}$, while, after switching off the excitation light, the final magnetic field is zero. Iterating (7.1) twice, we can relate the inverse nuclear spin temperature at the beginning of the probe pulse with the one at the end of the pump pulse. We denote these respective quantities as β_{probe} and β_{pump} and find

$$\beta_{\mathrm{probe}} = \beta_{\mathrm{pump}} \frac{B_{\mathrm{loc}}^2}{B_{\mathrm{el}}^2 + B_{\mathrm{loc}}^2}. \tag{7.2}$$

Equations (7.1) and (7.2) are valid in the limit of high nuclear spin temperatures, where $\langle I_z \rangle \propto \beta B_{\mathrm{tot}}$. Therefore, the OS at the end of the pump pulse and the OS at the beginning of the probe pulse at $B_{\mathrm{ext}} = 0$ are related through the same relation (7.2) as the respective inverse nuclear spin temperatures.

In our experiment, the measured average Knight field of $B_{\mathrm{el}} \approx 0.6$ mT is about a factor of five higher than the estimated local field B_{loc}. We would therefore expect a 26-fold decrease of the OS in our pump-probe measuring sequence for a non-adiabatic switching of the light pulses. The data presented in Fig. 7.1 allows for a comparison of DNSP with and without measurement pulses: The data point at $\tau_{\mathrm{wait}} = 0$ in Fig. 7.1(c) corresponds to a measurement of DNSP under continuous QD excitation, while the data points at $\tau_{\mathrm{wait}} \geq 40$ ms in Fig. 7.1(b) correspond to a measurement of DNSP after switching off the excitation light for 0.5 ms. The corresponding values of the OS differ by 2 μeV, which is at the edge of our energy resolution but certainly much smaller than the drop expected from the considerations discussed before.

We explain this discrepancy between our experimental data and the expectations from the theory of nuclear spin temperature by the role of QI already discussed in Chap. 6. The QI stabilizes the nuclear spins at $B_{\mathrm{ext}} = 0$ and suppresses the effect of the nuclear dipolar interactions. Only for a fraction of the QD nuclei the local strain field is small enough neglect the influence of QI. These nuclei are responsible for the effects discussed in Chap. 4 (Fig. 4.2) and might also cause the small drop in OS when applying a pump-probe measurement sequence to the nuclei at $B_{\mathrm{ext}} = 0$. At external magnetic fields largely exceeding B_{loc}, the effects of a non-adiabatic switching of the excitation light are of course negligible, as one can see from (7.1).

7.2 Nonlinear nuclear spin dynamics in high magnetic fields

In view of the nonlinear coupling between the electron and the nuclear spin system that was demonstrated in Chap. 5, the purely exponential buildup and decay curves measured in Sect. 7.1 might come as a surprise. Since the nuclear spin relaxation rate $T_{1\mathrm{e}}$ due to the QD electron depends on electron spin detuning, the buildup and decay rates of DNSP should depend on the degree of nuclear spin polarization and therefore change during the time traces presented in Fig. 7.1. These nonlinear effects are most prominent at the moment where the external and nuclear magnetic fields cancel. Since at low external magnetic fields this corresponds to the regime of almost zero nuclear spin polarization (i.e., to the beginning of the buildup- resp. to the end of the decay-curves), the experimental signature of the nonlinear character of the electron-nuclear spin system is not very pronounced there.

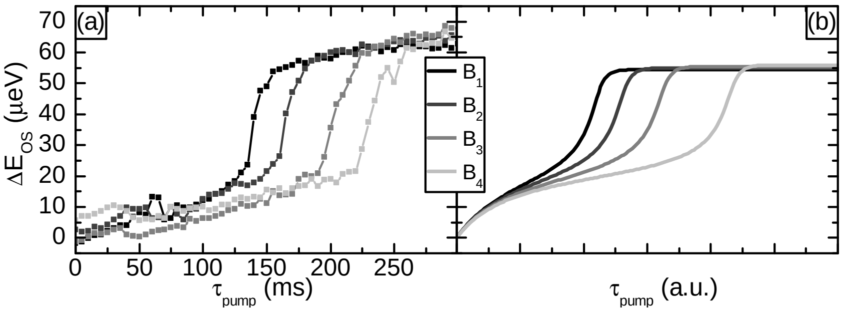

Figure 7.5: (a) Buildup of DNSP in external magnetic fields on the order of the Overhauser field. The experiment was performed with the procedure and external parameters described in the main text at magnetic fields $B_1 = 1.1$ T, $B_2 = 1.2$ T, $B_3 = 1.3$ T and $B_4 = 1.4$ T. (b) Simulations according to the classical nonlinear rate equation (5.3) with the parameters found in the fit for the data presented in Fig. 5.2. The magnetic fields used for the simulation are $B_1 = 1.22$ T, $B_2 = 1.24$ T, $B_3 = 1.26$ T and $B_4 = 1.28$ T.

When increasing the external magnetic field, the nuclear spin dynamics slow down due to the increasing electron Zeeman splitting. However, in a configuration where B_{nuc} opposes B_{ext}, the total magnetic field felt by the QD electron crosses through zero at some point during the buildup and the decay of DNSP (cf. Fig. 5.3(b)). At this point, the nuclear spin dynamics speed up again and $T_{1\text{e}} = T^0_{1\text{e}}$.

In order to observe the nonlinear buildup and decay curves discussed above, we performed the pump-probe measurement of DNSP described in Sect. 7.1.1 in a regime of positive magnetic fields and with excitation light of positive helicity (σ^+). Additionally, the nuclear spin polarization is reset between every pump-probe pulse pair by illumination with linearly polarized light for 100 ms. This ensures that individual pump-probe sequences are independent of each other.

7.2.1 Buildup and decay of nuclear spin polarization

Figure 7.5(a) shows the buildup curves of DNSP measured at various external magnetic fields. The nonlinear effects discussed before are clearly visible in this measurement. A numerical simulation of the dynamics described by the nonlinear equation of motion (5.3) at the corresponding magnetic fields is presented in Fig. 7.5(a). The parameters for these curves are directly taken from the fit to the data shown in Fig. 5.2 without any further adjustments[2]. We note that the magnetic fields applied in the measurement do not completely agree with the magnetic fields used in the simulation. This is most probably due to slightly different excitation conditions (in terms of excitation power and energy) between this experiment and the one presented in Chap. 5. Changing these parameters can significantly alter the critical magnetic fields $B^{\text{c}}_{1,2}$ defined in Chap. 5 and therefore influence the magnetic field dependence of the buildup of DNSP.

A much more interesting situation arises for the decay of DNSP in sizable external magnetic fields. Since the nuclear spin decay rate depends strongly on the electronic environment of the nuclei, the dependence on $\Delta E_{\mathrm{el}}^{\mathrm{Z}}$ of the electron-mediated DNSP decay rate can have various forms, depending on the relative importance of the different possible mechanisms discussed in Sect. 7.1.3.

---

[2] Since these fits only gave the relative time-constants of buildup and decay but not their absolute values, the time axis in Fig. 7.5(b) is given in arbitrary units.

A good picture of the different decay characteristics at various QD gate voltages in high magnetic fields can be obtained by measuring DNSP simultaneously as a function of gate voltage and time. The nuclei are initialized in a state of maximal DNSP at a gate voltage V_1 corresponding to the center of the X^{-1} plateau. The gate voltage is then switched to a value V_2 and DNSP is measured after a waiting time τ_{wait}. In this measurement we scan τ_{wait} first and step to the next value in V_2 after a full time trace is recorded. The measurement result as a function of V_2 and τ_{wait} is shown in Fig. 7.6(a), where the final degree of DNSP is encoded in gray-scale. The voltages corresponding to the crossover between the (n)- and $(n+1)$-electron regimes as determined from a gate voltage dependent PL experiment (at the lowest possible excitation power) are marked in the figure[3]. In agreement with the discussion in Chap. 7, the measurement shows three clearly distinct regions of DNSP decay: When the QD is occupied by a single electron, DNSP decays in tens of ms; when zero or two electrons are present, there is no decay of DNSP on the timescale of the presented measurements. Even when increasing the measurement time to 5min, DNSP shows virtually no decay in these regions. We speculate that the corresponding nuclear T_1 time is on the order of hours.

In the region where the QD is occupied with one electron, the fast DNSP decay shows a much richer behavior. The decay rate shows a marked increase when V_2 approaches the edge of the $1e^-$-plateau, where co-tunnelling rates increase substantially [30]. This illustrates the importance of co-tunneling in electron-mediated DNSP decay, which is twofold: Co-tunneling ensures that the mean electron spin polarization is zero due to the coupling to the (unpolarized) electron reservoir; this sets the equilibrium nuclear spin polarization through (3.6). Furthermore, co-tunneling limits the electron spin correlation time τ_{el}, which broadens the electron spin states and allows for electron-nuclear spin flips to happen at first place.

7.2.2 Motional narrowing of nuclear spins

When approaching the $1e^-$-$2e^-$ transition point however ($0.02V < V_2 < 0.04V$), nuclear spin lifetime increases again, even though the stable configuration of the QD is still singly charged. This observation is a signature of motional narrowing of the nuclear spins: While a finite τ_{el} is necessary to overcome the energy mismatch of the initial and final states of an electron-nuclear spin flip-flop, the nuclei cannot undergo such a transition if the electron spin fluctuations become too fast. This becomes apparent by inspecting (5.1) which shows that T_{1e} has a maximum for $\tau_{\mathrm{el}} = 1/\Omega_{\mathrm{el}}$. We observe the maximal electron-nuclear spin relaxation rate at a gate voltage $V_2 = 0.02$ V. Since at $\tau_{\mathrm{wait}} = 0$ the total electron Zeeman splitting, $g_{\mathrm{el}}^{*}\mu_B(B_{\mathrm{nuc}} + B_{\mathrm{ext}})$, amounts to ~ 20 μeV, the corresponding electron co-tunnelling

---

[3] We note that these voltages do not correspond to the same voltages indicated in Fig. 2.5. The reason for this is light-induced accumulation of space-charges in our gated structures during laser excitation. These charges screen the applied gate voltage, thereby shifting it to lower values. During the interval τ_{wait}, however, no space charges are present in the QD structure, causing the apparent shift of V_g between Fig 7.6 and Fig 2.5.

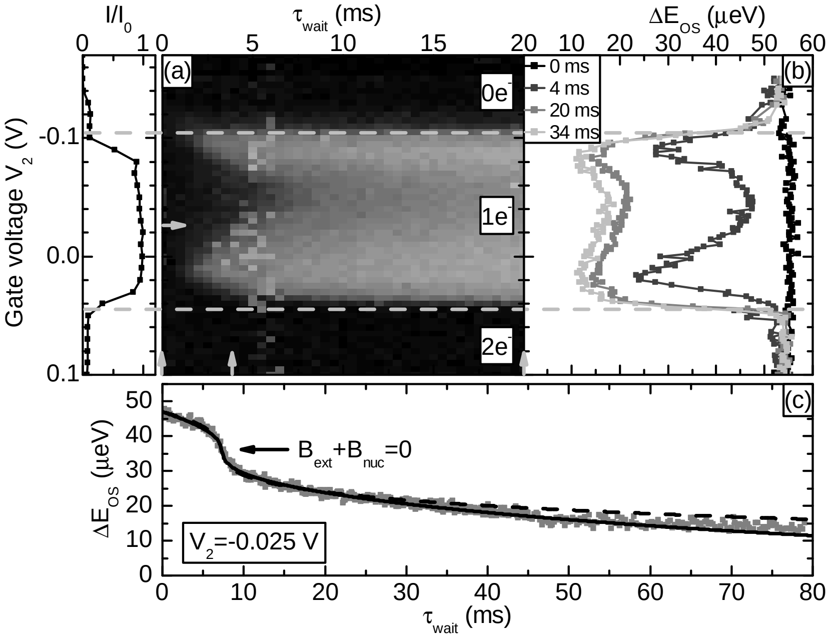

Figure 7.6: Decay of DNSP in an external magnetic field of $B_{\text{ext}} = 1$ T. The nuclear spin polarization was initialized with a 100 ms, σ^+-polarized pump pulse at a gate voltage V_1 corresponding to the middle of the $1e^-$-plateau, resulting in an initial Overhauser shift $\Delta E_{\text{OS}}(\tau_{\text{wait}} = 0) \approx 55$ μeV. Immediately after this nuclear spin initialization, the gate voltage was switched to a value V_2. (a) Measurement of ΔE_{OS} as a function of waiting time t_{wait} and gate voltage V_2. The dashed, gray lines indicate the transition between the QD charging states identified by the low power PL experiment shown in the left panel. (b) and (c) are line-cuts through figure (a) at fixed t_{wait} and V_2, respectively, as indicated by the gray arrows in (a) ((a), (b) and (c) have all been obtained by independent measurements). The black curves in (c) are fits according to (5.3), which are discussed in more detail in the text

rate at this gate voltage should be on the order of 30 GHz, according to (5.1). This is in reasonable agreement with independent calculations of the electron co-tunnelling rate in QD structures similar to the one studied here [30]. Motional narrowing is not observed on the $0e^-$-$1e^-$ transition, where one would at first expect a similar behavior as in the $1e^-$-$2e^-$ transition since co-tunneling processes are equivalent for these two regimes. However, this is not strictly true since the tunneling rate is exponentially growing when increasing the gate voltage. Therefore, co-tunneling is slower on the $0e^-$-$1e^-$ transition than on the $1e^-$-$2e^-$ transition and τ_{el} might never reach the value $1/\Omega_{\text{el}}$ on the low-voltage side of the $1e^-$-plateau.

The fact that increasing fluctuations of the electron spin can lead to and increase of DNSP lifetime (as long as $\tau_{\text{el}} < 1/\Omega_{\text{el}}$) can be illustrated by two additional, independent experiments. Fig. 7.3(b) shows the remaining OS after a free evolution of the nuclear spin system at $B_{\text{ext}} = 1.5$ T and at a QD gate voltage V_g, which sets the QD charge state. The dependence of τ_{decay} on V_g is qualitatively different in the $1e^-$- plateau, compared to the $3e^-$-plateau. While in the first case, DNSP decay is mediated by co-tunneling of an s-shell QD electron, in the latter case a p-shell electron leads to depolarization of the nuclear spins. Due to the exponential dependence of the tunneling rate on the height of the tunneling barrier, we estimate the co-tunneling rate of the p-shell electron to be about one order of magnitude higher than the one for the s-shell electron[4]. As a result, DNSP is slower in the three-electron case compared to the case where only one electron occupies the QD. The data suggests, that in the center of the $1e^-$-plateau, $\tau_{\mathrm{el}} > 1/\Omega_{\mathrm{el}}$, while the opposite is true for the $3e^-$-plateau. This would explain why τ_{decay} has a local maximum in the center of the $1e^-$-plateau, while it has a local minimum in the center of the $3e^-$-region.

The second surprising consequence of motional narrowing is that the nuclear spin lifetime increases if we excite the QD with light of linear polarization during the period τ_{wait} (not shown here). Again, the light excitation shortens τ_{el} which explains why τ_{decay} is prolonged in this case. The resulting relaxation of DNSP to zero resembles the buildup curves presented in Fig. 7.5 with a reversed time evolution. This result is reasonable, since the decay of DNSP under illumination with linearly polarized light is a driven relaxation, similar to the buildup of DNSP.

7.2.3 Nonlinear decay of nuclear spin polarization

The center of the $1e^-$-plateau shows a lifetime of DNSP of roughly 10 ms, limited by the interactions of the QD nuclei with the residual QD electron which is randomized by co-tunnelling with the reservoir. Due to the nonlinear electron-nuclear spin coupling, the decay in this region is highly non-exponential as illustrated by the data presented in Fig. 7.6(c). Nuclear spin depolarization initially happens at a rather slow rate but speeds up as soon as B_{nuc} and B_{ext} cancel after $\tau_{\mathrm{wait}} \approx 7$ ms and at $\Delta E_{\mathrm{OS}} \approx 36$ μeV. Once $|B_{\mathrm{nuc}}| < |B_{\mathrm{ext}}|$, the electron Zeeman splitting increases with time and DNSP decay slows down again. We fitted the measured decay curve by a numerical solution of the rate equation (5.2) for $S_z = 0$ and an initial condition $\Delta E_{\mathrm{OS}}(0)$. The parameters found for the best fit[5] were $\Delta E_{\mathrm{OS}}(0) = 47$ μeV, $T_{1\mathrm{e}}^0 = 3.3$ ms, $T_{\mathrm{d}} = 110$ ms, $\tau_{\mathrm{el}} = 360$ ps and $g_{\mathrm{el}}^* = -0.62$, in agreement with the corresponding numbers found in Sect. 5.2. However, the electron spin correlation time we found is surprisingly short given that here, the measurement was performed in the absence of optical excitation. We would expect τ_{el} to be on the order of 1 ns with a slight reduction due to the fact that the DNSP decay curve was not measured exactly at the center of the $1e^-$-stability plateau (cf. Fig. 7.6(a)). Another surprising feature is the remaining nuclear spin depolarization time of $T_{\mathrm{d}} = 110$ ms. We note that this nuclear spin relaxation cannot be due to spin diffusion mediated by nuclear dipole-dipole interactions, since this rate would have to be much smaller given the long DNSP lifetime found by the measurement in the $0e^-$- and the $2e^-$-regions of Fig. 7.6(a). We tried to fit the data in Fig. 7.6(c) using a corresponding nuclear spin decay time of $T_{\mathrm{d}} = 100$ s (dashed, black curve). While this gives a reasonable fit to the experimental data for short timescales, the fit underestimates the nuclear spin decay rate for longer times. All fitting parameters for the dashed curve were the same as for the first fit, only that τ_{el} had to be reduced to 275 ps. This value is even shorter than the previously quoted electron spin correlation time and renders these fitting parameters less realistic. We therefore deduce that for modelling the data in Fig. 7.6(c), an additional nuclear spin decay rate of $T_\mathrm{d} = 110$ ms, caused by the presence of the QD electron, has to be introduced. Possibly, indirect nuclear spin interactions mediated by the QD electron cause this decay through the mechanism discussed in Sect. 3.4. This decay is not expected to be exponential and further study of the DNSP decay dynamics in this regime is required to fully understand the measurement presented in Fig. 7.6(c).

---

[4] This rough estimate can be made based on the sample geometry and trap depths sketched in Fig. 2.3 and Fig. 2.4.

[5] We note that the quality of the fit is very sensitive to even small changes of the fitting parameters, which is a consequence of the nonlinear character of (5.2).

7.2.4 Open questions and conclusions

A surprising feature arises in the transition between the $1e^-$ and $0e^-$ regimes ($-0.14V < V_2 < -0.1V$). Fig. 7.6(b) shows that in this regime, DNSP has an initial, fast decay (on a timescale $\ll 1$ ms, not resolved in this measurement) after which it settles at a finite value of DNSP and shows no further decay on the timescale of our experiments. This unexplained observation is very surprising since it occurs in a regime where the QD electron is strongly coupled to the electron reservoir and electron spin fluctuations should become very large. Furthermore, decay of DNSP seems to stop at a value where the total electron Zeeman splitting is smaller than its value at $\tau_\mathrm{wait} = 0$ and where one would therefore expect DNSP decay to be enhanced. A possible, but highly speculative interpretation of the observed signature is the following: The strong coupling of the QD electron with the reservoir could lead to the formation of a spin-correlated (singlet) state between the localized electron and its reservoir. In this case, DNSP decay would stop, if this electron spin state is energetically well separated from a state where the QD electron is flipped. The formation of such a correlated spin state would be assisted by minimizing ΔE_Z^el, which the situation in which we observe the suppression of DNSP decay in Fig. 7.6(b). Full understanding of the interesting dynamics of DNSP decay in this QD charging regime, however, requires further investigation.

We note that we have repeated the experiment discussed above for external magnetic fields of $B_\mathrm{ext} = 0$, 0.5 and 1.5 T. All the features we previously described have been observed at all those fields. At $B_\mathrm{ext} = 0$, however, DNSP decay in the $1e^-$-region is too fast for our experimental setup to observe a variation of co-tunnelling rates over the $1e^-$-stability plateau. We also checked the dependence of our results on the exact form of the gate voltage-overshoots used to switch V_g between V_1 and V_2 (cf. Fig. 7.2) and found that the gate voltage-switching does not influence our results. A further check for the validity of our results was to change the order in which τ_wait and V_2 were measured. Sweeping V_2 and stepping τ_wait gave results identical to the ones depicted in Fig. 7.6.

We conclude that we have good understanding of the decay dynamics of DNSP in the regimes where the QD electron occupancy number is well defined. In the crossover regions where the QD charging state is changed, DNSP decay shows unexpected features that warrant further investigation. Especially a systematic investigation of the temperature dependance of the decay of DNSP could shed light on the processes that cause the unexplained behavior of DNSP decay in the region where the QD electron is strongly coupled to its reservoir.

8 Conclusion & Outlook

One of the principal experimental findings presented in this work was the identification of the QD electron as an efficient source of nuclear spin decay. While in our approach the electron is indispensable for building up a nuclear spin polarization in the first place, it also acts against this buildup by inducing indirect nuclear spin interactions as well as co-tunnelling mediated depolarization. In order to increase the maximal attainable degree of nuclear spin polarization it would therefore be interesting to investigate possibilities of suppressing this electron-mediated DNSP decay. This could be achieved by increasing the tunnelling barrier between the QD and the electron reservoir in our structures. However, changing this parameter also has the consequence of changing the electron spin correlation time τ_{el} and the fraction of QD electron occupation, f_{el}. Both these factors crucially influence the QD nuclear spin dynamics in various ways. Systematically studying the dependence of DNSP on the QD tunneling barrier thickness could therefore yield valuable information on how to enhance DNSP in self-assembled QDs.

For the interpretation of all of our experimental results, considering the nuclear spins as an ensemble of classical magnetic moments was sufficient. Investigating their quantum mechanical nature would be interesting for both fundamental reasons and applications that aim at tailoring the fluctuations of the mean nuclear spin [8]. The back-action of a (quantum-mechanical) measurement of the nuclear spin polarization along a given axis would be an interesting experiment in this direction. In order to perform a projective measurement on the QD nuclear spin system, the accuracy of the detection of the Overhauser-shift has to be greatly improved as compared to our experimental technique. The necessary energy resolution for such an experiment has recently been estimated to be on the order of $A/N^{3/2}$ [8]. Using optimistic numbers, this corresponds to an energy resolution of ~ 0.1 neV or ~ 25 kHz. While this resolution is out of reach with our present spectroscopic techniques, more advanced methods like optically detected electron spin resonance [70] or EIT [71] are close to reaching the required sensitivity. A first step in this direction would be the use of differential transmission measurements [72] to prepare and detect DNSP.

Our measurements of the Overhauser-shift of a QD electron give information about the mean nuclear field that the electron is exposed to. Investigating the role that the different nuclear species play in the dynamics of the nuclear field requires a further extension of our experimental techniques. Applying an NMR field resonant with a given nuclear spin species could induce additional heating for those spins, thereby giving information about the contribution of the different spin species to the measured Overhauser-shift. Such experiments are complicated by the large inhomogeneous broadening of the corresponding NMR lines caused by strain-induced quadrupolar shifts. Using more refined NMR- and optical detection techniques, however, NMR experiments could prove useful in investigating the dynamics of QD nuclear spins in greater detail.

Another exciting perspective is the experimental observation of the onset of nuclear order in a single QD. Different theoretical scenarios for these nuclear phase transitions have been proposed. Based on the experimental results presented in this work, realizing these proposals seems to be within experimental reach. Nuclear self polarization was predicted to occur for the case where nuclear spins couple to an electron spin system which is artificially maintained in a disordered spin state at sufficiently low temperatures [54]. Combining recent advances in electron spin resonance in self-assembled QDs [70] with the fast, non-invasive measurement of DNSP via pulsed PL could allow us to observe this spontaneous nuclear spin polarization which was predicted to occur at moderate temperatures of a few K. At much lower temperatures, a true ferromagnetic phase transition of the nuclear spins was recently predicted to occur in semiconductor nano-structures [73]. A possibility for reaching low nuclear spin temperatures in the μK range is adiabatic demagnetization of QD nuclear spins. Bringing the optically cooled nuclear spin system from a field on the order of 1 T adiabatically to zero field could result in a nuclear spin temperature being $2-3$ orders of magnitude lower than what can be achieved through direct optical cooling.

A Appendix

A.1 Experimental setup

This Appendix gives a sketch of the experimental setup and a short list of the most important optical components used in this work to perform measurements of the PL on an individual QD. Figure A.1 shows the schematics of the experimental setup, while Table A.1 gives a more detailed list of the optical components.

A schematic drawing of our setup is sketched in Fig. A.1. It corresponds to a standard PL setup with a few modifications that we will describe in the following. All optical elements of the PL setup were oriented on the optical axis marked by the black, dashed line. Laser light for PL excitation was directed onto the optical axis using a small gold mirror (GM) which replaces the beam-splitter which is used for this purpose in most other PL experiments. The advantages of using the gold mirror over a beam splitter are twofold. First, a beam splitter necessarily leads to a loss of PL light, which in our case was reduced due to the small diameter of the gold mirror compared to the diameter of the PL beam path. Second, a gold mirror provides excellent preservation of excitation light polarization if this polarization is linear and parallel to the mirror surface.

Lens L_1 in combination with the SIL was used to focus the excitation light onto the sample and to collect PL light from the QDs. The SIL - if properly mounted on the sample surface - had the advantages of increasing the PL collection efficiency by increasing the NA of the collection optics and by reducing total internal reflection of PL light from the sample surface [74]. We observed a corresponding $\sim$ 10-fold increase of photon collection efficiency by comparing PL from the same sample with and without SIL.

The lens pair L_2 and L_3 was mounted in a confocal geometry, so that a virtual image plane of the sample was created at the focal point. A pinhole (PH) placed in this image plane can be used to block stray laser- or PL-light and only observe PL from an individual QD. Furthermore, an external spectrometer shutter (Sh) was placed near the confocal point, where the effective switching speed for PL light is maximized. The narrow bandpass interference filter (F) was used to block the excitation laser light, while letting the PL light pass. It was mounted on a rotating stage for fine-adjusting its pass-band to the PL emission wavelength.

The polarization optics of the experiment was based on a combination of liquid crystal devices (W and R) with linear polarizers (P_1 and P_2), as shown in Fig. A.1. Polarizer P_1 (in a fixed, vertical orientation) together with the liquid crystal wave plate W (with its fast axis oriented at $-45°$[1] with respect to the orientation of polarizer P_1) were used to set the light polarization at the QD location. The liquid crystal wave plate allowed for a setting of the retardance between $\lambda/4$ and $3\lambda/4$

---

[1] The sign of this angle refers to an observation in the direction of excitation light propagation.

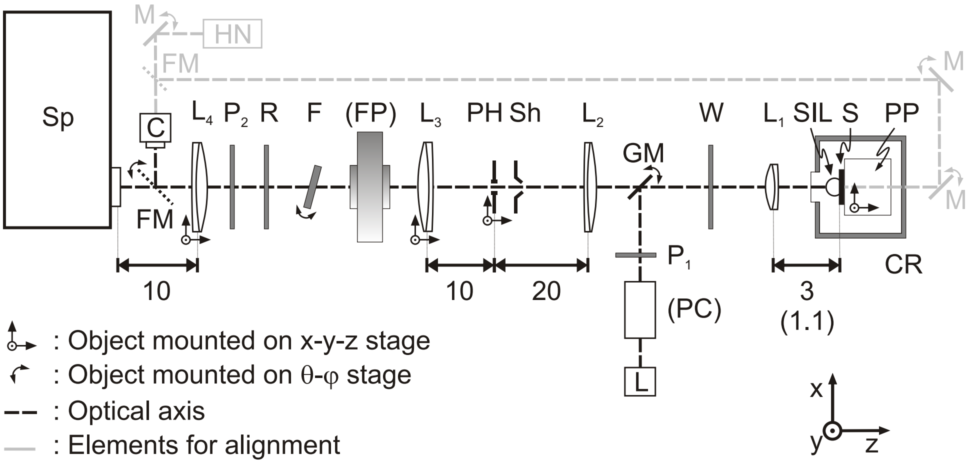
Sp
C
FM
M
HN
FM
L_4 P_2 R F (FP) L_3 PH Sh L_2
GM
W
L_1 SIL S PP
M
M
CR
10
10 20
P_1
(PC)
L
3
(1.1)
: Object mounted on x-y-z stage
: Object mounted on θ-φ stage
: Optical axis
: Elements for alignment
x
y z

Figure A.1: Schematics of the PL setup used in the experiments discussed in this thesis. The drawing is not to scale, relevant length scales are given in cm. The elements are, respectively: Sp: Spectrometer, C: CCD camera FM: Flip mirror L_4: Focussing lens, P_2: Polarizer (orientation horizontal, fixed), R: Linear polarization rotator, F: Bandpass filter for QD PL, FP: Fabry-Perot etalon, L_3: Collimation lens, PH: Pinhole, Sh: Shutter, L_2: Focussing lens, GM: Miniature gold mirror, W: Variable wave plate (principal axis at 45° to vertical, fixed), L_1: Collection lens, SIL: Solid immersion lens, S: Sample, PP: Piezoelectric positioner, CR: Cryostat, P_1: polarizer (orientation vertical, fixed), PC: Pockels cell (principal axis at 45° to vertical, fixed), L: Laser source, M: Mirror, HN: HeNe Laser. Elements described in brackets in the figure were optional and elements marked in light gray are used for alignment purposes only. Table A.1 gives a detailed description of the individual components.

corresponding to excitation with σ^-- and σ^+-polarized light [60]. The liquid crystal polarization rotator R together with the fixed analyzer P_2 were then used to analyze the polarization of the PL light. The combination of R and P_2 is equivalent to a single, rotatable analyzer, with the great advantage of having no mechanically moving parts. This greatly facilitated the coupling of PL into spectrometer S and avoided artifacts in the PL polarization measurements due to mechanical rotation of an analyzer. The polarization rotator allowed for a voltage controlled rotation of the axis of polarization of linearly polarized light over a total angle exceeding 180°. By setting the rotation such that the combination of R and P_2 corresponded to an analyzer setting perpendicular (parallel) to the orientation of P_1, PL polarization with co-circular (cross-circular) polarization with respect to the excitation light polarization was observed.

For experiments, where a high switching speed of the excitation light helicity was required, the liquid crystal devices operating at a maximal modulation frequency of 10 Hz were too slow. In this case, the setup was extended by the Pockels cell (PC) which was used to turn the linear polarization of the excitation light after P_1 by 90°, resulting in a fast switching of the excitation light helicity on the sample. Using a suitable high voltage amplifier, this switching could be achieved in less than 10 μs.

For the measurement of PL polarization under modulated excitation helicity presented in Sect. 6.2, the wave plate W was replaced by the Pockels cell PC, with its fast axis oriented at $-45°$ from vertical. By switching the PC retardance from $\lambda/4$ and $3\lambda/4$, we were able to modulate the excitation light helicity at a frequency of up to 100 kHz. Since the PL light was collected through the PC aperture as well, the detection would always remain co- or cross-circularly polarized with respect to the actual excitation light polarization. While this technique allows for a measurement of DNSP even under polarization modulation of the excitation light, it has the disadvantage of reducing light collection efficiency due to the inevitably small aperture of the PC of 2 mm.

The gray elements in Fig. A.1 were used for the initial alignment of the optical elements as well as for aligning the sample with respect to the light excitation direction z and the external magnetic field. The alignment was based on observing the back-reflection of the HeNe laser (HN) beam from either one of the optical elements or from the rear surface of the sample, which was optically accessible. Before mounting the optical elements, the HeNe laser beam was aligned with the optical axis. Successively, each optical element was introduced into the setup, starting with elements close to the cryostat and moving towards the spectrometer. Each element was centered and aligned with respect to the HeNe beam by observing the HeNe back-reflection on a white screen. Lenses L_1, L_3 and L_4 were then put into their focal position with the help of camera C, which for this purpose was equipped with an infinitely corrected focussing lens. The camera was positioned successively after each of the two collimating lenses (L_1, L_3), and the lenses were adjusted to give a clear image of the sample structure on the camera screen. Similarly, L_4 was brought into focus by imaging the spectrometer slit with the camera through L_4.

The setup used for the creation of the pump and probe laser pulses necessary for the measurements presented in Chap. 7 is discussed in great detail elsewhere [75]. The acousto-optical modulator (AOM) and the driver used in our setup were produced by Crystal Technology, the AOM was model no. 3080-125 together with driver model no. 1080AF-AIF0-2.0. After the AOM setup, the laser beam was coupled into a fiber and directed to the PL setup. The fiber coupling served two purposes. First, passing the laser-beam through the fiber resulted in a cleaner spatial mode-profile, which in turn led to an improved focussing of the excitation laser onto the sample. Second, the fiber coupling decoupled the alignment of the AOM setup from the alignment of the PL setup, which was of great practical advantage compared to the case of free space propagation of the laser beam.

The whole experiment, including the applied gate voltage V_g, the setting of the AOM drive power, the opening of the spectrometer shutter as well as the readout of the spectrometer CCD was controlled by a digital acquisition card (DAQ), which allowed for the output of digital as well as analog channels. The DAQ card used in this experiment was model no. PCI-6229 from National Instruments.

Item	Description	Manufacturer
Sp	Spectrometer Detector	Princeton Instruments/Acton Research, SpectraPro 2759, f= 0.750 m Princeton Instruments, Spec-10:100BR/LN. 1340 × 100 pixel back-illuminated CCD array
C	CCD camera	Watec, WAT-120N
FM	Flip mirror	Thorlabs, BB1-E03
L_3,L_4	Achromatic lens,$f = 0.1$ m	Thorlabs, AC508-100-B
P_1, P_2	Polarizer	Newport, Glen-Laser polarizer, 10GL08AR.16
R	Liquid crystal polarization rotator	Meadowlark, LPR-200-0915
F	Bandpass filter	Thorlabs FB950-10, $\lambda = 950$ nm,$\Delta\lambda =$ 10 nm
FP	Fabry-Perot etalon	Burleigh, TL-15
PH	Pinhole, ø100 (20) μm	Thorlabs, P100S (P20S)
Sh	Shutter	Uniblitz, LS6ZM2
L_2	Achromatic lens,$f = 0.2$ m	Thorlabs, AC508-200-B
GM	Miniature gold mirror	Homemade, 250 nm gold evaporated on 10 nm Ti on a GaAs substrate. Cut to 2 × 2 mm and glued onto thin glass-strip
W	Liquid crystal wave plate	Meadowlark, LRC-200-0915
L1	Achromatic lens (with bath cryostat) Microscope objective (with flow cryostat)	Thorlabs, C220TME, NA=0.25, f= 11 mm Mitutoyo, 378-823-4. M Plan Apo NIR 10x, NA= 0.26, W.D.= 30.5 mm
SIL	Solid immersion lens	A.W.I. Industries, E14571. Hyper-hemispherical ball lens, ZrO_2, uncoated. Mounted to sample surface using “Quick stick 135” TEM mounting wax
S	Sample	Described in detail in Sect. 2.2
PP	Piezoelectric positioners	Attocube, ANPx50/LT and ANPz50/LT. Controller ANC150/3
CR	Flow cryostat Bath cryostat	Oxford instruments, MicrostatHe Oxford instruments, Spectromag with 12T split-coil magnet
PC	Pockels cell Pockels cell driver	Linos, LM0202 SI, HVA 3/450
L	Ti:Saph laser (for PL) Diode Laser (for imaging)	Tekhnoscan, TIS-SF-07. Pumped by a Coherent, Verdi-V5 (5W) Melles Griot, 56IC5210, $\lambda = 780\ nm$, $P_{max} =$ 50 mW
M	Mirror	Thorlabs, BB1-E03
HN	HeNe Laser	Melles Griot, 05-SRP-812

Table A.1: Detailed list of the most important elements used for the PL setup sketched in Fig. A.1

A.2 Measurement of the gate voltage switching time and sample RC time constant

For the experiments involving a rapid switching of the QD gate voltage V_g that were discussed in Chap. 7 it was important to measure the speed at which the electric field E at the position of the QD could be switched. This electric field controls the charging state of the QD which has to be set faster than the dynamical timescales of the QD nuclear spins. In order to measure E in a time-resolved way, we employed a stroboscopic measurement technique. During acquisition of a single QD PL spectrum, the excitation laser was chopped into a periodic sequence of light pulses of length 10 μs, using the AOM setup described in Appendix A.1. Simultaneously, a periodic modulation of the gate voltage was applied to the sample, where the period was the same as for the laser modulation and where the shape of the modulation corresponded to the gate voltage switching sequences to be employed in the experiment. The phase between the modulated light intensity and the gate voltage modulation was thereby changed in steps in order to trace the time evolution of E. Owing to the quantum confined stark effect (cf. Fig. 2.5), the energy of the QD emission lines can be used as a measure for the electric field E.

Figure A.2 shows the resulting measurement of the gate voltage switching time with and without the application of gate voltage "spikes" to increase the switching time. The data presented in Fig. A.2(a) show a direct measurement of the RC time constant τ_{RC} of the QD gate structure (Fig. 2.3). By fitting an exponential to the experimental data, we find $\tau_{\mathrm{RC}} = 61.2$ μs. We note that this RC time constant was strongly dependent on the way the sample was contacted. Bad contacts resulted in a prolonged τ_{RC} of up to 2 ms. The gate voltage "spikes" we applied in order to decrease the switching time of V_g consisted in constant overshoots with an amplitude of 0.25 V and a length of 30 μs. The amplitude was adjusted to obtain the best switching behavior for V_g and the final switching time was limited by the length of the overshoots. Fig. A.2(b) shows the resulting gate switching performance. With the gate voltage "spikes", we can switch the gate voltage between two fixed gate voltages in 30 μs. The final emission QD energy after the gate voltage switching was stable within a few μeV.

We note that the method presented here is very convenient to determine the RC time constant of gated QD samples based on PL of a single QD. This time constant is a relevant parameter in all experiments where QD gate voltage modulation is required, such as single QD absorption experiments [76].

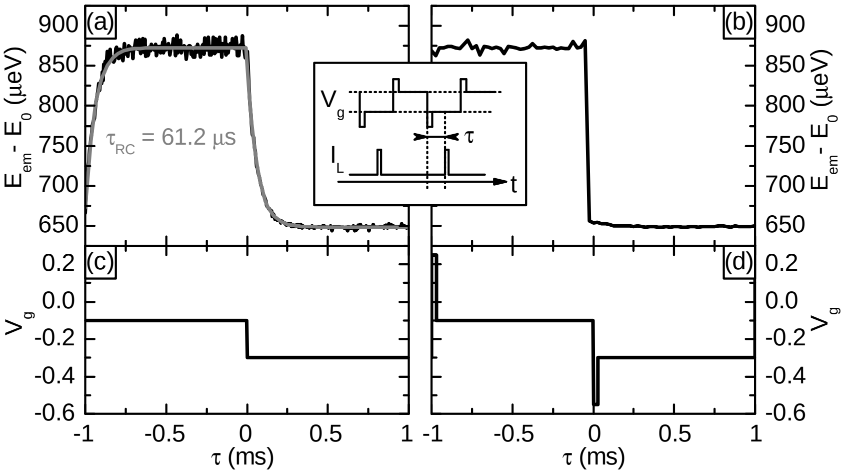

Figure A.2: Measurement of the spectral response of X^0 PL emission energy to a change of the gate voltage. A constant offset of $E_0 = 1.149$ eV is subtracted from the data. The measurement is based on a stroboscopic detection which is illustrated in the insert of the figure and discussed in more detail in the text. The length of the repeated probe pulses was 10 μs; I_L stands for the laser intensity. The energy of the emitted photons directly measures the electric field E the QD is exposed to. (a) Gate voltage switching behavior under square wave modulation of the gate voltage (c). The measured RC time constant of the diode structure is ~ 61.2 μs. (b) Applying overshooting "spikes" (illustrated in (d)) to the gate voltage modulation, the electric field at the QD site can be switched much faster. Here, the switching speed is limited by the length of the "spikes", which is 30 μs. After the gate voltage switching, E_{em} is stable within a few μeV.

B Bibliography

[1] A. Overhauser, *Polarization of Nuclei in Metals*, Phys. Rev. **92**, 411 (1953), URL. 1

[2] G. Lampel, *Nuclear Dynamic Polarization by Optical Electronic Saturation and Optical Pumping in Semiconductors*, Phys. Rev. Lett. **20**, 491 (1968), URL. 1

[3] D. Paget, G. Lampel, B. Sapoval, and V. I. Safarov, *Low Field Electron-Nuclear Spin Coupling in Gallium-Arsenide under Optical-Pumping Conditions*, Phys. Rev. B **15**, 5780 (1977), URL. 1, 15, 17, 18, 24, 40

[4] G. Chen, D. L. Bergman, and L. Balents, *Semiclassical dynamics and long-time asymptotics of the central-spin problem in a quantum dot*, Physical Review B (Condensed Matter and Materials Physics) **76**, 045312 (2007), URL. 1

[5] A. V. Khaetskii, D. Loss, and L. Glazman, *Electron spin decoherence in quantum dots due to interaction with nuclei*, Phys. Rev. Lett. **88**, 186802 (2002), URL. 1, 17, 20, 21

[6] A. C. Johnson, J. R. Petta, J. M. Taylor, A. Yacoby, M. D. Lukin, C. M. Marcus, M. P. Hanson, and A. C. Gossard, *Triplet-singlet spin relaxation via nuclei in a double quantum dot*, Nature **435**, 925 (2005), URL. 1

[7] F. H. L. Koppens, J. A. Folk, J. M. Elzerman, R. Hanson, L. H. W. van Beveren, I. T. Vink, H. P. Tranitz, W. Wegscheider, L. P. Kouwenhoven, and L. M. K. Vandersypen, *Control and Detection of Singlet-Triplet Mixing in a Random Nuclear Field*, Science **309**, 1346 (2005), URL. 1

[8] D. Klauser, W. A. Coish, and D. Loss, *Nuclear spin dynamics and Zeno effect in quantum dots and defect centers* (2008), arXiv:0802.2463v1, URL. 1, 21, 63

[9] W. A. Coish and D. Loss, *Hyperfine interaction in a quantum dot: Non-Markovian electron spin dynamics*, Phys. Rev. B **70**, 195340 (2004), URL. 1

[10] D. Gammon, S. W. Brown, E. S. Snow, T. A. Kennedy, D. S. Katzer, and D. Park, *Nuclear Spectroscopy in Single Quantum Dots: Nanoscopic Raman scattering and Nuclear Magnetic Resonance*, Science **277**, 85 (1997), URL. 2

[11] S. W. Brown, T. A. Kennedy, D. Gammon, and E. S. Snow, *Spectrally resolved overhauser shifts in single GaAs/*$Al_xGa_{1-x}As$ *quantum dots*, Phys. Rev. B **54**, R17339 (1996), URL. 2

[12] K. Ono and S. Tarucha, *Nuclear-spin-induced oscillatory current in spin-blockaded quantum dots*, Phys. Rev. Lett. **92**, 256803 (2004), URL. 2

[13] A. S. Bracker, E. A. Stinaff, D. Gammon, M. E. Ware, J. G. Tischler, A. Shabaev, A. L. Efros, D. Park, D. Gershoni, V. L. Korenev, et al., *Optical pumping of the electronic and nuclear spin of single charge-tunable quantum dots*, Phys. Rev. Lett. **94**, 047402 (2005), URL. 2, 12

[14] B. Eble, O. Krebs, A. Lemaitre, K. Kowalik, A. Kudelski, P. Voisin, B. Urbaszek, X. Marie, and T. Amand, *Dynamic nuclear polarization of a single charge-tunable InAs/GaAs quantum dot*, Phys. Rev. B **74**, 081306 (2006), URL. 2, 23, 24, 31

[15] C. W. Lai, P. Maletinsky, A. Badolato, and A. Imamoglu, *Knight-field-enabled nuclear spin polarization in single quantum dots*, Phys. Rev. Lett. **96**, 167403 (2006), URL. 2, 3, 10, 20

[16] A. I. Tartakovskii, T. Wright, A. Russell, V. I. Fal'ko, A. B. Van'kov, J. Skiba-Szymanska, I. Drouzas, R. S. Kolodka, M. S. Skolnick, P. Fry, et al., *Nuclear Spin Switch in Semiconductor Quantum Dot*, Phys. Rev. Lett. **98**, 26806 (2007), URL. 2

[17] I. A. Akimov, D. H. Feng, and F. Henneberger, *Electron Spin Dynamics in a Self-Assembled Semiconductor Quantum Dot: The Limit of Low Magnetic Fields*, Phys. Rev. Lett. **97**, 056602 (2006), URL. 2

[18] I. A. Merkulov, A. L. Efros, and M. Rosen, *Electron spin relaxation by nuclei in semiconductor quantum dots*, Phys. Rev. B **65**, 205309 (2002), URL. 2, 49

[19] P. Maletinsky, C. W. Lai, A. Badolato, and A. Imamoglu, *Nonlinear dynamics of quantum dot nuclear spins*, Phys. Rev. B **75**, 35409 (2007), URL. 3, 10, 50

[20] P. Maletinsky, A. Badolato, and A. Imamoglu, *Dynamics of Quantum Dot Nuclear Spin Polarization Controlled by a Single Electron*, Phys. Rev. Lett. **99**, 056804 (2007), URL. 3, 49

[21] *Ioffe Physico-Technical Institute, Physical Properties of Semiconductors*, URL. 5, 6

[22] P. Y. Yu and M. Cardona, *Fundamentals of Semiconductors: Physics and Materials Properties* (Springer, Berlin, 2001), 3rd ed., URL. 6, 12

[23] F. Meier, *Optical orientation* (North-Holland, Amsterdam, 1984). 6, 17, 24, 32, 42, 45, 46, 47, 54, 56

[24] P. Petroff, *Epitaxial Growth and Electronic Structure of Self-Assembled Quantum Dots*, Topics Appl. Phys. **90**, 1 (2003), URL. 7

[25] D. Leonard, K. Pond, and P. M. Petroff, *Critical layer thickness for self-assembled InAs islands on GaAs*, Phys. Rev. B **50**, 11687 (1994), URL. 7

[26] R. J. Warburton, C. Schaflein, D. Haft, F. Bickel, A. Lorke, K. Karrai, J. M. Garcia, W. Schoenfeld, and P. M. Petroff, *Optical emission from a charge-tunable quantum ring*, Nature **405**, 926 (2000), URL. 8, 10

[27] R. J. Warburton, B. T. Miller, C. S. Dürr, C. Bödefeld, K. Karrai, J. P. Kotthaus, G. Medeiros-Ribeiro, P. M. Petroff, and S. Huant, *Coulomb interactions in small charge-tunable quantum dots: A simple model*, Phys. Rev. B **58**, 16221 (1998), URL. 10, 52

[28] B. Urbaszek, R. J. Warburton, K. Karrai, B. D. Gerardot, P. M. Petroff, and J. M. Garcia, *Fine structure of highly charged excitons in semiconductor quantum dots*, Phys. Rev. Lett. **90**, 247403 (2003), URL. 10, 52

[29] M. Bayer, G. Ortner, O. Stern, A. Kuther, A. A. Gorbunov, A. Forchel, P. Hawrylak, S. Fafard, K. Hinzer, T. L. Reinecke, et al., *Fine structure of neutral and charged excitons in self-assembled In(Ga)As/(Al)GaAs quantum dots*, Phys. Rev. B **65**, 195315 (2002), URL. 10, 14, 18

[30] J. M. Smith, P. A. Dalgarno, R. J. Warburton, A. O. Govorov, K. Karrai, B. D. Gerardot, and P. M. Petroff, *Voltage control of the spin dynamics of an exciton in a semiconductor quantum dot*, Phys. Rev. Lett. **94**, 197402 (2005), URL. 11, 14, 26, 53, 59, 60

[31] M. E. Ware, E. A. Stinaff, D. Gammon, M. F. Doty, A. S. Bracker, D. Gershoni, V. L. Korenev, S. C. Badescu, Y. Lyanda-Geller, and T. L. Reinecke, *Polarized Fine Structure in the Photoluminescence Excitation Spectrum of a Negatively Charged Quantum Dot*, Phys. Rev. Lett. **95**, 177403 (2005), URL. 11, 12

[32] M. J. Snelling, E. Blackwood, C. J. McDonagh, R. T. Harley, and C. T. B. Foxon, *Exciton, heavy-hole, and electron g factors in type-I GaAs/$Al_xGa_{1-x}As$ quantum wells*, Phys. Rev. B **45**, 3922 (1992), URL. 14

[33] S. Amasha, K. MacLean, I. P. Radu, D. M. Zumbühl, M. A. Kastner, M. P. Hanson, and A. C. Gossard, *Electrical Control of Spin Relaxation in a Quantum Dot*, Phys. Rev. Lett. **100**, 046803 (2008), URL. 14

[34] A. Abragam, *The principles of nuclear magnetism* (Clarendon Press, Oxford, 1961). 15, 31, 54

[35] J. A. McNeil and W. G. Clark, *Nuclear quadrupolar spin-lattice relaxation in some III-V compounds*, Phys. Rev. B **13**, 4705 (1976), URL. 15, 16

[36] D. Paget, *Optical-Detection of NMR in High-Purity GaAs - Direct Study of the Relaxation of Nuclei Close to Shallow Donors*, Phys. Rev. B **25**, 4444 (1982), URL. 16, 50, 55

[37] A. Malinowski, M. A. Brand, and R. T. Harley, *Nuclear effects in unltrafast quantum-well spin-dynamics*, Physica E **10**, 13 (2001), URL. 16, 50

[38] M. Goldman, *Spin Temperature and nuclear Magnetic Resonance in Solids* (Oxford University Press, 1970). 16, 17, 23, 38, 56

[39] R. V. Pound, *Nuclear Spin Relaxation Times in Single Crystals of LiF*, Phys. Rev. **81**, 156 (1951), URL. 16

[40] I. Merkulov, *spin system of quantum dots*, Physics Uspekhi **45**, 1293 (2002), URL. 17, 19, 31, 33

[41] P.-F. Braun, B. Urbaszek, T. Amand, X. Marie, O. Krebs, B. Eble, A. Lemaitre, and P. Voisin, *Bistability of the nuclear polarization created through optical pumping in $In_{1-x}Ga_xAs$ quantum dots*, Phys. Rev. B **74**, 245306 (2006), URL. 17, 37

[42] E. I. Gryncharova and V. I. Perel, *Relaxation of Nuclear Spins Interacting with Holes in Semiconductors*, Sov. Phys. Semicond. **11**, 997 (1977). 17

[43] M. I. Dyakonov and V. I. Perel, *Optical Orientation in a System of Electrons and Lattice Nuclei in Semiconductors - Theory*, Sov. Phys. JETP **38**, 177 (1974). 17, 24

[44] J. R. Petta, A. C. Johnson, J. M. Taylor, E. A. Laird, A. Yacoby, M. D. Lukin, C. M. Marcus, M. P. Hanson, and A. C. Gossard, *Coherent Manipulation of Coupled Electron Spins in Semiconductor Quantum Dots*, Science **309**, 2180 (2005), URL. 19, 20

[45] E. L. Hahn, *Spin Echoes*, Phys. Rev. **80**, 580 (1950), URL. 19

[46] G. Giedke, J. M. Taylor, D. D'Alessandro, M. D. Lukin, and A. Imamoglu, *Quantum measurement of a mesoscopic spin ensemble*, Phys. Rev. A **74**, 032316 (2006), URL. 20

[47] D. Klauser, W. A. Coish, and D. Loss, *Nuclear spin state narrowing via gate-controlled Rabi oscillations in a double quantum dot*, Phys. Rev. B **73**, 205302 (2006), URL. 20

[48] R. Hanson, L. P. Kouwenhoven, J. R. Petta, S. Tarucha, and L. M. K. Vandersypen, *Spins in few-electron quantum dots*, Rev. Mod. Phys. **79**, 1217 (2007), URL. 20

[49] W. Yao, R.-B. Liu, and L. J. Sham, *Theory of electron spin decoherence by interacting nuclear spins in a quantum dot*, Phys. Rev. B **74**, 195301 (2006), URL. 20

[50] D. Gammon, A. L. Efros, T. A. Kennedy, M. Rosen, D. S. Katzer, D. Park, S. W. Brown, V. L. Korenev, and I. A. Merkulov, *Electron and nuclear spin interactions in the optical spectra of single GaAs quantum dots*, Phys. Rev. Lett. **86**, 5176 (2001), URL. 23, 31, 33, 34, 50

[51] V. L. Berkovits, C. Hermann, G. Lampel, and A. Nakamura, *Giant Overhauser Shift of Conduction-Electron Spin-Resonance Due to Optical Polarization of Nuclei in Semiconductors*, Phys. Rev. B **18**, 1767 (1978), URL. 24

[52] S. Laurent, B. Eble, O. Krebs, A. Lemaitre, B. Urbaszek, X. Marie, T. Amand, and P. Voisin, *Electrical control of hole spin relaxation in charge tunable InAs/GaAs quantum dots*, Phys. Rev. Lett. **94**, 147401 (2005), URL. 26

[53] E. L. Ivchenko, *Spectroscopy of Spin-Polarized Excitons in Semiconductors*, Pure Appl. Chem. **67**, 463 (1995), URL. 27

[54] M. I. Dyakonov and V. I. Perel, *Dynamic Self-polarization of Nuclei in Solids*, JETP Lett. **16**, 398 (1972), URL. 31, 64

[55] R. Kaji, S. Adachi, H. Sasakura, and S. Muto, *Precise measurements of electron and hole g factors of single quantum dots by using nuclear field*, Appl. Phys. Lett. **91**, 261904 (2007), URL. 37

[56] R. Kaji, S. Adachi, H. Sasakura, and S. Muto, *Hysteretic response of the electron-nuclear spin system in single* $In_{0.75}Al_{0.25}As$ *quantum dots: Dependences on excitation power and polarization*, Phys. Rev. B **77**, 115345 (2008), URL. 37

[57] D. Paget, T. Amand, and J. Korb, *Light-induced nuclear quadrupolar relaxation in semiconductors* (2008), arXiv:0801.2894v1, URL. 38

[58] C. Ramanathan, *Dynamic nuclear polarization and spin-diffusion in non-conducting solids* (2008), arXiv.org:0801.2170, URL. 38

[59] R. I. Dzhioev and V. L. Korenev, *Stabilization of the Electron-Nuclear Spin Orientation in Quantum Dots by the Nuclear Quadrupole Interaction*, Phys. Rev. Lett. **99**, 037401 (2007), URL. 41, 42, 56

[60] J. Jackson, *Classical Electrodynamics* (John Wiley, New York, 1998). 41, B

[61] C. P. Slichter, *Principles of Magnetic Resonance* (Springer, 1996), 3rd ed. 42

[62] R. K. Sundfors, R. K. Tsui, and C. Schwab, *Experimental gradient elastic tensors: Measurement in I-VII semiconductors and the ionic contribution in III-V and I-VII compounds*, Phys. Rev. B **13**, 4504 (1976), URL. 42

[63] A. J. Williamson and A. Zunger, *InAs quantum dots: Predicted electronic structure of free-standing versus GaAs-embedded structures*, Phys. Rev. B **59**, 15819 (1999), URL. 42, 47

[64] B. D. Gerardot, D. Brunner, P. A. Dalgarno, P. Ohberg, S. Seidl, M. Kroner, K. Karrai, N. G. Stoltz, P. M. Petroff, and R. J. Warburton, *Optical pumping of a single hole spin in a quantum dot*, Nature **451**, 441 (2008), URL. 43

[65] X. Marie, T. Amand, P. Le Jeune, M. Paillard, P. Renucci, L. E. Golub, V. D. Dymnikov, and E. L. Ivchenko, *Hole spin quantum beats in quantum-well structures*, Phys. Rev. B **60**, 5811 (1999), URL. 43

[66] K. and Karrai, R. J. Warburton, C. Schulhauser, A. Hogele, B. Urbaszek, E. J. McGhee, A. O. Govorov, J. M. Garcia, B. D. Gerardot, and P. M. Petroff, *Hybridization of electronic states in quantum dots through photon emission*, Nature **427**, 135 (2004), URL. 53

[67] C. Schulhauser, Ph.D. thesis, LMU Mnchen (2004), URL. 53

[68] G. Bester, D. Reuter, L. He, A. Zunger, P. Kailuweit, A. D. Wieck, U. Zeitler, J. C. Maan, O. Wibbelhoff, and A. Lorke, *Experimental imaging and atomistic modeling of electron and hole quasiparticle wave functions in InAs/GaAs quantum dots*, Phys. Rev. B **76**, 075338 (2007), URL. 53

[69] V. Kalevich, K. Kavokin, and I. Merkulov, private communication (2008). 56

[70] M. Kroner, K. M. Weiss, B. Biedermann, S. Seidl, S. Manus, A. W. Holleitner, A. Badolato, P. M. Petroff, B. D. Gerardot, R. J. Warburton, et al., *Optical Detection of Single-Electron Spin Resonance in a Quantum Dot*, Phys. Rev. Lett. **100**, 156803 (2008), URL. 63, 64

[71] A. Imamoglu, *Coherent population trapping in a single-hole-charged quantum dot*, Phys. Stat. Sol. (b) **243**, 3725 (2006), URL. 63

[72] A. Hogele, M. Kroner, S. Seidl, K. Karrai, M. Atature, J. Dreiser, A. Imamoglu, R. J. Warburton, A. Badolato, B. D. Gerardot, et al., *Spin-selective optical absorption of singly charged excitons in a quantum dot*, Appl. Phys. Lett. **86**, 221905 (2005), URL. 63

[73] P. Simon and D. Loss, *Nuclear Spin Ferromagnetic Phase Transition in an Interacting Two Dimensional Electron Gas*, Phys. Rev. Lett. **98**, 156401 (2007), URL. 64

[74] V. Zwiller and G. Bjork, *Improved light extraction from emitters in high refractive index materials using solid immersion lenses*, Journal of Applied Physics **92**, 660 (2002), URL. A

[75] E. A. Donley, T. P. Heavner, F. Levi, M. O. Tataw, and S. R. Jefferts, *Double-pass acousto-optic modulator system*, Review of Scientific Instruments **76**, 063112 (2005), URL. C

[76] A. Hogele, S. Seidl, M. Kroner, K. Karrai, , R. J. Warburton, B. D. Gerardot, and P. M. Petroff, *Voltage-Controlled Optics of a Quantum Dot*, Phys. Rev. Lett. **93**, 217401 (2004), URL. E

List of publications

1. C. W. Lai, P. Maletinsky, A. Badolato, and A. Imamoglu, *Knight-field-enabled nuclear spin polarization in single quantum dots*, Phys. Rev. Lett. **96**, 167403 (2006), URL
2. P. Maletinsky, C. W. Lai, A. Badolato, and A. Imamoglu, *Nonlinear dynamics of quantum dot nuclear spins*, Phys. Rev. B **75**, 35409 (2007), URL
3. P. Maletinsky, A. Badolato, and A. Imamoglu, *Dynamics of Quantum Dot Nuclear Spin Polarization Controlled by a Single Electron*, Phys. Rev. Lett. **99**, 056804 (2007), URL
4. P. Maletinsky and A. Imamoglu, *Quantum Dot Nuclear Spin Polarization* in *Single Semiconductor Quantum Dots*, edited by P. Michler (Springer, Berlin, 2008)

Acknowledgement

As it is the case with most scientific endeavors, this work was certainly not the product of one individual person. Conducting this Ph.D. work would neither have been possible without the consoling and encouraging words of friends during the difficult, initial times when our quantum dots were very efficient in hiding any sign of nuclear spin polarization nor without the inspiring and motivating inputs of colleges in times when my experiment produced more data than I could possibly have digested on my own. In that sense, I thank everybody who contributed to this work as a friend, a collegue or a member of my family.

Most and foremost, my gratitude goes to ATAC IMAMOGLU who let me accomplish my Ph.D. in his group. Atacs inputs on my experiment were always most inspiring and the ease with which he was able to analyze and explain even the most difficult experimental situations often left me with astonishment, new insight and a day to digest the contents of our discussions. What I am most grateful for is the great scientific liberty and confidence Atac always gave me. I never felt “obliged” to conduct any of my experiments and was mostly left to work on the problem I was most motivated to investigate. While such an attitude can usually not be taken for granted, in my opinion and at least for my case, this is a most fruitful way to make progress in science.

Not knowing anything about the experimental techniques of photoluminescence and semiconductor spectroscopy at the beginning of my Ph.D., it would have been very difficult to start my project without a good teacher in the lab. With CHIH-WEI LAI, I possibly had the best and most patient mentor for this task. A good part of the experiments presented in this work can only be performed on a system having an excellent photon collection efficiency. Chih-Wei is probably the world-champion in not loosing photons and if I only inherited a part of his experimental perfectionism in this and many other respects I already owe him a lot. I thank Chih-Wei for the year we spent together in the lab and for the support he kept giving me even after leaving our lab in 2005.

If meeting people in a lab not only leads to good collaborations but also to very good friends, this is certainly an ideal combination. With ALEX HÖGELE I believe to have found such a combination and I happily think back to the many days and evenings we spent together in G17. Alex always showed greatest interest in my experimental results for many of which he deserves big credits for his inspiring comments and his help in solving experimental problems. Last but not least, the present form of this manuscript owes a lot to his patient and critical proof-reading for which I am very grateful.

Laboratory G17 was a fun place to be and to work. This was to a good part due to the presence of CHRISTIAN LATTA whose ambition to push his experiment forward was highly contagious. I thank Christian for keeping me from wasting too much of my time by surfing the internet and for his many helpful inputs during my clumsy attempts to master Matlab. I wish him all the best for the rest of his Ph.D. which I'm sure he will finish with distinction but hopefully also in a relaxed manner.

For the little time of my Ph.D. that I spent on my desk, I was lucky to have JEROEN ELZERMAN as an office-mate. Jeroen always gave helpful input on papers and presentations I tried to produce and always surprised me with the original plants he introduce into our office, where they had a life-expectancy of not more than two weeks.

THIERRY AMAND kindly agreed to take the long journey from Toulouse to Zürich to co-examine my Ph.D. defense. I thank him for doing so and for the inputs he gave me for our experiments regarding quadrupolar interactions.

Furthermore, I thank thank all the members of the Quantum Photonics group for creating such a lovely working atmosphere. Particularly, I thank A. BADOLATO for providing us with very nice samples and J. DREISER for the gating of our QD structures.

I would also like to thank ILJA GERHARD for providing me with a very nice template for writing up this Ph.D. thesis. His effort in preparing a good environment to create such a thesis certainly saved me many hours of painful LaTeX debugging.

Working long hours on an experiment that mostly works but sometimes not is mostly fun - but sometimes not! In either case, leaving the lab after a long day in the lab would only be half as fun without a place to live, where one truly feels at home. I want to thank my roommates LORENZ, RAHEL, BINE and RONA from the "Luther-WG" for of sharing this home with me over the last 3 years and for making it such an enjoyable place to live.

As an "associate roommate", SEBI HUBER deserves a special credit at this place. Not only was he a best fiend and constant companion since the early time of our common studies in physics, he also provided most helpful input to my Ph.D. work. He always was a critical listener who constantly challenged me to find a good way to overcome the language barrier between experimental and theoretical physicists. I thank him for all the time we spent together, including our countless common climbing trips which rarely lacked discussions about Sebis latest crazy calculations.

Being a consequent defender of work-free weekends, I luckily had time enough for physics-free activities over the last three years. This time was mostly filled by spending time with friends, be it for climbing in the mountains or for taking advantage of the the many activities that Zürich and Switzerland in general can offer. For this, I thank all my friends, in particular, the Schaffhauserner climbing crew with DAVE, ANNINA, LUKI and others. Furthermore I thank TOTT, DARIO, NICOLE, SINA and BRICE, for being good friends that I always enjoy seeing and hope for their understanding that this was not much the case in recent times.

My biggest thank however goes to my family and most of all to MY PARENTS. Their constant support and motivating words always gave and give me the confidence to move on in my current direction. Thanks to them and to a big extent also thanks to our newest family members, our common family gatherings are always most enjoyable and warming events. For those, I'd like to thank DAVID, MARTIN, CORINNE, ANNE, ELENA, NILS, LUANA, MELANIE and of course my godson NOA.

Finally, I thank NINA♡♡♡.

Curriculum Vitae

Personal Details

Name	Patrick Maletinsky
Date of Birth	3rd of June, 1979
Place of Birth	Baden, Switzerland
email	patrickm@phys.ethz.ch

Education

1993-1998	Kantonsschule Schaffhausen
1998-2004	ETH Zürich, Diploma in Physics
2000-2001	ENS Paris, MIP I
2004-2005	JILA, University of Colorado, research internship
2005-2008	ETH Zürich, Quantum Photonics Group, Ph.D.

Experience

Languages	German, English, French, Czech
Programming	Visual Basic, Matlab, Mathematica

October 3, 2008

List of Figures

2.1 Band structure of bulk III-V semiconductors 6
2.2 Quantum dot growth schematics 7
2.3 Quantum dot field effect structure 8
2.4 Trapping potential for charge carriers in quantum dots 9
2.5 Gate voltage dependent quantum dot photoluminescence spectrum . . 11

4.1 Exciton spin splitting induced by the Overhauser field 24
4.2 Measurement of the QD Knight field 26

5.1 Magneto PL of X^{-1} under circularly polarized excitation 30
5.2 Magnetic field dependence of nuclear spin polarization 32
5.3 Graphical solution of the nonlinear rate equation 5.3 35
5.4 Hysteretic behavior of nuclear spin polarization in a magnetic field . . 36
5.5 High nuclear spin polarization at $B_{\text{ext}} = 4T$ 38

6.1 Theory for the anomalous Hanle effect 41
6.2 Hanle curve of X^{-1} in an individual QD 44
6.3 Hanle curve of X^{+1} in an individual QD 46

7.1 Buildup and decay of quantum dot nuclear spin polarization 51
7.2 Nuclear spin relaxation controlled by a QD electron 52
7.3 Nuclear spin relaxation for different QD electron occupation numbers 53
7.4 Nuclear spin dynamics in low magnetic fields 55
7.5 Buildup of nuclear spin polarization in high magnetic fields 58
7.6 Decay of nuclear spin polarization in high magnetic fields 60

A.1 Sketch of the photoluminescence setup . . . . B
A.2 Fast switching of the QD gate voltage . . . . F